ผลของการเติมพอลิโพรพิลีนออกไซด์ ต่อโครงสร้างและสมบัติของ
พอลิเมอร์อิเล็กโทรไลต์ของแข็ง:ระบบพอลิเอทธิลีนออกไซด์/เกลือ

นางสาวพนิตา   เดชา

EFFECT OF ADDING POLY(PROPYLENE OXIDE) ON STRUCTURES

AND PROPERTIES OF SOLID POLYMER ELECTROLYTES:

POLY(ETHYLENE OXIDE)/SALT SYSTEM

Miss Panita   Decha

EFFECT OF ADDING POLY(PROPYLENE OXIDE) ON STRUCTURES AND
PROPERTIES OF SOLID POLYMER ELECTROLYTES:
POLY(ETHYLENE OXIDE)/SALT SYSTEM

Suranaree University of Technology has approved this thesis submitted in partial fulfillment of the requirements for a Master's Degree

Thesis Examining Committee

………………………………………….………….

(Asst. Prof. Dr. Malee Tangsathitkulchai)

Chairman

………………………………………….………….

(Dr. Visit Vao-Soongnern)

Member (Thesis Advisor)

………………………………………….…………

(Asst. Prof. Dr. Kunwadee Rangsriwatananon)

Member

………………………………………….………….

(Asst. Prof. Dr. Anan Tongraar)

Member

………..…..……………………… ………………………………….…………

(Assoc. Prof. Dr. Tawit Chitsomboon) (Assoc. Prof. Dr. Prasart Suebka)

Vice Rector for Academic affairs Dean of the Institute of Science

พนิตา เดชา: ผลของการเติมพอลิโพรพิลีนออกไซด์ต่อโครงสร้างและสมบัติของพอลิเมอร์อิเล็กโทร
ไลต์ของแข็ง:ระบบพอลิเอทธิลีนออกไซด์/เกลือ (EFFECT OF ADDING POLY(PROPYLENE
OXIDE) ON STRUCTURES AND PROPERTIES OF SOLID POLYMER ELECTROLYTES:
POLY(ETHYLENE OXIDE)/SALT SYSTEM)
อ. ที่ปรึกษา: ดร. วิสิษฐ์ แววสูงเนิน, 118 หน้า ISBN 974-533-193-7

      งานวิจัยนี้มีจุดประสงค์เพื่อเพิ่มการนำไฟฟ้าเชิงไอออนิกของระบบพอลิเอทธิลีนออกไซด์/
เกลือ (PEO/salt) ผู้วิจัยใช้การเติมพอลิโพรพิลีนออกไซด์ (PPO) ซึ่งเป็นพลาสติไซเซอร์ลงไปใน
ระบบดังกล่าวโดยคาดว่าจะเพิ่มส่วนที่เป็นอสัณฐานของพอลิเอทธิลีนออกไซด์และทำให้การนำไฟ
ฟ้าเพิ่มขึ้น ผลของการเติมพอลิโพรพิลีนออกไซด์ต่อโครงสร้างและสมบัติการนำไฟฟ้าของพอลิ
เอทธิลีนออกไซด์/เกลือได้ศึกษาโดยใช้เทคนิคต่างๆ ดังนี้ เอกซเรย์ดิฟแฟรกชัน (XRD), อินฟราเรด
สเปกโทรสโกปี (FTIR), ดิฟเฟอเรนเชียลสแกนนิงคาลอริมิเตอร์ (DSC) และ เครื่องวัดความต้าน
ทาน เนื่องจากโครงรูปของพอลิเมอร์มีบทบาทสำคัญต่อความเข้าใจที่ดีขึ้นของการนำไฟฟ้าและ
อันตรกิริยาระหว่างไอออน–พอลิเมอร์ของพอลิเมอร์อิเล็กโทรไลต์ของแข็ง ดังนั้นจึงมีการศึกษา
ลักษณะจำเพาะเชิงโครงรูปของพอลิโพรพิลีนออกไซด์โดยการใช้ทฤษฎีไอโซเมอร์เชิงโครงรูป
(RIS Theory)

      ผลการทดลองที่ได้จากเทคนิค XRD, DSC, FTIR และเครื่องวัดความต้านทาน พบว่าพอลิ
โพรพิลีนออกไซด์ลดส่วนที่เป็นผลึกของพอลิเอทธิลีนออกไซด์ได้และทำให้สภาพนำไฟฟ้าเชิง
ไอออนของระบบพอลิเอทธิลีนออกไซด์/เกลือ (เกลือ $LiCF_3SO_3$ หรือ KSCN) สูงขึ้น แนวโน้มของ
การนำไฟฟ้าจะเพิ่มขึ้นตามความเข้มข้นของเกลือซึ่งมีค่าสูงสุดที่ความเข้มข้นจุดหนึ่งและจะลดลง
เมื่อความเข้มข้นของเกลือมากๆ ระบบ $PEO/PPO/LiCF_3SO_3$ จะมีสภาพนำไฟฟ้าเชิงไอออนสูงกว่า
ระบบ PEO/PPO/KSCN โดยส่วนประกอบที่ทำให้ค่าการนำไฟฟ้าเชิงไอออนสูงที่สุดของระบบดัง
กล่าว คือ (1) PEO:salt ในอัตราส่วน O:M 16:1 + 80 %wt PPO สำหรับระบบ $PEO/PPO/LiCF_3SO_3$
และ (2) PEO:salt ในอัตราส่วน O:M 16:1 + 100 %wt PPO สำหรับระบบ PEO/PPO/KSCN
สมบัติเชิงโครงรูปของ PPO คำนวณได้จากทฤษฎีไอโซเมอร์เชิงโครงรูปซึ่งให้ค่าที่ใกล้เคียงกับการ
ทดลอง

สาขาวิชาเคมี	ลายมือชื่อนักศึกษา……………………………………
ปีการศึกษา 2545	ลายมือชื่ออาจารย์ที่ปรึกษา………………………….…..

MISS PANITA DECHA: EFFECT OF ADDING POLY(PROPYLENE OXIDE) ON STRUCTURES AND PROPERTIES OF SOLID POLYMER ELECTROLYTES: POLY (ETHYLENE OXIDE)/SALT SYSTEM:

THESIS ADVISOR: VISIT VAO-SOONGNERN, Ph.D. 118 PP. ISBN 974-533-193-7

The objective of this research was to improve the ionic conductivity of poly(ethylene oxide) (PEO) based electrolytes. We added poly(propylene oxide) (PPO) which was used as the plasticizer to increase the fraction of the conductive amorphous phase. Variety of techniques, such as x-ray diffraction (XRD), infrared spectroscopy (FTIR), differential scanning calorimeter (DSC) and high resistance meter were employed to analyze the effect of adding PPO on the structure and ionic conductivity of PEO-salt ($LiCF_3SO_3$ and KSCN) solid electrolytes. The conformation of polymer played an important role for a better understanding of the conductivity and ion-polymer interaction of solid polymer electrolytes. Therefore, the conformational characteristics of PPO were studied by using the Rotational Isomeric State (RIS) Theory.

The results from XRD, DSC, FTIR and, high resistance meter suggested that PPO was able to decrease the crystallinity of PEO and improve the ionic conductivity of PEO-salts ($LiCF_3SO_3$ or KSCN) electrolytes. The PEO/PPO/$LiCF_3SO_3$ electrolyte exhibited higher ionic conductivity than that of PEO/PPO/KSCN electrolyte. The trend was observed in which the conductivity increased with increasing salt concentration to a maximum, then it decreased at very high salt concentration. The best compositions that gave the highest ionic conductivity of PEO:salt electrolytes were (1) the PEO:salt (O:M) ratio of 16:1 + 80 %wt PPO for PEO/PPO/$LiCF_3SO_3$ electrolyte and (2) the PEO:salt (O:M) ratio of 16:1 + 100 %wt PPO for PEO/PPO/KSCN electrolyte. Conformational dependent properties of PPO calculated from the RIS Theory gave the values that were closed to the experimental results.

สาขาวิชาเคมี   ลายมือชื่อนักศึกษา……………………………………………

ปีการศึกษา 2545   ลายมือชื่ออาจารย์ที่ปรึกษา……………………………………

Acknowledgment

Panita Decha

Contents

Contents (Continued)

Contents (Continued)

List of Tables

List of Tables (Continued)

Table **Page**

List of Figures

List of Figures (Continued)

List of Figures (Continued)

List of Figures (Continued)

List of Abbreviations

SPEs	Solid polymer electrolytes
PEO	Poly(ethylene oxide)
PPO	Poly(propylene oxide)
TEGDME	Tetraethylene glycol dimethylether
TEG	Tetraethylene glycol
DME	Dimethylether
PC	Propylene carbonate
EC	Ethylene carbonate
DMP	Dimethoxypropane
PTMO	Poly (tetramethylene oxide)
POM	Poly(oxytrimethylene)
KSCN	Potassium Thiocyanate
$LiCF_3SO_3$	Lithium trifluorosulfonate
XRD	X-ray diffraction
DSC	Differential Scanning Calorimeter
FTIR	Fourier Transform Infrared
NMR	Nuclear Magnetic Resonance
DEPT	Distortionless Enhancement by Polarization Transfer
H-H COSY	H-H COrrelated SpectroscopY
HETCOR	Heteronuclear Chemical Shift Correlation
RIS	Rotational Isomeric State
MM	Molecular Mechanics
VTF	Vogel-Tammann-Fulcher
σ	Conductivity
S/cm	Seimen/centimeter
I	Current

List of Abbreviations (Continued)

V	Voltage
R	Resistance
iso	Isotactic
syn	Syndiotactic
$\left\langle r^2 \right\rangle_0$	Mean square unperturbed end-to-end distance
$\left\langle r^2 \right\rangle_0 / nl^2$	Characteristic ratio
C_n	Characteristic ratio
$\left\langle S^2 \right\rangle$	Mean-square radius of gyration
$\left\langle S^2 \right\rangle_0 / nl^2$	Mean-square unperturbed radius of gyration ratio
$\left\langle \mu^2 \right\rangle_0 / nm^2$	Mean-square unperturbed dipole moment
$t,$	Trans
g^+	Gauche$^+$
$g-$	Gauche$^-$
Z	Conformational partition function
U	Statistical weight matrix
$E_i(\phi_i)$	Single bond energy
$\langle...\rangle$	Ensemble average for all possible conformations
G	Super generator matrix
I	Identity matrix
$\otimes$	Direct product
θ	Bond angle
ϕ	Torsion angle
$[\eta]$	Intrinsic viscosity
η_{rel}	Relative viscosity
η_{red}	Reduced viscosity
η_{inh}	Inherent viscosity
g/dl	Gram/deciliter

List of Abbreviations (Continued)

Φ	Hydrodynamic factor
M	Average molecular weight
MW	Molecular weight
O:M	Molar ratios of the ether oxygen in the polymer to metal cation of salt
T_g	Glass transition temperature
T_m	Melting temperature
ΔH_f	Heat of fusion
%wt	Percent weight
°C	Degree celcius
K	Degree Kelvin
Å	Angstrom
$\Omega.cm^{-1}$	Ohms/centimeter
cm^{-1}	Per centimeter
A	Absorbance
Sec.	Second
e.g.	For example
et al.	et alia (and others)

CHAPTER I

INTRODUCTION

Polymers are substances consisting of very large molecules made up of many repeating subunits (Billmeyer, 1984). They are interesting both from a fundamental scientific point of view and from their importances in a wide variety of technological applications. In general, polymeric materials are well known as insulators. Furthermore, they can be modified into partially conductive materials.

Solid polymer electrolytes (SPEs) exhibit an ionic conductivity when they are modified by dissolving of alkali salts in suitable polymer matrix. SPEs have a wide range of electrochemical applications such as batteries, fuel cells, electrochromic devices, sensors and electrochemical switching (Dias et al., 2000; Quartarone et al., 1998; Song et al., 1999).

PEO and its derivatives have been used as matrix polymers in most of SPEs studies (Bruce, 1995; Chintapalli, 1996). PEO contains ether coordination sites, which assist the dissociation of incorporated salts in polymer matrix as well as a flexible macromolecular structure, which promotes facile ionic transport (Chintapalli, 1996; Nishimoto et al., 1999). However, PEO-based polymer electrolytes show comparatively low ionic conductivity at an ambient temperature due to the existence of crystalline domains, which interfere the ionic transport. Since the ion mobility in polymer electrolytes was found to be accompanied by polymer chain mobilities, conductivity and ion transport were restricted to the amorphous phase of the polymer electrolyte (Dias et al., 2000). Decreasing of the crystalline domains and increasing of the ionic transport on main-chain segmental motions of SPEs was able to enhance the ionic conductivity of SPEs (Song et al., 1999). The most striking advancements in the ionic conductivity of SPEs have been attained through the incorporation of substantial amounts of plasticizers to reduce the crystalline content and to increase the polymer segmental mobility. For example, low molecular weight polyethers and polar organic solvents are two commonly used plasticizers (Chintapalli, 1996; Dias et al., 2000; Quartarone et al., 1998; Song et al., 1999)

In this work, attempt to improve the conductivity of PEO based electrolytes has come up with plasticization of polymer electrolytes with low molecular weight species to disrupt PEO crytallinity and increase the fraction of the conductive amorphous phase. Poly(propylene oxide) (PPO) has a similar backbone structure as PEO and it is possible to be used as a plasticizer. Since PPO is inherently amorphous due to the extra methyl group in the repeating unit the introduction of PPO can prevent the crystallization of the matrix polymer (Nishimoto et al., 1999). At room temperature, PPO is highly flexible with the transition to the glassy state (Ahlstrom et al., 2000). The conformation of polymer plays an important role for a better understanding of the conductivity, ion-polymer interaction of SPEs. Therefore, the conformational characteristics and conformational dependent properties of PPO will be studied by using the Rotational Isomeric State (RIS) Theory which made possible the fast and accurate calculations by generating properties of a single chain and an accurate representation of chain conformational statistics for molecule (Chen, 1991).

In this research work, we are interested in polymer electrolytes based on PEO/PPO/salt and analyze the effect of adding PPO on the structure and ionic conductivity of these systems. In particular the system in which PEO, PPO and salt have been used as a polymer host, a plasticizer and ionic charge, respectively. The conformational characteristics of PPO are determined by using the RIS Theory.

Research Objectives

1. To study the conformational characteristics of PPO by using the RIS Theory and compare their conformational dependent properties with those obtained from the experiments.
2. To determine the best composition of PEO/PPO/salt electrolytes that give the highest ionic conductivity.
3. To study the effect of adding low molecular weight PPO as plasticizer on the structure and properties of PEO-salt electrolytes.

Scope of the Study

Poly(propylene oxide) Characterization

In this research work, the elements of statistical weight matrices of PPO are investigated first. These quantities can be estimated from the conformational energy calculations of small representative segments of a PPO chain by using Molecular Mechanics (MM) technique. Secondly, some conformational dependent properties (the unperturbed mean square end-to-end distance $\left\langle r^2 \right\rangle_0$, characteristic ratio C_n, mean-square radius of gyration $\left\langle S^2 \right\rangle$ and fraction of bond conformer are calculated by using the RIS Theory and then compare them with experimental results.

Solid Polymer Electrolytes Film Characterization

Solid polymer electrolytes based on PEO/PPO/salt are prepared in the form of thin film. Structure and properties are characterized by variety of techniques, such as X-ray diffraction, Differential Scanning Calorimeter (DSC), Fourier Transform Infrared Spectroscopy (FTIR) and High resistance meter.

CHAPTER II

LITERATURE REVIEW

2.1 Polymer Electrolytes

Solid polymer electrolytes (SPEs) have an ionic conductivity when modified by dissolving of alkali salts in suitable polymer matrix. SPEs are typically thin films, which have a wide range of electrochemical applications such as batteries and electrochromic devices. They have several advantages when used in a battery can be formed into very thin films of large surface area giving high power levels. The flexibility of the films allows space-efficient batteries to be constructed (Quartarone et al., 1998).

Polymer electrolytes were first launched by Fenton *et al.* in 1973, but their technological significance was not appreciated until the research undertaken by Amand and co-worker a few years later (Song et al., 1999). These latter authors claimed that the complexes formed from alkali metal salts and PEO were capable of demonstrating significant ionic conductivity and highlighted their possible application as battery electrolytes. This work inspired intense research and development on the synthesis of new polymer electrolytes, physical studies of their structure and charge transport, theoretical modeling of the charge transport processes, and the physical and chemical properties at the electrolyte/electrode interface (Quartarone et al., 1998). The rapid progress in this field in which starting in 1987 by Armand to recent years, has led to many reviews.

The important criteria for a polymer to act as a host for complex formation include:

(i)   Having atoms or groups of atoms with sufficient donor ability to coordinate cations.

(ii)   Low bond rotational energy barriers to facilitate polymers segmental motion.

(iii)   A suitable distance between coordinating heteroatoms allowing interaction with the ions.

Oxygen, nitrogen and sulfur containing polymers such as poly ethers, poly(ethylene imine), poly (N-propylaziridene) and poly(alkylene sulfides) have been used as polymer host, their formula are shown in Figure 2.1 (Stowe, 2001). However little success has been seen with nitrogen and sulfur containing polymers. Crystallinity and hydrogen bonding in poly(ethylene imine) and low salt solubility in poly(N-propylaziridene) result in low conductivity. Sulfur containing polymers have similar problems.

Polymer Name	Formula
Poly(methylene oxide)	$-\!\!\left(OCH_2\right)\!\!-$
Poly(ethylene oxide)	$-\!\!\left(OCH_2CH_2\right)\!\!-$
Poly(trimethylene oxide)	$-\!\!\left(OCH_2CH_2CH_2\right)\!\!-$
Poly(propylene oxide)	$-\!\!\left(OCH_2CH\right)\!\!-$ $\quad\quad\quad\;\;\, CH_3$
Poly(alkylene sulfides)	$-\!\!\left(OCH_2CH_2\text{-}S\right)\!\!-$
Poly(ethylene imine)	$-\!\!\left(OCH_2CH_2\text{-}NH\right)\!\!-$
Poly(N-propylaziridine)	$-\!\!\left(OCH_2CH_2\text{-}N\right)\!\!-$ $\quad\quad\quad\quad\;\, CH_2CH_2CH_3$

Figure 2.1 Structures of potential host polymer for SPEs.

2.2 Basic Structure and Characteristics of Poly(ethylene oxide)

By far the most successful host to date is the ether based polymer poly(ethlene oxide) (PEO). PEO is made by the cationic or anionic ring opening polymerization of ethylene and can result in polymers ranging in molecular weights (MW) ranging from 1000 to 5×10^6. Below MW = 600 is a viscous liquid. At higher MW's PEO is waxy solid with a glass transition temperature (T_g) near -60 °C and the melting temperature (T_m) anywhere from 60 to 70 °C, depending on MW and thermal history. The electrostatic interactions ($\varepsilon \cong 5$), electronpair donating ability ($\approx$ 22), and the most important, the optimal spatial solvating oxygen units, make PEO a superior SPEs candidate (Stowe, 2001).

The chemical structure of PEO consists of the series of polyethers ($[-(CH_2)_mO-]_n$ where m=2). It has recently used in wide applications such as denture adhesives and water-soluble packaging materials. PEO is a linear polymer and the regularity of the structure unit allows a high degree of crystallinity of about 70 to 80 % usually with a density 1.2 g/cc (Armand, 1987), and a heat of fusion value of 188.2 J/g. PEO readily crystallizes in 7_2 helical structure as shown in Figure 2.2, which contains seven ethylene oxide repeat units with two turns in a fiber period of 19.3 Å.

1.93 nm
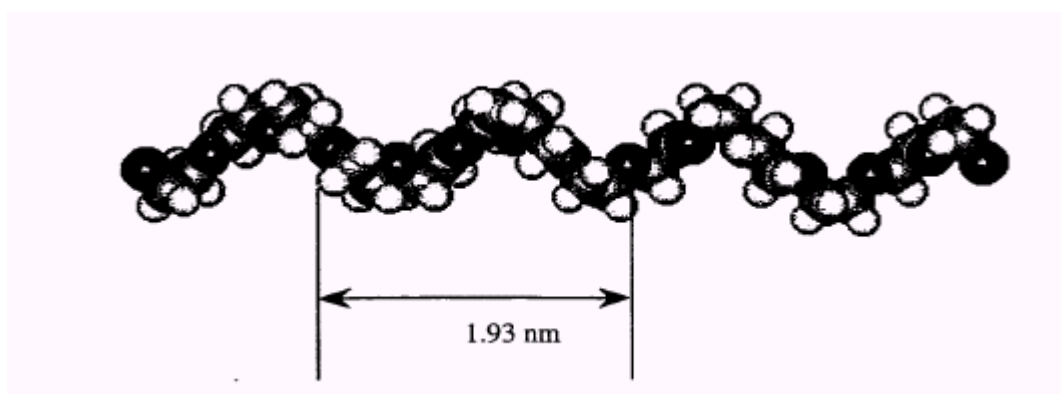
Figure 2.2 The helical structure of PEO.

Takahashi and Tadokoro (1973) showed that the crystalline structure of PEO is monoclinic unit cell as displayed in Figure 2.3. From XRD analysis confirmed that PEO molecules are well

packed and that the molecules are neither unreasonably close nor too far apart. The internal rotation angles are considerably distorted from the uniform helix, as a result of intermolecular forces. This distortion and the ability of the PEO to orient when stressed show the high degree of flexibility of the PEO chains.
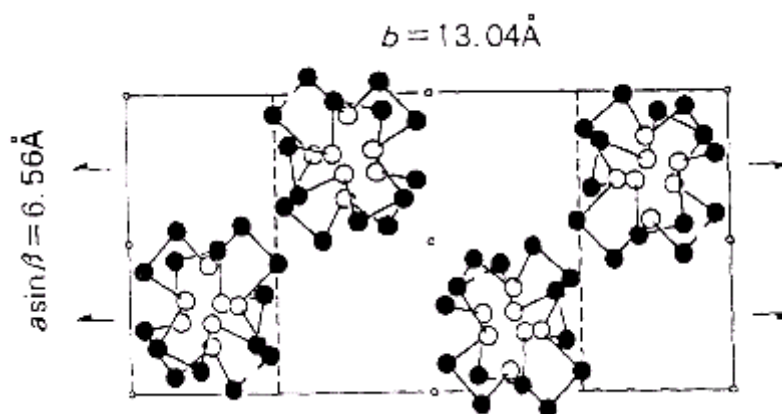
Figure 2.3 Crystal structure of PEO .

2.3 PEO-salt Electrolytes

Over the year, PEO has been the most widely studied host polymer in these systems, because it has oxygen atom with sufficient electron donor power to form coordinate bonds with cations (Gauthier et al., 1988). It also yields the stable formation of multiple intrapolymer bonds with cations due to a proper distance between co-ordinating sites. In addition, the low barriers to bond rotation in PEO promote the segmental motion of the polymer chain. Figure 2.4 illustrates the possible conformations of PEO chain around the cations (Gray, 1991). This lead to easy migration of cations from one solvating sits to another.
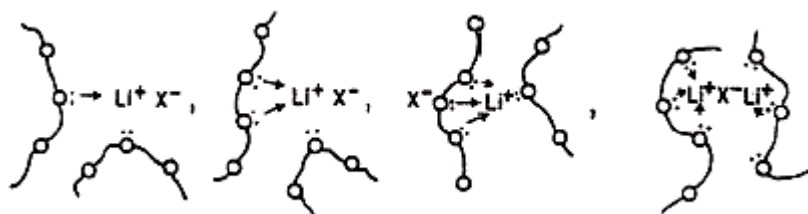
Figure 2.4 Schematic of conformational flexibility of linear polyether enhancing ion solvation.

It is clear that PEO is able to solvate a wide range of metal salts, including alkali metals, alkaline earth metals and transition metals. The different of salt influence the electrolyte properties. The hard-soft acid-base principle, proposed by Pearson (1963), is likely to give a good prediction for stability of acids-bases complexes. The hard acids and bases have high electronegativity (electron held tightly), but low polarizability and to oxidize. The soft acids and bases are opposite. Generally, the strongest interactions occur by matching between hard acids and bases or soft acids and bases. Thus, ether oxygen in PEO may be regarded as hard bases having oxygen as donor atoms with electronegativity and low polarizability. Consequently, Armand (1987) suggested that the strongest solvation in PEO would be with a hard cation, *e.g.* Li^+, Na^+, Mg^{2+} and Ca^{2+}. This is reasonable that these cations have been widely used as a lightweight, high energy density polymer electrolyte battery. MacCallum and Vincent (1987) explained that in water or hydrogen bonded solvent such as alcohols, hydrogen bonding is crucial for specific anion solvation. On the other hand in less polar solvents such as acetonitrile or polymer solvent charge dispersion is main factor for the stability of the anion solvation. Due to the fact that large anion with delocalized charge, ether "soft" (*e.g.* I^-) or "hard" bases (*e.g.* $CF_3SO_3^-$), requires little solvation, the most appropriate anions for polyether-type polymer electrolyte formation would be expected to follow the order (Gray, 1991):

$$F^- \gg Cl^- > Br^- > I^- \sim SCN^- > ClO_4^- \sim CF_3SO_3^- > BF_4^- \sim AsF_6^-$$
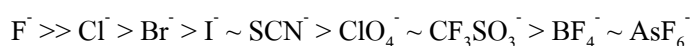
In general, salts of singly charged polyatomic anions such as $LiCF_3SO_3$ or $LiClO_4$ will dissolve in polyethers. Ratner *et al.* (1987) discusses the formation of a complex as the result of the competition between solvation energy of salt, according to equation (2.1).

$$[—AB—]n + MX \longrightarrow [—AB—]n \bullet MX \qquad \_\_\_\_\_ (2.1)$$
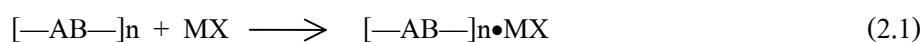
where [—AB—] represents the polymer repeating unit, M is generally an alkali metal and X is an anion. In the case of PEO and PPO, the repeating unit consists of lone pair oxygen as hard base. The solvation of the ions must be strong enough to overcome the lattice energy of the salt in order to form complex (Puatrakul, 2000).

PEO has been found to form complexes with lithium salts such as LiI, LiCl, LiSCN, $LiClO_4$, $LiCF_3SO_3$, $LiBF_4$, and $LiAsF_6$ (Kovac et al., 1998; Smith et al., 1996). Crystal structure

of polymer-salt determination from powder x-ray diffraction data have been shown to provide valuable information on ion-polymer an ion-ion interactions since the local environment in the melt is likely to be very similar to that in the crystal from which it was obtained. Lightfoot *et al.* (1993) determined the crystal structure of $PEO_3LiCF_3SO_3$ from powder x-ray diffraction data. They found that the Li^+ is coordinated with five oxygen atoms, consisted of three ether oxygens from PEO and one oxygen from each of two $LiCF_3SO_3^-$ groups as shown in Figure 2.5. Each $LiCF_3SO_3^-$ in turn bridges two Li^+ ions to from chain running parallel to and interwinded with the PEO chain as illustrated Figure 2.6.
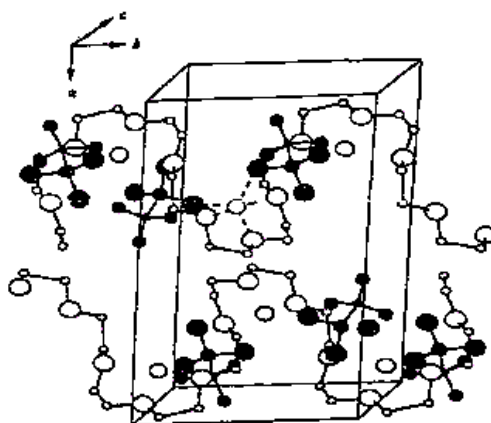
Figure 2.5 Crystal structure of $PEO_3LiCF_3SO_3$ along the axis. $LiCF_3SO_3^-$ groups are shaded and coordination around one Li^+ ion is shown in dashed lines.
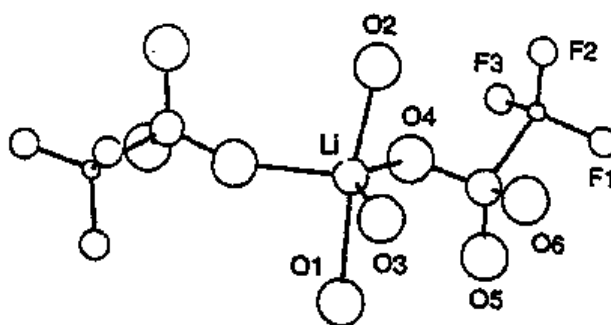
Figure 2.6 Local environment around Li^+, showing coordination by three ether oxygens and oxygens from neighboring trifate groups.

Preechatiwong and Schultz (1996) studied the conductivity of PEO-salt systems, the effect of mixed salts and mixed molecular weight. They found that mixed salt and mixed anion can increase the ionic conductivity of these SPEs systems. Up to date, many types of salts have been used in polymer complex, as shown in Table 2.1.

Table 2.1 Lists of salts used in polymer complex systems.

Host Polymer	Salt	Conductivity about 10^{-5} (S/cm)at T (°C)	Ref.
PEO	NaI	70	(Wright, 1975)
	NaSCN	70	
	KSCN	90	
	NH_4SCN	90	
PEO	LiSCN	70	(Armand, 1987)
	KSCN	60	
	CsSCN	50	
PEO	$MgCl_2$	80	(Yang et al., 1986)
Crosslinked PEO	$LiCLO_4$	30	(Watanabe et al., 1986)
PEO/PPO	$Cu(AA)_2$	10^{-7} at room temperature	(Tandel, 1994)

However, PEO-based polymer electrolytes show comparatively low ionic conductivity at an ambient temperature. The reasons are due to (a) the existence of crystalline domains, which interfere with the ionic transport, and (b) the dependence of the ionic transport on main-chain segmental motions which rapidly diminish with decreasing temperature (Nishimoto et al., 1999).

It is essential to know the microscopic structure and morphology of polymer electrolytes systems that form crystalline phases, as ionic conduction takes place only in the amorphous phase (Chintapalli, 1996). The construction of phase diagrams has been quite useful in understanding the behavior of these systems over a wide range of composition and temperature. The characterization of phase behavior for the PEO-salt system is qualitative as these systems often consist of several phases which greatly influence their properties. While phase diagrams can be used to interpret the dependence of the conductivity on salt concentration and temperature. The phase diagram of PEO-LiCF$_3$SO$_3$ system based on Nuclear Magnetic Resonance (NMR), DSC, conductivity and optical microscopy studies (Chintapalli, 1996) are shown in Figure 2.7. Their phase diagram show the present of a eutectic and at least one salt-rich crystalline intermediate compound with n =3 stoichiometry.
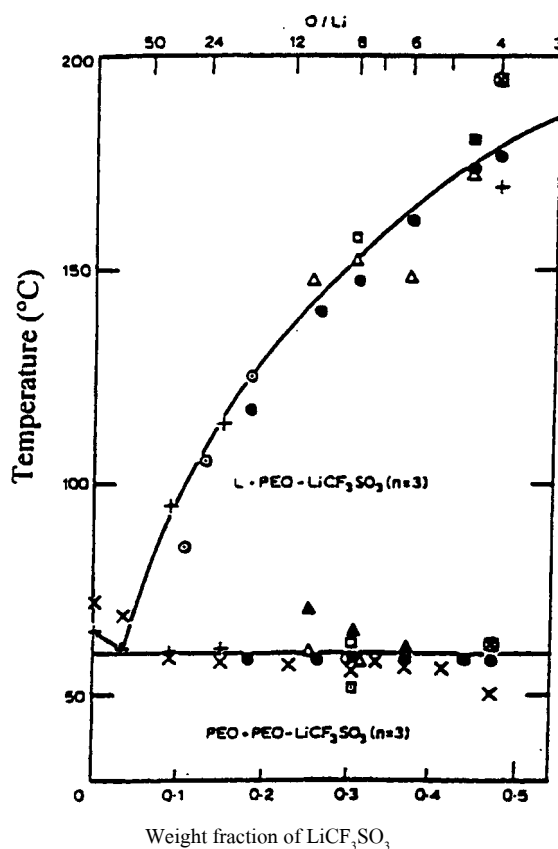
Figure 2.7 Phase diagram of the PEO-LiCF$_3$SO$_3$ system.

Figure 2.8 illustrates the temperature dependent behavior of PEO at O/Li = 6/1 (Stowe, 2001). It is clearly seen that although PEO is good conductor above 60 °C, its performance drops off rapidly as the electrolyte crystallizes. It seems that the good mechanical properties at room temperature come at the expense of immobile ions, and hence low ionic conductivity.
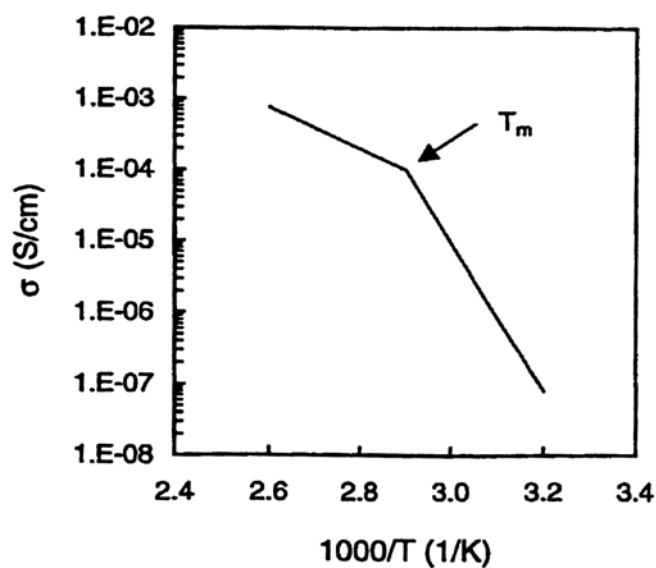
Figure 2.8 Temperature dependent conductivity of PEO/LiClO$_4$ (O/Li=6/1).

Armand *et al*. (1979) proposed a regular helix model for crystalline PEO, below and above the melting temperature. The appearance of highly conductive phase below the melting point was attributed by the formation of cation vacancies in the crystalline phase as shown in Figure 2.9a. At the melting point of PEO, the pure polymer was said to become slighly soluble in the stoichiometric complex, creation the vacancies needed for condition as illustrated in Figure 2.9b.

(a)

(b)

M^{+} Cation X^{-} Anion

○ Oxygen ◉ Carbon
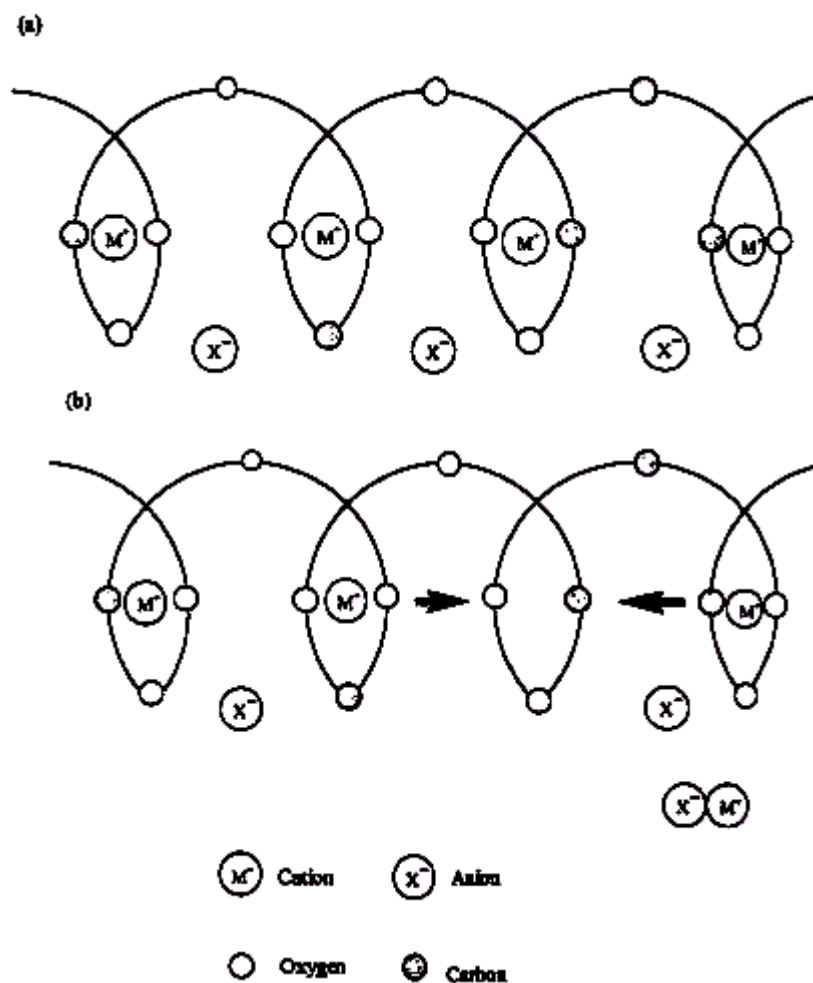
Figure 2.9 A regular helix model of the crystalline PPO complex (a) below the melting transition temperature (b) above the melting transition temperature.

Based on vibrational spectroscopy, Oapke *et al*. (1694) showed that the alkali ions (M) in the electrolytes MX: PEO are tightly coordinated by oxide. In this case, it is oversimplified for ion transport occurring though helical channels. Since amorphous regions link the lamellar crystalline versions, the cation must be able to break all metal oxygen and move out of the helix and though amorphous region under the influence of direct current electric field. This suggested that fewer cation-oxygen interactions were broken in the conduction mechanism. A more resonable microscopic mobility mechanism in salt-complex electrolytes would then involve the cations moving by the breaking one or two M-O bond. Then it replacing these bonds by links to

different oxygen, while the anion X^- move freely into available holes in the structure, as schematically shown in Figure 2.10 later by Shriver and Farrington (1985).
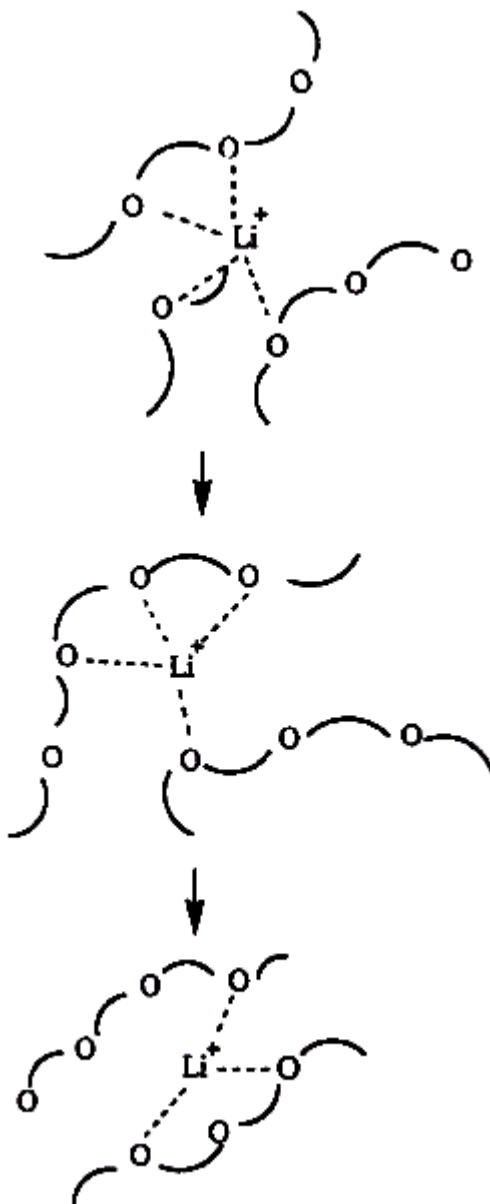
Figure 2.10 Representation of ionic transport in polymer chain Li^+ is transport by the local motion of the polymer chain.

2.4 Enhancement Conductivity of SPEs

It is generally believed that ion conduction takes place in the amorphous domains of the polymer matrix and is assisted by large-amplitude segmental motion (Chintapalli, 1996). Decreasing of the crystalline domains and increasing of the ionic transport on main-chain segmental motions of SPEs can enhance the ionic conductivity of SPEs (Song et al., 1999). Many investigations have focused primarily on the enhancement of room temperature conductivity via various approaches such as using blends, copolymers, comb branch polymers and cross-linked 'networks' (as shown in Figure 2.11). All these enhancements have been done by reducing the crystalline order, trying to create an amorphous phase or decreasing the glass-transition temperature (Dias et al., 2000; Quartarone et al., 1998; Song, et al., 1999). Acosta *et al.* (1996) improved the ionic conductivity by synthesizing different polymer electrolytes based on PEO/PPO blends. They studied the effect of lithium salt on the microstructure and electrical conductivity. It was found that the conductivity was lower for the higher salt concentration than the lower salt concentration (Chintapalli 1996). Nishimoto *et al.* (1999) developed comblike networks polymer electrolytes with hyperbranched ether side chains. They found that the hyperbranched side chains would contribute to fast ionic transport.
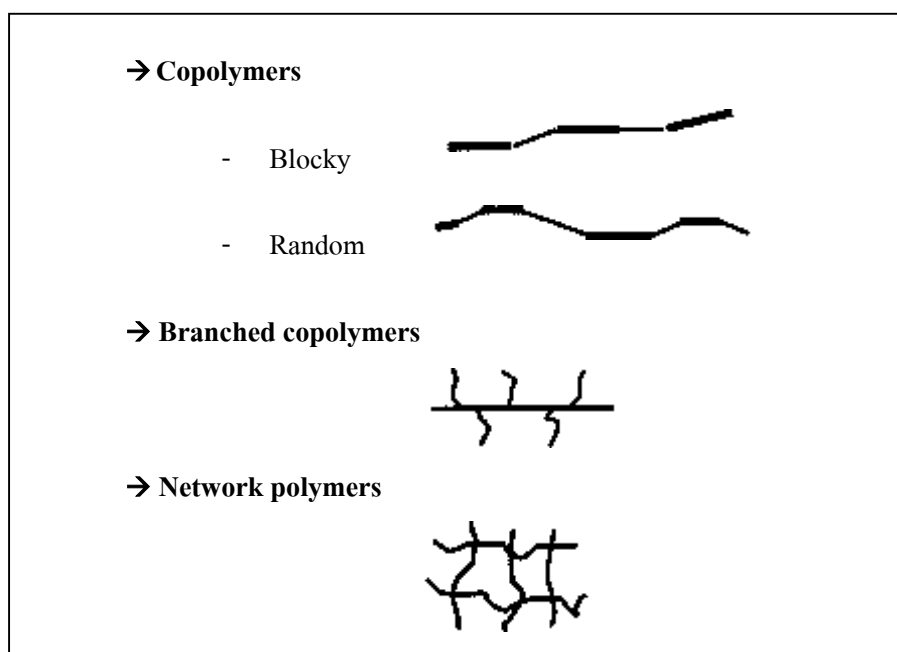
Figure 2.11 Polymer structures designed to limit crystalline.

2.5 Plasticizers

The most striking advancements in the ionic conductivity of SPEs have been attained through the incorporation of substantial amounts of plasticizers. In addition to reducing the crystalline content and increasing the polymer segmental mobility. Low molecular weight polyethers and polar organic solvents are two commonly used plasticizers (Dias et al., 2000; Quartarone, 1998; Song et al., 1999). Chintapalli (1996) studied the effect of adding plasticizers such as propylene carbonate (PC), ethylene carbonate (EC), tetraethylene glycol (TEG) and tetraethylene glycol dimethylether (TEGDME) on ionic association and conductivity in the PEO-LiCF$_3$SO$_3$ system. It was found that both PC and EC interact with the crystalline PEO rendering the complexes amorphous and hence the increases of 3-4 orders of magnitude in the conductivity. In contrast with the addition of TEGME, which increases the associated ionic species, and the addition of TEG, which decreases the number of "free" ions. Kovac *et al.* (1998) studied the effect of plasticizer for a (PEO)$_n$ LiAl(SO$_3$Cl)$_4$ using a mixture of PC and DME as a plasticizer. It was found that this combination reduces the crystallinity of PEO by more than 50 %. The reduction of crystallinity is proportional to the increasing of Li-salt concentration. In this work, attempts will be made to plasticize the polymer matrix with low molecular weight species. PPO has the same backbone structure as PEO, is possible to be used as a plasticizer. Since PPO is inherently amorphous at ambient temperature due to the extra methyl group in the repeating unit, as displayed in Figure 2.12. The introduction of propylene oxide can prevent the crystallization of the matrix polymer (Nishimoto et al., 1999; Ahlstrom et al., 2000). At room temperature, PPO is highly flexible with the transition to the glassy state and the T$_g$ of PPO is–70 °C (Ahlstrom et al., 2000).
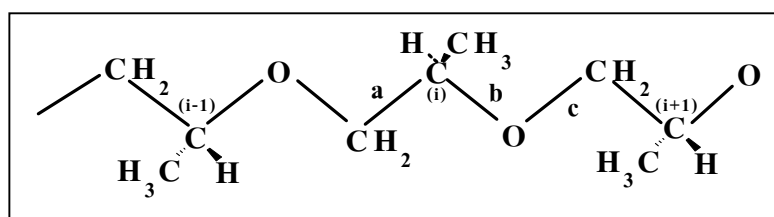
Figure 2.12 Schematic diagram of the isotactic poly (*(R)* propylene oxide) chain in its planar, all-trans conformation.

2.6 General Concepts of Electrically and Ionically Conducting Polymers

The range of electrical conductivity in materials is one of the largest vibrations in any material property (Blythe, 1979). While one tend to regard polymers primarily as insulators, it been recognized that polymer could be a conductive material even at low level. The conductivity, σ, of material are defined by Duke and Gibson (1978) as in Eq. (2.2).

$$J = \underline{\sigma} E \quad \underline{\quad\quad} (2.2)$$

where J is the steady-state current density in A/cm^2 and induced by an applied electric field (E) in V/cm. Both J and E are vectors. As a consequence, $\underline{\sigma}$ is a tensor. By assuming that the induced current flows parallel to the imposed fields, Gutmann and Lyons (1976) and Duke and Gibson. (1978) stated that a tensor, $\underline{\sigma}$, can be treat as a scalar and simply expressed as the general conduction process contributing from several types of charge carriers as the following;

$$\sigma = \sum_i q_i n_i \mu_i \quad \underline{\quad\quad} (2.3)$$

Here, conductivity (σ) is the charge transport across a unit cross-sectional area per second per unit electric field applied. q_i is the charge on ith species having the concentration, or density, n_i per cubic centimeter and mobility of the μ_i. The latter parameter is the velocity with which the carrier moves under unit electric field, i.e., under potential gradient of 1 volt/cm. It dimension is cm^2/volt-sec. Therefor, the unit of conductivity is given as ohm^{-1} cm^{-1} or Siemen cm^{-1}, where Siemen = ohm^{-1} [18]. High ionic conductivity is a result of ions being able to diffuse though an electrolyte medium. Since it is difficult for ions to move freely in a crystal lattice, electrolytes are rarely used below their melting, T$_m$, or glass transition, T$_g$, temperatures where ion mobility is hindered. The relationship of the conductivity of a homogeneous electrolyte can be described by an Arrhenius type equation called the Vogel-Tammann-Fulcher (VTF) equation 2.4.

$$\sigma(T) = A \exp\left(-E_a / (T - T_0)\right) \quad \underline{\quad\quad} (2.4)$$

Here A is the pre-exponential factor and is related to the number of charge carriers and E_a is the apparent activation energy for ion transport. T_0 is the temperature at which the conductivity is zero and is usually taken to be 50 K lower than T_m or T_g. The larger the difference between T_0 and the use temperature, T, the higher the conductivity (Stowe, 2001).

2.7 Measuring Ionic Conductivity

Ohm's law, Eq. (2.5), describes the current (I) as a function of the applied voltage (V) and the resistance (R) of electrolyte.

$$R \ = \ \frac{V}{I} \qquad \qquad \underline{\quad} (2.5)$$

Conductivity (σ) is directly related to Ohms in that σ (in S/cm) is defined as the reciprocal of resistivity (ρ) in Ω cm unit, as shown in Eq. (2.6).

$$\sigma \ = \ \frac{1}{\rho} \qquad \qquad \underline{\quad} (2.6)$$

and

$$\rho \ = \ R\left(\frac{A}{l}\right) \qquad \qquad \underline{\quad} (2.7)$$

Where A (in cm^2) is the area and l (in cm) is the length of the electrolyte sample. It follows then that

$$\rho \ = \ \frac{1}{RA} \qquad \qquad \underline{\quad} (2.8)$$

In order to characterize the conductive properties of the electrolyte alone, it is necessary to minimize the resistive components of the electrode materials. In practice, electrodes of highly electronically conductive and inert material, such as stainless steel or platinum, are used in place of actual working electrode materials. Here, in the intercalation of ion and reactions with the electrode surface are minimized and hence, only the resistive components of the electrolyte are measured (Stowe, 2001).

2.8 The Conformation and Rotational Isomeric State (RIS) Theory

The conformation of polymer plays an important role for a better understanding of the conductivity, ion-polymer interaction of SPEs. Therefore, the conformational characteristics and conformational dependent properties of PPO will be studied using the Rotational Isomeric State (RIS) Theory. RIS Theory can be used to calculate the conformational dependent properties of polymer chains with ease and speed, while also accounting for the detailed chemical structure of the chain. Rotational isomers, local minima produced by internal rotation about main-chain bond, are considered as discrete state. The relative energies of these states determining the probability as given conformation will be studied. Under an additional assumption of fixed bond lengths and bond angles, a set of rotational states along the bonds of a chain completely determines the chain geometry. RIS Theory made possible the fast and accurate calculations by generating properties of a single chain and an accurate representation of chain conformational statistics for molecule (Chen, 1991).

The conformations of small ether molecules have been the subject of extensive experimental and computational studies. These molecules serve as models for larger structure, technological important molecules such as polyethers and crown ethers. Therefore, better understanding of conformational properties of the polymer would greatly facilitate the development of new material (Smith, G. D., et al.,). Conformational analysis of PPO and its model compound 1,2 dimethoxypropane (DMP) (Abe, 1979; Sasanuma, 1995; Sasanuma et al., 2001) and poly (tetramethylene oxide) (PTMO) (Law and Sasanuma 1998), have been investigated by using *ab initio* Molecular Orbital calculations in an effort to better understanding of the conformational properties. The results of *ab initio* quantum chemistry can provide the geometry, conformational energy map and the element of statistical weight matrices. The latter quantities can be estimated from the conformational energy calculations for small molecules and they are required for the parameterization of RIS models. This model with statistical weight matrices can be used to predict the unperturbed mean-square end-to-end distances characteristic ratio, mean-square dipole moments and their temperature coefficients. RIS Theory approximation has been investigated for these conformational dependence properties of PPO, POM and DMP in reasonably good agreement with experimental results.

Thus structure-conductivity investigations relationships are of fundamental importance to the technological applications of the SPEs. A wide range of techniques can be employed to investigate their structure and properties. In this research work, we are interested in polymer electrolytes based on PEO/PPO/salt and analyze the effect of adding PPO on the structure and ionic conductivity of these systems. In particular the system in which PEO, PPO and salt have been used as a polymer host, a plasticizer and ionic charge, respectively. The conformational characteristics of PPO are determined by using the RIS Theory.

CHAPTER III

RESEARCH METHODOLOGY

This work was conducted through a dual gateway, computational method and experimental method. For the computational part, the elements of statistical weight matrices of PPO which were used as numerical input for the RIS model were calculated first. These quantities can be estimated from the conformational energy map of small representative segments of a PPO chain using force field based Molecular Mechanics (MM) technique. Next, some conformational dependent properties such as the unperturbed mean square end-to-end distance $\langle r^2 \rangle_0$, the characteristic ratio $\langle r^2 \rangle_0 / nl^2$, the unperturbed mean-square radius of gyration $\langle s^2 \rangle_0 / nl^2$ and the fraction of bond conformer for the PPO chain were calculated by the matrix multiplication method or the RIS theory. Then these findings were compared with the experimental results.

In an experimental part, solid polymer electrolytes (SPEs) based on PEO/salt and PEO/PPO/salt complexes were prepared in the form of thin film. Structure and properties of these SPE films were characterized using various analytical techniques, such as X-ray diffraction (XRD), Differential Scanning Calorimeter (DSC), Fourier Transform Infrared Spectroscopy (FTIR), Hewlett Packard 4339B high resistance meter.

3.1 Apparatus and Materials

- Glassware for SPE preparation and viscosity measurement
- Magnetic stirrers and magnetic bars
- Oven and vacuum oven for salt drying and solvent removing
- Microscope slides for sample casting
- Viscometer (Cannon-Ubbelohde type) No.150
- Thermostated water bath (range of temperature $20 - 60\ °C$) with stability $\pm\ 0.1\ °C$

- Stop watch

- Poly(ethylene oxide) (PEO MW 4 x 10^6), Aldrich Chemical Company, Inc., USA

- Poly(propylene oxide) (PPO MW 4000 with OCH_3 end group), Aldrich Chemical Company, Inc., USA

- Potassium Thiocyanate (KSCN), APS Finechem

- Lithium trifluorosulfonate ($LiCF_3SO_3$), APS Finechem

- Acetonitrile (CH_3CN), Analytical Reagent, Merck, Germany

- Methanol (CH_3OH), Analytical Reagent, Merck, Germany

- Benzene (C_6H_6), Analytical Reagent, Merck, Germany

3.2 Poly(propylene oxide) Characterization

3.2.1 Rotational Isomeric State (RIS) Theory

RIS Theory is an important method used for the calculation of the conformational dependent properties of a single polymer molecule with ease and speed and also accounting for the detaile chemical structure of the chain. Rotational isomers, local minima produced by internal rotation about main-chain bond, are considered as discrete state so that the degree of freedom of this problem will largely be reduced. The relative energies of these states determining the probability at a given conformation will be studied. Under an additional assumption of fixed bond lengths and bond angles, a set of rotational states along the bonds of a chain completely determines the chain geometry. RIS Theory makes possible the fast and accurate calculations by generating properties of a single chain and an accurate representation of chain conformational statistics for a molecule.

The most frequently used theoretical quantities in RIS Theory, which can be compared with an experimentally measurable quantity are conformational dependent properties such as $\left\langle r^2 \right\rangle_0$, $\left\langle r^2 \right\rangle_0 / nl^2$ and the fraction of bond conformer for a polymer chain. These properties depend significantly on the quality of statistical weights employed in the calculation. The techniques to find statistical weight is to derive from portions of the conformational energy map.

Contour plot denotes the change in energetics of a molecule for each pair of two consecutive torsion angles.

Advantages of RIS Theory

- RIS Theory assumes that the conformations of a chain differ from each other only to the extent that values of the dihedral (torsion) angles of the backbone bonds differ.

- RIS Theory approximates the continuum of possible torsion angles in a chain backbone by a small number of discrete states.

- RIS Theory considers only *short-range* intramolecular interactions.

- RIS Theory makes use of matrix formalism that allows sums over all possible chain conformations to be computed by simply multiplying series of matrices.

Drawbacks of RIS Theory

- RIS Theory normally does not yield analytically expressions that can be evaluated by hand. A computer is usually necessary (PC or Mac is sufficient).

- RIS Theory is set up primarily to handle polymer chains in their unperturbed (θ) states.

- RIS Theory does not concern itself with solution thermodynamics (beyond the default assumption of an unperturbed state).

Foundation of the RIS Theory

Volkenstein used the first RIS model in his pioneering work. The mathematical treatment was adapted independently around 1960 by Gotlib, Brishtein, Ptitsyn, Lifson, Nagai, and Hoeve. It is Flory who introduces versatile methods involving serial multiplication of generator matrices that populated this calculation technique into polymer science community. Quantitative treatment of the conformation-dependent properties of a macromolecular chain by their detail molecular structure has been obtained with the similar accuracy as is achieved in the conformational analysis of small molecules.

The RIS program uses Flory's RIS theory to calculate properties of a flexible polymer chain. This theory accounts for effects of the torsional states of bonds in the chain on their near neighbors in cases where long-range excluded volume effects may be neglected. RIS model tries

to find the conformational partition function from the energy that arises from the torsion angle of polymer chain in the unperturbed or theta condition. In the RIS scheme, the conformational partition function may be written as

$$Z = \sum_{\phi_1}...\sum_{\phi_n}\exp\left[-E(\phi_1...\phi_n)/RT\right] \qquad _____(3.1)$$

If the rotational states of all bonds were completely *independent* of each other, this expression could be simplified to a product of independent sums over *single* torsion angles as

$$Z = \prod_i\left[\sum_{\phi_i}\exp\left[-E_i(\phi_i)/RT\right]\right] \qquad _____(3.2)$$

where $E_i(\phi_i)$ is a single bond energy, independent of the states of all other bonds, such that the total energy is

$$E(\phi_1...\phi_n) = E_1(\phi_1) + E_2(\phi_2) + ... + E_n(\phi_n) \qquad _____(3.3)$$

For most polymer chains, this is a poor approximation because the state of a bond is influenced by the states of its neighbors. This is due to the *pentane effect* effect or the *second-order interaction*, named after the smallest molecule in which the phenomenon occurs. When nearest neighbor dependence is taken into account, the weight associated with a given conformation is

$$\prod_i\exp\left[-E(\phi_{i-1},\phi_i)/RT\right] \qquad _____(3.4)$$

The statistical weight for a bond pair in a given conformation is then given by

$$u_i(\phi_{i-1},\phi_i) = \exp\left[-E(\phi_{i-1},\phi_i)/RT\right] \qquad _____(3.5)$$

The partition function can then be expressed as the sum over all rotational states of the product of these weights. That is

$$Z = \sum_{\phi_i} \cdots \sum_{\phi_n} \prod_i u_i(\phi_{i-1}, \phi_i) \qquad \underline{\qquad}(3.6)$$

In matrix form, this can be rewritten as

$$Z = \prod_i \mathbf{U}_i \qquad \underline{\qquad}(3.7)$$

where U_i is the statistical weight matrix

3.2.2 Statistical Weight Matrices of PPO

Statistical weight matrices were estimated from the conformational energy map of representative small segments of the polymer chain by the force-field based MM technique. In this work, MM was carried out by using Chem3D program that was installed on a PC computer. The descriptive procedures of our calculation were as followed:

- The portions of a PPO chain of which conformations depend on one or both of two neighboring backbones bond rotation angles were selected. Figure 3.1 illustrates constituent bonds of a repeating unit, designated as C-C bond, C-O bond, and O-C bond, respectively.

- Before performing the simulations, the atom coordinates were adjusted to minimize the energy while the torsional angles were kept fixed.

- The conformational energies for each of these fragments were calculated as a function of the rotation angles $E(\phi_1, \phi_2)$. ϕ_2 torsion was rotated from 10° to 360° then ϕ_1 was rotated from 10° to 360° (10° for each step of torsional rotation).

- The conformational energy maps were constructed with respect to ϕ_1 and ϕ_2 for each segment.

- The statistical weight $\text{SW}_{\alpha\beta}$ was evaluated for each of the nine pair-wise dependent rotational states ($\alpha\beta = tt, tg^{\pm}, g^{\pm}t, g^{\pm}g^{\pm}, g^{\pm}g^{\mp}$). As an example, $SW_{g^+g^+}$ was obtained by

$$SW_{g^+g^+} = \frac{\displaystyle\sum_{\phi_1=10°}^{120°}\sum_{\phi_2=10°}^{120°} \exp\left[-E(\phi_1,\phi_2)/RT\right]}{\displaystyle\sum_{\phi_1=0°}^{360°}\sum_{\phi_2=0°}^{360°} \exp\left[-E(\phi_1,\phi_2)/RT\right]} \underline{\qquad}(3.8)$$

where $E(\phi_1,\phi_2)$ is the conformational energy (kcal/mole) at torsional angles ϕ_1 and ϕ_2, R is the gas constant, and T is the absolute temperature. The RIS approximation for chain molecules were usually based on the first- and second-order interactions for three rotational isomeric states i.e. trans *(t)*, gauche$^+$ *(g$^+$)*, and gauche$^-$ *(g$^-$)*. Then, all the statistical weight matrices assigned to the skeletal bonds were 3 x 3 dimension [41].

$$U_{C-C} = \begin{bmatrix} SW_{tt} & SW_{tg^+} & SW_{tg^-} \\ SW_{g^+t} & SW_{g^+g^+} & SW_{g^+g^-} \\ SW_{g^-t} & SW_{g^-g^+} & SW_{g^-g^-} \end{bmatrix} \underline{\qquad}(3.9)$$

3.2.3 Molecular Mechanics

Molecular mechanics describes the energetics of a molecule in terms of a set of classically derived potential energy functions. The potential function and their parameters used for an evaluation of molecular energy are known as force-field. Molecular mechanics typically treats atoms as spheres, and bonds as springs. The mathematics of spring deformation (Hooke's Law) is used to describe the ability of bonds to stretch, bend, and twist. Non-bonded atoms (greater than two bonds apart) interact through van der Waals attraction, steric repulsion, and electrostatic attraction and repulsion. These properties are easiest to describe mathematically when atoms are considered as spheres of characteristic radii. The total potential energy, E, of a molecule can be described by the following summation of interactions:

Energy = Stretching + Bending +Torsion + Non-Bonded Interaction Energy

The first three terms, given as bond stretching, angle bending, and torsion energy , are the so-called bonded interactions. In general, these bonding interactions can be viewed as a strain energy imposed by a model moving from some ideal zero strain conformation. The last term,

which represents the non-bonded interactions, includes the two interactions as repulsion (van der Waals interaction) and interaction from charges, dipoles, quadrupoles (electrostaticinteractions). The Figure 3.2 shows the major interactions (CambridgeSoft Corporation, 1986-2000).
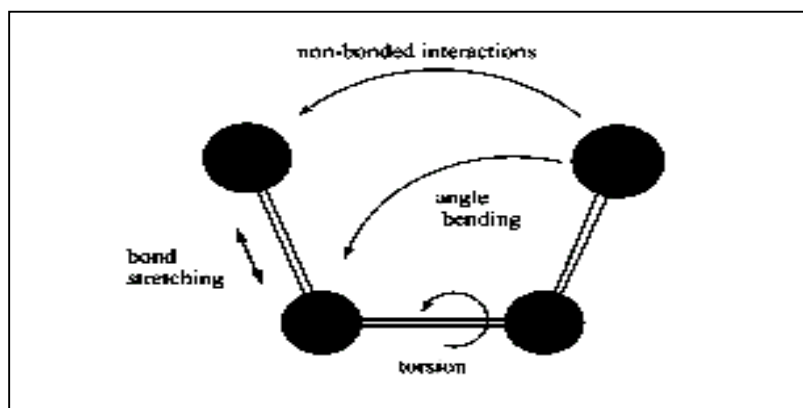
Figure 3.1 Major interactions, including bond stretching, angle bending, torsion and non-bond interaction.

3.2.4 Conformational Dependent Properties Calculated from RIS Theory

It was constructive to consider the relative conformational energies for the model compounds of PPO to be the sum of conformation-dependent interaction depending on single torsions (first-order) and consecutive pairs of torsions (second-order). Such an RIS analysis was useful in gaining greater insight into conformational-dependent interaction in these molecules. The quantities of interest in this work were $\left\langle r^2 \right\rangle_0$, the $\left\langle r^2 \right\rangle_0 / nl^2$, $\left\langle s^2 \right\rangle_0 / nl^2$ and the fraction of bond conformer, all being tested to investigate the characteristics of the polymers. Some useful mathematical formulae following the original framework of the RIS model were given below.

For example, $\left\langle r^2 \right\rangle_0$ for the chain was obtained by evaluating the following matrix multiplication scheme.

$$\left\langle r^2 \right\rangle_0 = Z^{-1} G_1 \left\langle G_2 \right\rangle \cdots \left\langle G_{n-1} \right\rangle G_n \qquad \qquad \_\_\_\_(3.10)$$

where Z is the conformational partition function

         U is the statistical weight matrices in the form as shown in Eq. (3.9)

         $\langle ... \rangle$ is the ensemble average for all possible conformations

$$\langle G_i \rangle = \begin{bmatrix} U & (U \otimes I^T)\|T\| & 0 \\ 0 & (U \otimes I^T)\|T\| & U \otimes I \\ 0 & 0 & U \end{bmatrix}_i \quad\quad \_\_\_\_(3.11)$$

G_i is the super generator matrix, I denotes to the identity matrix and $\otimes$ denotes to the direct product. If U_i is of dimensions V_{i-1} x V_i and I_A is of dimensions 4x4, the direct product, in the sequence $U_i \otimes I_A$, is of dimensions $4V_{i-1}$ x $4V_i$, with the form

$$U_i \otimes I_A = \begin{bmatrix} u_{11}I_A & u_{12}I_A & \cdots \\ u_{21}I_A & u_{22}I_A & \cdots \\ \vdots & \vdots & \ddots \end{bmatrix} \quad\quad \_\_\_\_(3.12)$$

T is the transformation matrix of the form

$$T_i = \begin{bmatrix} -\cos\theta & \sin\theta & 0 \\ -\sin\theta\cos\phi & -\cos\theta\cos\phi & -\sin\phi \\ -\sin\theta\sin\phi & -\cos\theta\sin\phi & \cos\phi \end{bmatrix} \quad\quad \_\_\_\_(3.13)$$

where θ and ϕ denote the bond angle and the torsion angle, respectively.

The other conformational dependent properties such as $\langle s^2 \rangle_0 / nl^2$, and the fraction of bond conformer are calculated in the same way by changing only the super generator matrix for each of these properties.

3.2.5 The Intrinsic Viscosity

The intrinsic viscosity, $[\eta]$, of PPO was measured using a Ubbelohde capillary viscometer. The capillary viscometers used for dilute solution measurements were made of glass. They were operated by filling with a suitable volume of liquid, drawing the liquid level to a point

above the upper mark on the bulb, and measuring the time required for the liquid meniscus to fall from the upper mark to the lower mark. The flow time is related to the viscosity of the liquid and it determined by the driving pressure, using an equation known as Poiseuille's Law,

$$\eta = \frac{\pi R^4 P}{8lQ} = \frac{\pi R^4 Pt}{8lV} \underline{\hspace{2cm}}(3.14)$$

where R is the radius of the capillary, P is the pressure driving the fluid through the capillary, l is the length of capillary, $Q = V/t$ is the volumetric flow rate, V is the volume of liquid, and t is the time of flow. However, there are many sources of error in capillary viscometry depending upon the viscosity level, the nature of the fluid, and the geometric design of the capillary viscometer. Several corrections are important for dilute solutions of polymers.

The Poiseuille equation, after a kinetic energy correction and an entrance correction, has the form

$$\eta = A\rho t - \frac{B\rho}{t} = A\rho t\left(1 - \frac{B}{At^2}\right) \underline{\hspace{2cm}}(3.15)$$

where η is the viscosity of the liquid, ρ is the liquid density, and A and B are constants for the particular viscometer. A and B can be obtained graphically by plotting $\eta/\rho t$ versus $1/t^2$. The intercept of the line though the data point gives A and the slope gives $\left(-B/A\right)$. The relative viscosity, η_{rel}, is measured first and can be calculated by an equation

$$\eta_{rel} \equiv \frac{\eta}{\eta_0} = \frac{\rho t\left(1 - B/At^2\right)}{\rho_0 t_0\left(1 - B/At_0^2\right)} \underline{\hspace{2cm}}(3.16)$$

where the subscript 0 refers to the pure solvent.

In dilute solution, the ratio ρ/ρ_0 is usually closed to unity, so that

$$\eta_{rel} = \frac{t\left(1 - B/At^2\right)}{t_0\left(1 - B/At_0^2\right)} \underline{\hspace{2cm}}(3.17)$$

If the viscometer has an outflow time greater than 100 sec for the pure solvent, the kinetic energy correction B/At^2 are negligible compared to unity, and then

$$\eta_{rel} = \frac{t}{t_0} \qquad\qquad \underline{\qquad}(3.18)$$

The relative viscosity is used to calculate the reduced viscosity, (η_{red}), and the inherent viscosity, (η_{inh}). For given polymer solution, the reduced viscosity and inherent viscosity calculated according to the following equations.

$$\eta \equiv \frac{\eta_{sp}}{c} = \frac{\eta_{rel} - 1}{c} \qquad\qquad \underline{\qquad}(3.19)$$

$$\eta \equiv \frac{\ln \eta_{rel}}{c} \qquad\qquad \underline{\qquad}(3.20)$$

where η_{sp} is $\eta_{rel} - 1$ and c is the polymer concentration (g/dl).

After that, $[\eta]$ can be determined by using the Huggins and Kraemer Equation, which is the viscosity number (the reduced viscosity) or the logarithmic viscosity number (the inherent viscosity), extrapolated to c = 0. It is shown as follows:

$$[\eta] \equiv \lim_{c \to 0}\left(\frac{\eta_{sp}}{c}\right) = \lim_{c \to o}\left(\frac{\ln \eta_{rel}}{c}\right) \qquad\qquad \underline{\qquad}(3.21)$$

The unit of $[\eta]$ is g/dl.

An extrapolation to infinite dilution requires a measurement of the viscosity at several concentrations. The sample concentration should not be too large because additional effects may then arise from intermolecular forces and entanglements between chains. The Huggins and Kraemer Equation are used for this extrapolation.

The Huggins Equation is

$$\frac{\eta_{sp}}{c} = [\eta] + k'[\eta]^2 c \qquad\qquad \underline{\qquad}(3.22)$$

and the Kraemer Equation is

$$\frac{\ln \eta_{rel}}{c} = [\eta] + k''[\eta]^2 c \qquad\qquad \underline{\qquad}(3.23)$$

where both k' and k'' are constants.

Furthermore, the intrinsic viscosity is related to $\langle r^2 \rangle_0$, which can be predicted by the RIS model. The relation is equated as follows:

$$[\eta] = \Phi\left[\frac{\langle r^2 \rangle_0}{M}\right]^{\frac{3}{2}} \qquad \underline{\qquad} (3.24)$$

where Φ is the hydrodynamic factor and M is the average molecular weight.

The Intrinsic Viscosity Measurement

The intrinsic viscosity, $[\eta]$, of dilute PPO solutions were measured using a Cannon Ubbelohde capillary viscometer No 150 as shown in Figure 3.3. The solvent used for the viscosity measurements was benzene. The solutions of the PPO were usually prepared directly by dissolving a known weight of PPO in 25-ml benzene. Concentrations were expressed in g/dl of solution. Viscosity of the benzene solvent and PPO solutions were measured at 20, 25, 30, 40 and 50 °C to find the intrinsic viscosity $[\eta]$.

Figure 3.2 A Cannon Ubbelohde capillary viscometer No 150.

3.2.6 Nuclear Magnetic Resonance (NMR)

A. One-Dimensional NMR Spectroscopy (1D-NMR)

A one-dimensional mode of NMR gives spectra having just one frequency axis, the second axis being used to display the signal intensities. The nuclides of mainly interest are proton (^{1}H) and carbon-13 (^{13}C), as their resonances are the most important ones for determining the structures of organic molecules. In general, there is a weakness for the conventional 1D-NMR

techniques to distinguish the types of carbon (CH, CH_2 and CH_3). One of the most important techniques used to develop the pulse sequence of 1D-NMR in order to identify the types of carbon is DEPT.

Distortionless Enhancement by Polarization Transfer (DEPT)

The DEPT method is performed to determine the number of hydrogen attached to a given carbon atom. The pulse sequence is that carbon atoms with one, two, and three attached hydrogens exhibit different phases as they are recorded. DEPT-45 provides the information for methine (-CH-), methylene (-CH_2-), and methyl (-CH_3-) groups and DEP-90 give information of methine group. DEPT-135 distinguish carbon signals by giving positive carbon signals of methine and methyl groups and negative carbon signals of methylene carbon. The pulses of carbon 90-degree and proton 180-degree are applied simultaneously. The coupling between protons and carbons take place and the carbon chemical shift is refocused by 180 degree pules. Therefore, the acquisition is delayed by ½ J. The DEPT sequence transfers the larger proton magnetization to carbon and thereby enhances the signal. The pulse sequence of DEPT is displayed in Figure 3.3.
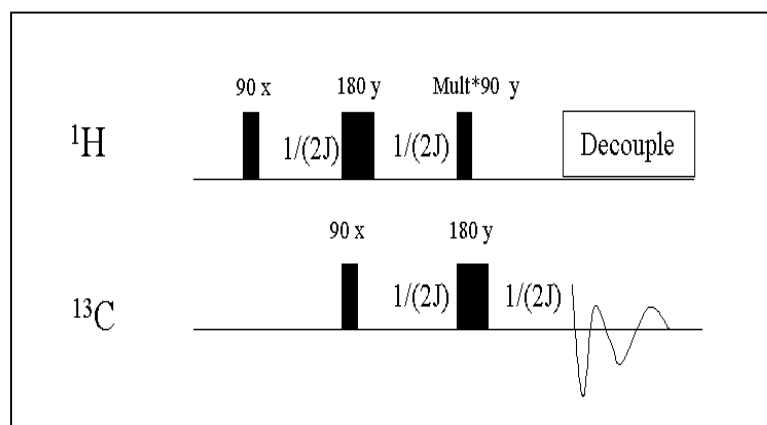
Figure 3.3 The pulse sequence for DEPT.

B. Two-Dimensional NMR Spectroscopy (2D-NMR)

For polymer molecules, 1D-NMR techniques are insufficient since there are many overlapped peaks occurring in the spectra. Then, 2D-NMR techniques are prominent for determining of the structure. In 2D-NMR, there are two coordinate axes. The data are plotted as a grid; one axis represents one chemical shift range, the second axis represents the second chemical shift range, and the third dimension constitutes the magnitude of the observed signal. The result is a form of contour plot where contour lines correspond to signal intensity. Of many types of 2D-NMR experiments, two techniques find the most frequent application. One of them is COSY and the other is HETCOR.

H-H Correlated-2D-NMR spectra (H-H COSY)

^{1}H-^{1}H COSY (COrrelated SpectroscopY) is useful for determining which signals arise from neighboring protons, especially when the multiplets overlap or there is extensive second order coupling. In the COSY experiment, the chemical shift range of the proton spectrum is plotted on both axes. In order to identify which protons couple to each other, the coupling interaction is allowed to take place during t_1. During the same period, the individual nuclear magnetization vectors is spread as a result of spin-coupling interactions. These interactions modify signal that is observed during t_2. The interaction of spin in a COSY experiment is too complexes to be described completely in a simple manner. The pulse sequence of COSY also contains only two pulses as shown in Figure 3.4
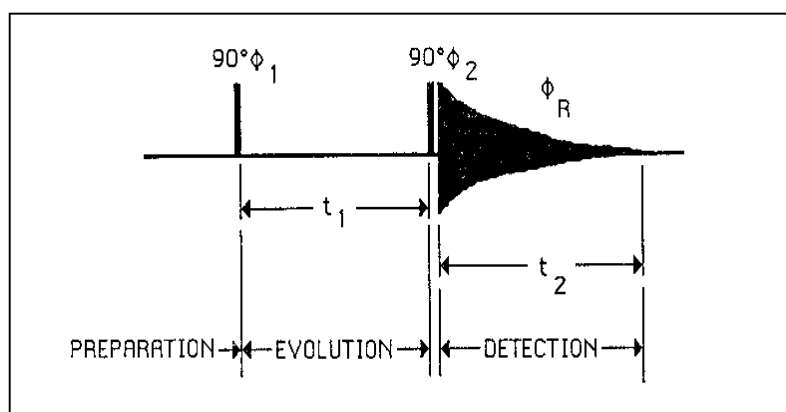
Figure 3.4 The pulse sequence for COSY.

^{1}H-^{13}C Correlated-2D-NMR spectra (HETCOR)

The HETCOR (Heteronuclear Chemical Shift Correlation) experiment is similar to the COSY experiment with the exception that it concerns two different nuclei (correlation between carbons and attached proton). The simplest pulse sequence that can be proposed for such 2D involves simply two 90-degree pulses, the last one being applied simultaneously to both nuclei. The first pulse excites proton nuclei whose chemical shift is detected during the evolution period t_1. The proton signal of interest is coupled not only to other protons but also to the heteronuclei (and therefore decoupled with a large coupling constant). The last proton pulse transfers proton magnetization to the carbon-nuclei whose intensity will be modulated by the proton chemical shift. The simplest sequence for HETCOR is displayed in Figure 3.5.
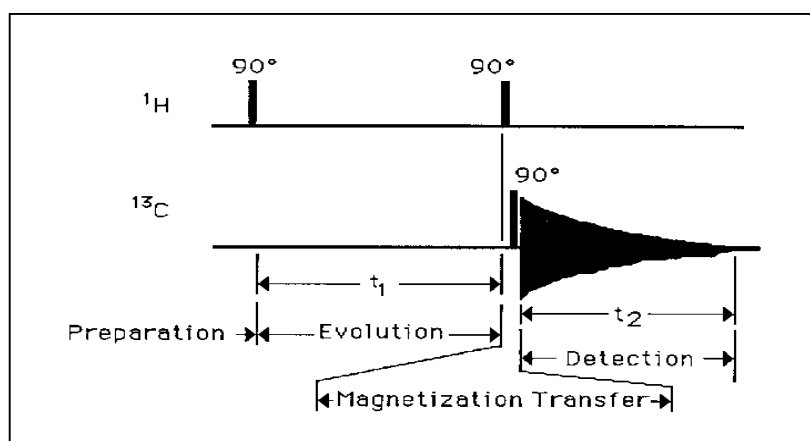
Figure 3.5 The pulse sequence for HETCOR.

NMR Experiments

In this work, the conformational statistics of PPO chain were identified on 300 MHz Unity Inova NMR spectrometer as shown Figure 3.6. C_6D_6 solvent was used in all measurements. The sample concentration was 5% by wt of PPO. 1D-NMR experiments are ^{1}H, ^{13}C and DEPT-45 was performed to characterize carbon signals such as methine (-CH-), methylene (-CH$_2$-) and methyl (-CH$_3$-) in the polymer structure. To assign all carbon peaks in PPO, 2D-NMR techniques

Heteronuclear Chemical Shift Correlation (HETCOR) will be used. HETCOR experiment provides a relationship between ^{1}H-NMR and ^{13}C-NMR spectra.

Figure 3.6 300 MHz Unity Inova NMR spectrometer.

3.3 Solid Polymer Electrolyte Film Characterization

3.3.1 Preparation of the PEO/PPO/salt Film

PEO (MW 4×10^6) and PPO (MW4000) were used as received while $LiCF_3SO_3$ and KSCN salts were dried at 100 °C in the oven for 24 h. A solution of the desired volume of PEO, PPO and salt dissolved in a sufficient amount of methanol was stirred overnight at room temperature. A set up of tools was shown in Figure 3.7a. The concentration of salt in polymer-salt complexes was expressed in term of molar ratios of the ether oxygen in the polymer to metal cation of salt (O:M). After continuous stirring, the solution was allowed to stand at room temperature for 24 h to facilitate degasing. These solutions were cast on the aluminum plate (see Figure 3.7b). Solvent was removed slowly in vacuum oven at 50 °C for 24 hour. The final films were stored in a dessicator before testing.

<center>(a)   (b)</center>

Figure 3.7 Preparation of SPEs films (a) sets up of tool for dissolve sample and (b) aluminum plate for cost sample.

The O:M ratios were followed by the following equation

$$w = w_{salt}/w_{polymer} = (M:O) \times \left(MW_{salt}/MW_{peroxygen}\right) \qquad \underline{\quad\quad}(3.25)$$

when $$MW_{peroxygen} = MW_{polymer}/(n+1)$$

The amount of PPO was expressed as a weight percent (wt %) of the PEO present, were followed by

$$y\% = [Wt(PPO)/Wt(PEO)]\,100 \qquad \underline{\quad\quad}(3.26)$$

Two main sets of solid polymer electrolytes were made as shown in Table 3.1. They are:

1. Various O:M ratio of PEO-salt with constant weight percent of PPO to studied effect of salt concentration

2. Various weight percent of PPO with constant O: M ratio of PEO-salt to studied effect of adding plasticizer.

Table 3.1 Two main sets of solid polymer electrolytes.

Effect of salt concentration (O:M$^+$)	Effect of adding wt %PPO
3:1	0%, 20%, 40%, 60%, 80%, 100%
5:1	"
12:1	"
16:1	"
20:1	"
30:1	"
40:1	"
60:1	"

3.3.2 Fourier Transform Infrared Spectroscopy (FTIR) Studies

Infrared spectroscopy is an important technique in organic chemistry. It is an easy way to identify the presence of certain functional groups in a molecule. Also, one can use the unique collection of absorption bands to confirm the identity of a pure compound or to detect the presence of specific impurities.

The interactions between PEO‑salt and salt association were investigated by FTIR. The study was carried out with FT‑IR spectrometer Perkin‑Elmer model: spectrum GX as shown in Figure 3.8. Absorbance mode was in the range 4000-400 cm^{-1} and at a resolution of 2 cm^{-1}.

Figure 3.8 FTIR spectrometer Perkin-Elmer model: spectrum GX.

3.3.3 X-ray Diffraction (XRD) Studies

X-ray diffraction is an important instrumental technique to the materials scientist. With many materials, this technique provides a quick and easy way to figure out what is happening after they are synthesized or reacted. Of course this is limited to crystalline materials, but with exceptions of solids such as gels, glasses, and polymers above their glass transition temperature, some degree of order is demonstrated. This allows a determination of what it is that we are dealing with at an atomic level, it gives a chance to model intermediate phases, and design ways to make out come suit our needs.

The sources of the x-rays are from the excitation of a Cu target (other metals can be used but, this was used in all of these experiments so it will be focused on here) that causes the removal of an electron from the atomic core. Upon relaxation of the atom by dropping an electron from an outer shell into the core, there is the emission of a photon. For the success of this, the electron used to excite the copper target much contain a high amount of kinetic energy. When the copper target is used, the process occurring is the removal of an electron in the 1s shell which is replenished by an electron dropping from the 2p orbital. The x-ray produced by this is termed K_α emission. K_β emission is when the replenishing electrons are provided by the 3d orbital. This occurs, but it is not so favorable as the K_α, which is more intense. Therefor, the x-ray from the

target is filtered through nickel prior to hitting the sample to absorb the K_β. the nickel can dispose of this energy as non-radiative decay.

XRD Experiment

The XRD patterns were recorded on Bruker, model D5005 X-ray diffractometer with Ni-filtered Cu K_α radiation as shown in Figure 3.9. All the measurements were made at room temperature between 2θ values ranging from $10°$ to $60°$ in $0.02°$ -steps with 0.4 s per step.

Figure 3.9 Bruker, model D5005 X-ray diffractometer with Ni-filtered Cu K_α radiation.

3.3.4 Differential Scanning Calorimeter (DSC) Studies

Differential scanning calorimeter is a technique to study the thermal transition of material in which the differential in heat flow to a sample and reference is monitored against time or temperature. DSC determines the specific heat, heat of fusion, heat of reaction or heat of polymerization of materials and is accomplished by heating or cooling a sample and reference under such conditions that they are always maintained at the same temperature. The additional heat required by the sample to maintain them at the same temperature is a function of the observed chemical or physical change. Typical applications include determination of melting point temperature and the heat of melting; measurement of the glass transition temperature;

curing and crystallization studies; and identification of phase transformations. After the analysis is complete, an endotherm (corresponding to heat absorption) and an exotherm (corresponding to energy release) are generated.

DSC Experiment

The melting temperature, T_m and the percentage cryatallinity of PEO and SPEs films were investigated using a PerkinElmer PYRIS (Dimond) Differential Scanning Calorimeters (DSC) as shown in Figure 3.10. Indium sample was employed to calibrate the machine. The amount of sample used in the study was about 10 mg, loaded using aluminum pans, the range of testing temperature was from 25 °C to 200 °C with the heating ramp 10 °C/min under an inert gas atmosphere. T_m was estimated at the extrapolated onset of melting. The percentage of crystallinity (%X) was evaluated from the following equation.

$$\%X = \frac{\Delta H_f}{\Delta H_f^0} \times 100 \qquad\qquad \_\_\_\_(3.27)$$

ΔH_f is the heat of fusion of each sample and ΔH_f^0 is the heat of fusion of a perfectly crystalline of PEO is 188.1 Jg^{-1}.

Figure 3.10 PerkinElmer PYRIS (Dimond) Differential Scanning Calorimeters (DSC).

3.3.5 High Resistance Meter

The resistance of material specimen is determined from a measurement of current or of voltage drop under specified conditions by using the appropriate volume resistivity. The volume resistance multiplied by that ratio of the d.c. voltage applied to two electrodes to the current in the volume of the specimen between the electrodes. Volume resistance is usually expressed in ohm-cm (preferred) or in ohm-meter and is the reciprocal of the volume conductivity.

Conductivity Experiment

Conductivity measurements were made under ASTM D257 standard method using a Hewlett-Packard 4339B high resistance meter as shown in Figure 3.11. The samples were held between the electrodes using compression springs. A potential difference of 1 volt was applied to the sample. Electrification time as 60 second was used for measurement. The d.c. resistance was calculated from the formula, $R = V*t/I*A$ of which the unit is $\Omega.cm^{-1}$. Here, V was applied voltage (1 Volt), t was the thickness of sample (1 mm), I was the resulting current (0.5 mA) and A was the area of electrode (5.06 cm^2).

Figure 3.11 Hewlett-Packard 4339B high resistance meter.

CHAPTER IV

RESULTS AND DISCUSSION

4.1 Poly(propylene oxide) Characterization

4.1.1 Conformational Energy Calculations

The energy contour maps were obtained from the conformational energy calculation of a PPO chain. The PPO chain was broken down into sequences of four skeletal bonds and pairs of dihedral angles, denoted by ϕ_1 and ϕ_2. The three repeating fragments for the isotactic PPO (R) chain are defined as follows:

Fragment 1 Pair of O-C and C-C bonds
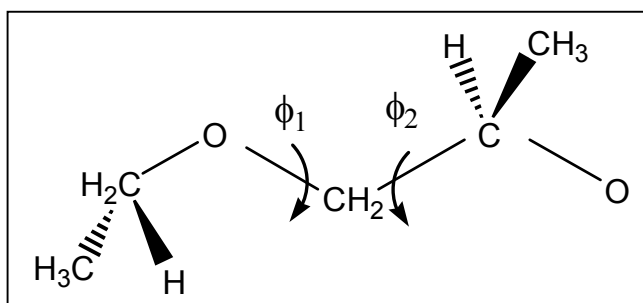
Fragment 2 Pair of C-C and C-O bonds
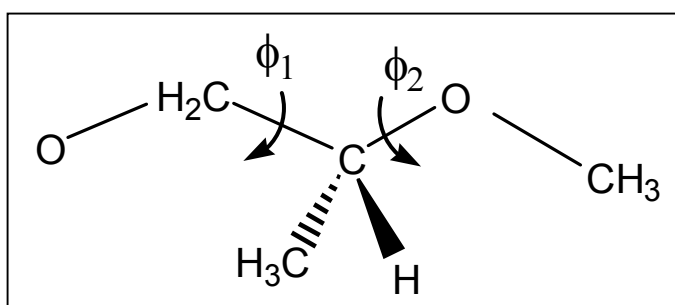
Fragment 3 Pair of C-O and O-C bonds
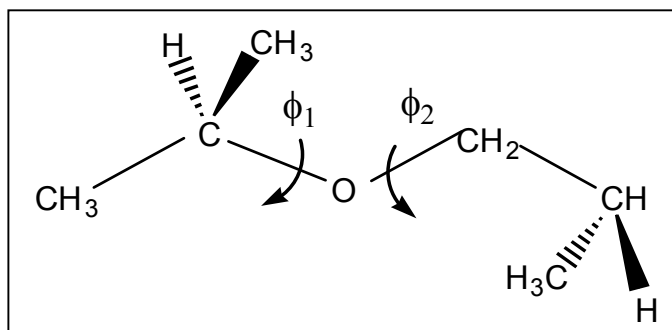
The *t*, g^+ and g^- bond conformations represented as Newman projections are shown in Figure 4.1. The g^+ conformer corresponds to a right-handed rotation relative to *trans (t)* conformer or a rotation which would increase the distance between the pairs of skeletal atoms, if the bond joining them is a right-hand screw, with the skeletal atoms threaded on it.
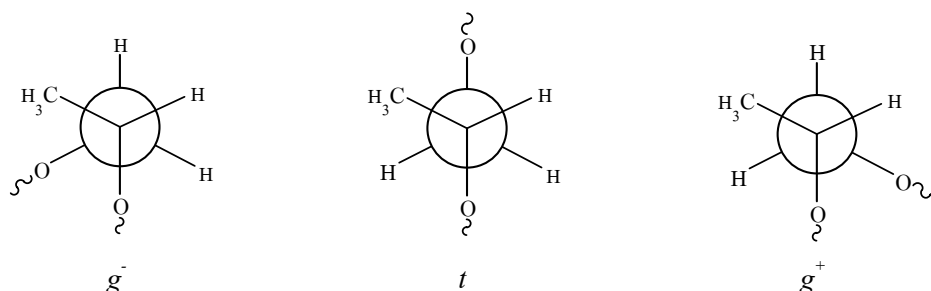
Figure 4.1 Newman projections of the *t*, g^+ and g^- conformations of the O-CH$_2$CH(CH$_3$)-O three-bond sequence.

The energy contour maps and the nine pair-wise dependent rotational isomeric states $(\alpha\beta = tt, tg^\pm, g^\pm t, g^\pm g^\pm, g^\pm g^\mp)$ for the three bonds of isotactic PPO are plotted in Figure 4.2-4.4. All figures were constructed using *trans* states (the ϕ_1 and ϕ_2 were set to 180°), where energies were in kcal mol^{-1}. The positions and magnitudes of the energy minima on the resulting energy-contour maps yield the values of the preferred rotational angles and their associated statistical-weights for each four-bond sequence. The conformational properties of the whole polymer chain can then be calculated from the properties of individual four-bond sequences using matrix-algebra techniques.

Contour map of rotational energy for O-C and C-C bond pair
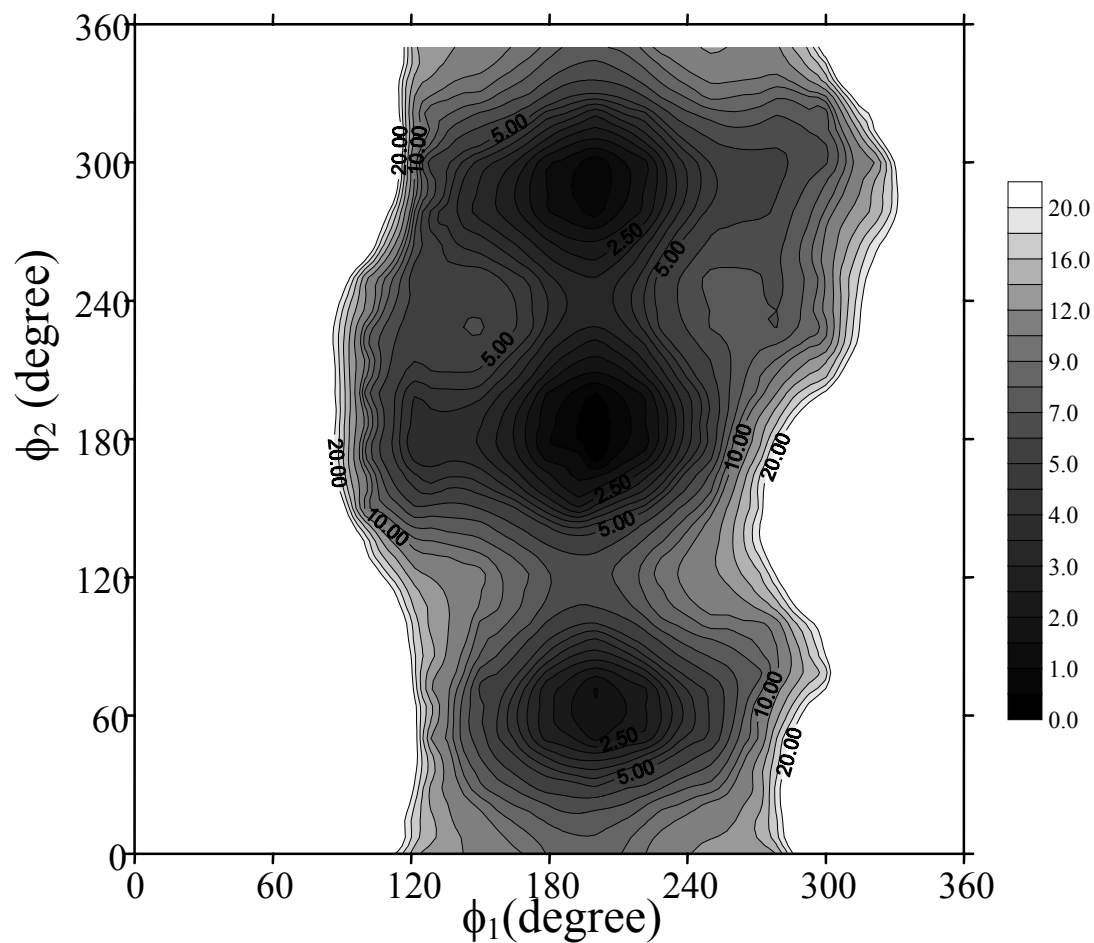
ϕ_1 ϕ_2	60°	180°	300°
300°	g^-g^+	tg^+	g^+g^+
180°	g^-t	tt	g^+t
60°	g^-g^-	tg^-	g^+g^-

Figure 4.2a Conformation energy map for the fragment 1 of the isotactic PPO (*R*). The location of minima was indicated by black color.
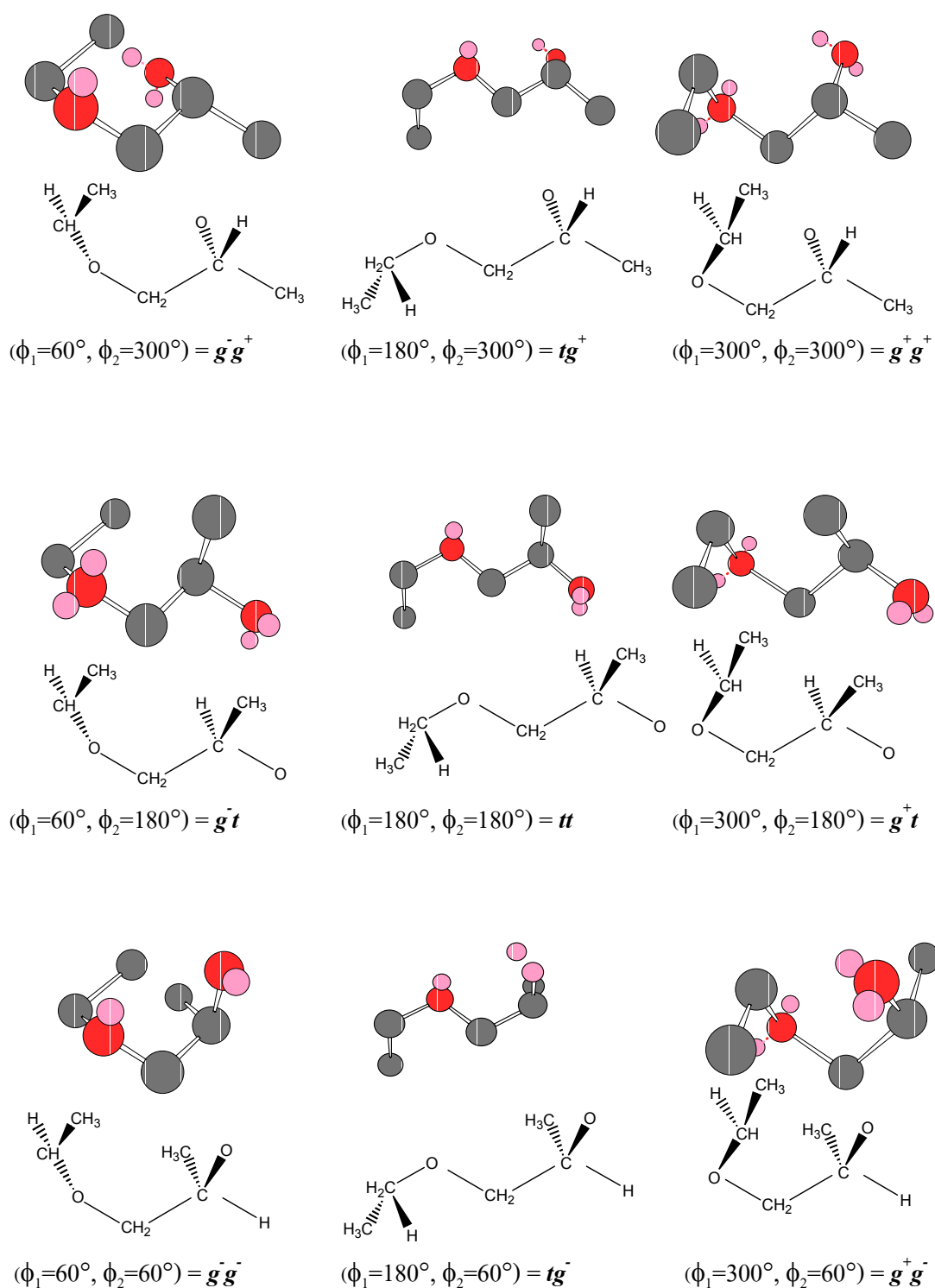
Figure 4.2b The nine pair-wise dependent rotational isomeric states for the fragment 1 of the isotactic PPO (*R*).

Contour map of rotational energy of C-C and C-O bond pair
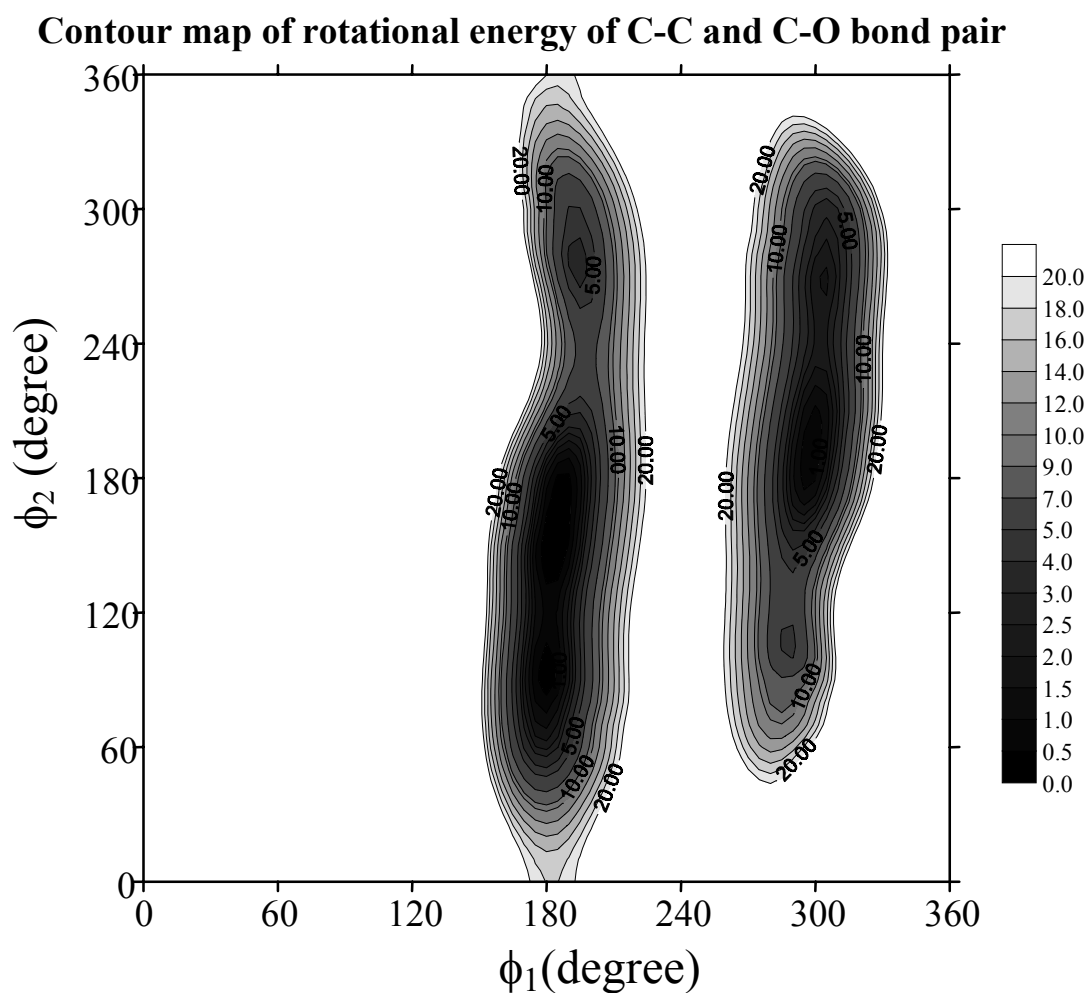
ϕ_2 \ ϕ_1	60°	180°	300°
300°	g^-g^+	tg^+	g^+g^+
180°	g^-t	tt	g^+t
60°	g^-g^-	tg^-	g^+g^-

Figure 4.3a Conformation energy map for the fragment 2 of the isotactic PPO (*R*). The location of minima was indicated by black color.

($\phi_1=60°$, $\phi_2=300°$) = g^-g^+

($\phi_1=180°$, $\phi_2=300°$) = tg^+

($\phi_1=300°$, $\phi_2=300°$) = g^+g^+

($\phi_1=60°$, $\phi_2=180°$) = g^-t

($\phi_1=180°$, $\phi_2=180°$) = tt

($\phi_1=300°$, $\phi_2=180°$) = g^+t

($\phi_1=60°$, $\phi_2=60°$) = g^-g^-

($\phi_1=180°$, $\phi_2=60°$) = tg^-

($\phi_1=300°$, $\phi_2=60°$) = g^+g^-
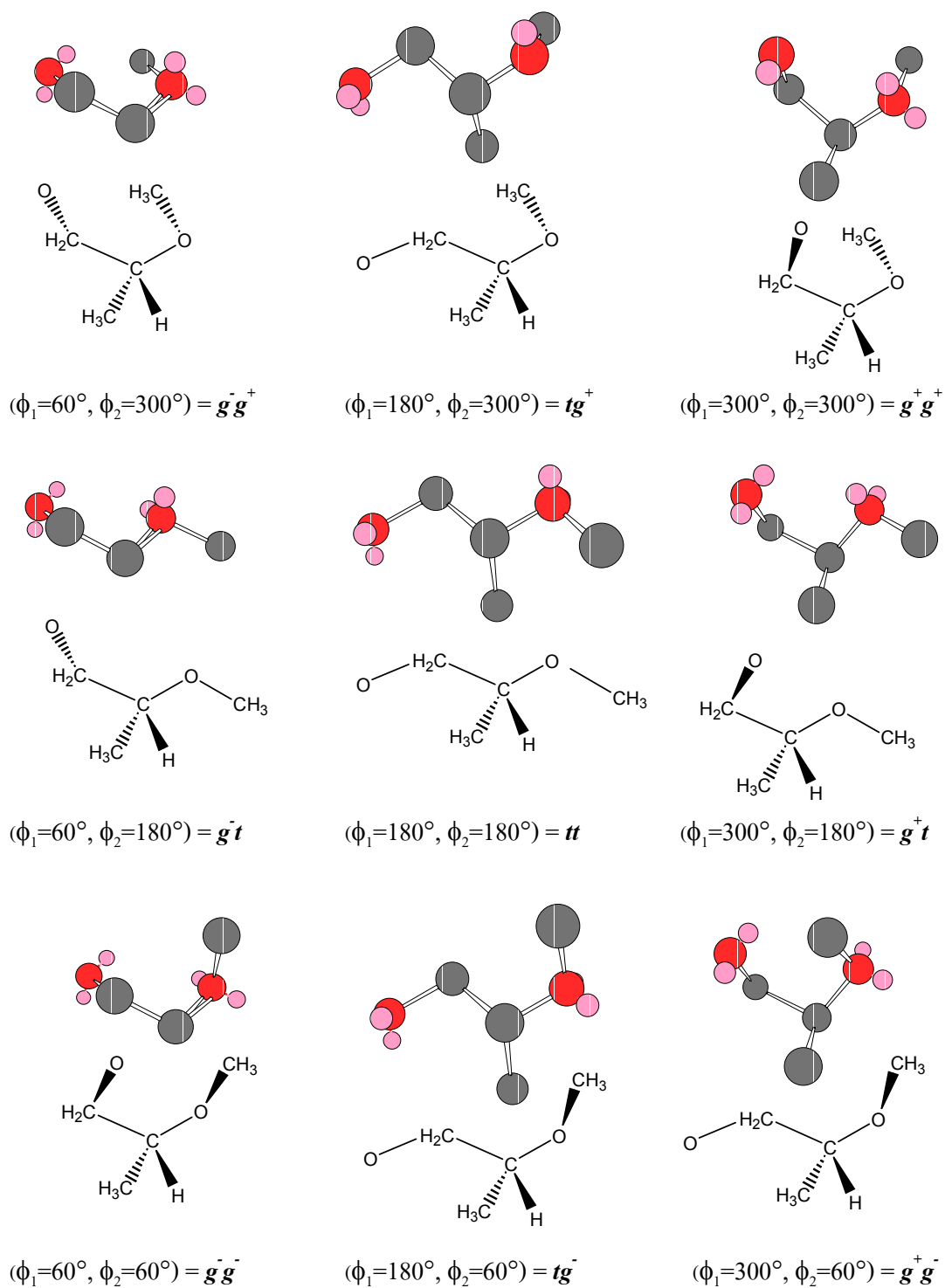
Figure 4.3b The nine pair-wise dependent rotational isomeric states for the fragment 2 of the isotactic PPO (*R*).

Contour map of the rotational energy of C-O and O-C bond pair
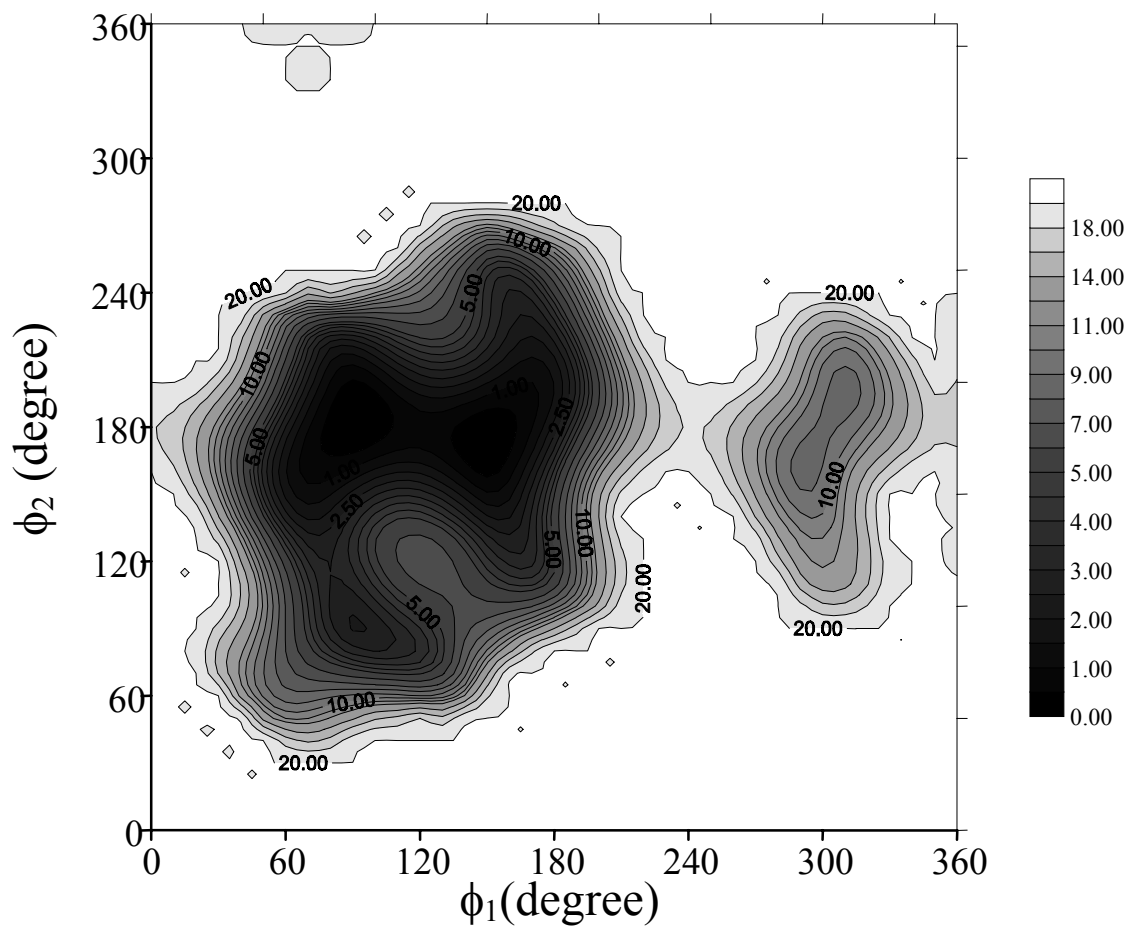
ϕ_1 / ϕ_2	60°	180°	300°
300°	g^-g^+	tg^+	g^+g^+
180°	g^-t	tt	g^+t
60°	g^-g^-	tg^-	g^+g^-

Figure 4.4a Conformation energy map for the fragment 3 of the isotactic PPO (*R*). The location of minima was indicated by black color.

$(\phi_1=60°, \phi_2=300°) = \boldsymbol{g^-g^+}$ $(\phi_1=180°, \phi_2=300°) = \boldsymbol{tg^+}$ $(\phi_1=300°, \phi_2=300°) = \boldsymbol{g^+g^+}$

$(\phi_1=60°, \phi_2=180°) = \boldsymbol{g^-t}$ $(\phi_1=180°, \phi_2=180°) = \boldsymbol{tt}$ $(\phi_1=300°, \phi_2=180°) = \boldsymbol{g^+t}$

$(\phi_1=60°, \phi_2=60°) = \boldsymbol{g^-g^-}$ $(\phi_1=180°, \phi_2=60°) = \boldsymbol{tg^-}$ $(\phi_1=300°, \phi_2=60°) = \boldsymbol{g^+g^-}$
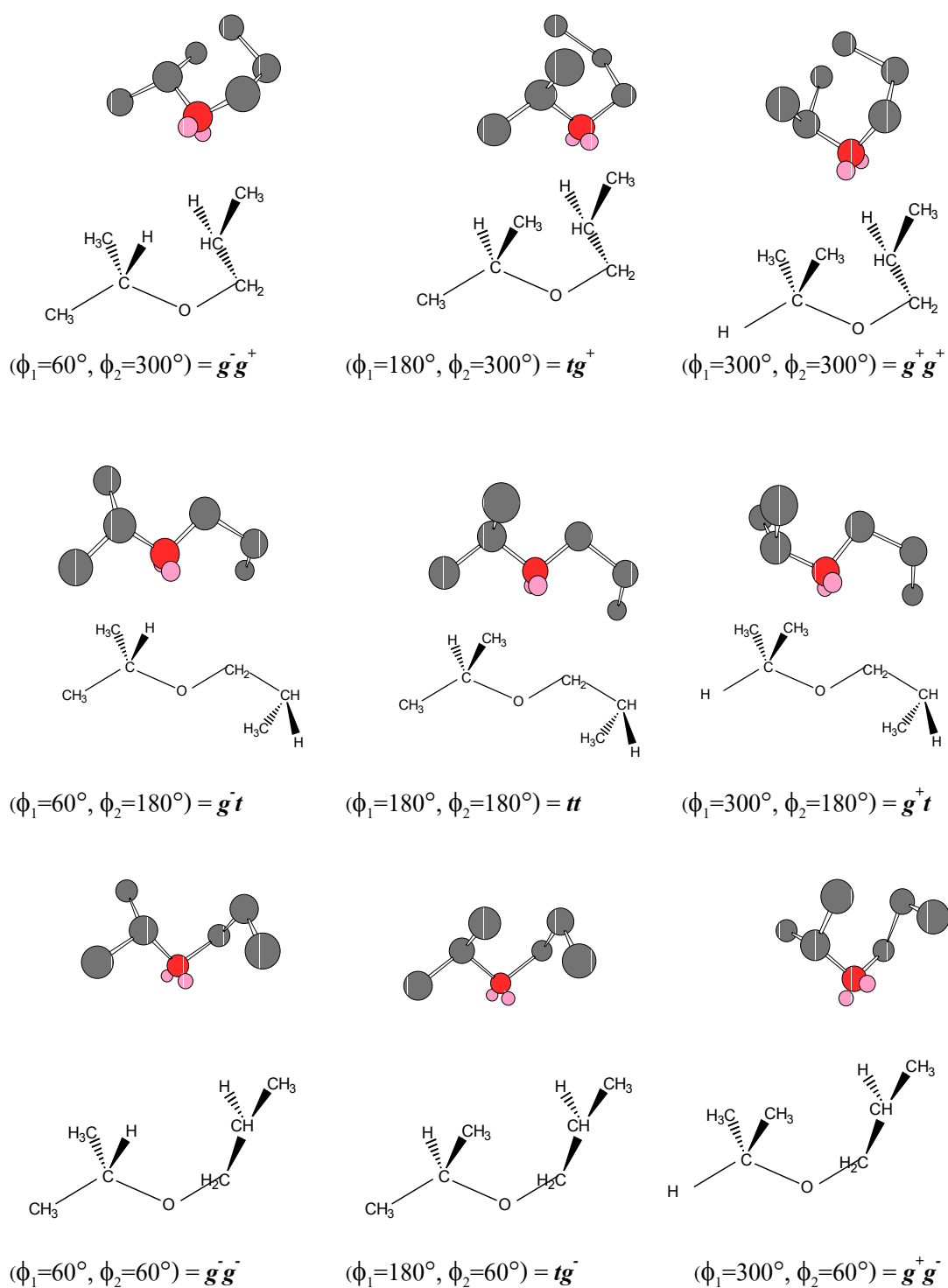
Figure 4.4b The nine pair-wise dependent rotational isomeric states for the fragment 3 of the isotactic PPO (*R*).

4.1.2 Statistical Weight Matrices of PPO

Statistical weight matrices were estimated from the energy contour map of representative small segments of a polymer chain using MM technique. These parameters were evaluated for each of the representative nine pair-wise dependent rotational isomeric states ($\alpha\beta = tt, tg^{\pm}, g^{\pm}t, g^{\pm}g^{\pm}, g^{\pm}g^{\mp}$) related to the conformational energies through the Boltzmann factor that calculated by Eq. (3.8). The bond lengths, bond angles, torsion angles and dipole moment vectors used in this calculation are listed in Table 4.1.

Table 4.1 Geometrical parameters used for PPO.

Bond length (Å)	μ (Debye)	Bond angle	Torsion angle		
O-C 1.402	O-C −1.7	∠COC 106.8°	180° (t)	320° (g^+)	40° (g^-)
C-O 1.402	C-O 1.7	∠CCO 107.4°	160° (t)	310° (g^+)	60° (g^-)
C-C 1.505	C-C 0.0	∠OCC 107.7°	180° (t)	290° (g^+)	60° (g^-)

The statistical weight matrices for each bond, $\mathbf{U_i}$, at temperature of 323 K, constructed for the set of R fragments, are written as follows:

$$U_{OC-CC} = \begin{pmatrix} SW_{tt} & SW_{tg^+} & SW_{tg^-} \\ SW_{g^+t} & SW_{g^+g^+} & SW_{g^+g^-} \\ SW_{g^-t} & SW_{g^-g^+} & SW_{g^-g^-} \end{pmatrix} \begin{pmatrix} 0.80 & 0.75 & 0.70 \\ 0.03 & 0.16 & 0.01 \\ 0.00 & 0.00 & 0.00 \end{pmatrix}$$

$$U_{CC-CO} = \begin{pmatrix} SW_{tt} & SW_{tg^+} & SW_{tg^-} \\ SW_{g^+t} & SW_{g^+g^+} & SW_{g^+g^-} \\ SW_{g^-t} & SW_{g^-g^+} & SW_{g^-g^-} \end{pmatrix} \begin{pmatrix} 0.13 & 0.06 & 0.19 \\ 0.11 & 0.06 & 0.01 \\ 0.00 & 0.00 & 0.00 \end{pmatrix}$$

$$U_{CO-OC} = \begin{pmatrix} SW_{tt} & SW_{tg^+} & SW_{tg^-} \\ SW_{g^+t} & SW_{g^+g^+} & SW_{g^+g^-} \\ SW_{g^-t} & SW_{g^-g^+} & SW_{g^-g^-} \end{pmatrix} \begin{pmatrix} 0.61 & 0.00 & 0.02 \\ 0.38 & 0.00 & 0.01 \\ 0.63 & 0.00 & 0.23 \end{pmatrix} \_\_ (4.1)$$

Matrix elements can be normalized to give maximum statistical weight of unity for the corresponding **tt** state. The matrices are arranged according to the following scheme:

$$
\begin{array}{ccccc}
 & & t & g & \overset{\phi_2}{} & g^- \\
 & t & & & & \\
\phi_1 & g^+ & & & & \\
 & g^- & & & &
\end{array}
$$

The statistical weight matrices for the S unit incorporated in a polymer chain may be easily derived from those of the R unit by a pre- and post multiplying an operator matrix Q. Thus in general,

$$
U_a^S = Q U_a^R Q
$$

where

$$
Q = \begin{bmatrix} 1 & 0 & 0 \\ 0 & 0 & 1 \\ 0 & 1 & 0 \end{bmatrix}
$$

Therefore, matrix Q performs an interchange of the second and third rows or columns. The matrices U_b^S and U_c^S can be derived in similarly way.

4.1.3 Conformational Dependent Properties of PPO

The RIS model with statistical weight matrices obtained in this work can be used to predict some conformational dependent properties, including the mean square unperturbed end-to-end distance, the mean-square unperturbed radius of gyration ratio and the mean-square unperturbed dipole moment, (expressed as $\langle r^2 \rangle_0 / nl^2$, $\langle S^2 \rangle_0 / nl^2$ and $\langle \mu^2 \rangle_0 / nm^2$, respectively, where n is the number of skeletal bonds, l^2 and m^2 are the average values of the square of their bond lengths and dipole moments). The radius of gyration is the mean distance of the atoms in the chain from the center of mass. If only backbone atoms are considered, the mean-squared radius of gyration is

$$s^2 = \frac{1}{(n+1)^2} \sum_{k=0}^{n-1} \sum_{j=k+1}^{n} r_{kj}^2 \qquad \underline{\qquad}(4.2)$$

These calculated properties depend largely on the statistical weight for all portions of the conformational energy map. Therefore, the validity of the theoretical study can be tested by the successful prediction of an experimentally measurement.

Values of $\langle r^2 \rangle_0 / nl^2$, $\langle S^2 \rangle_0 / nl^2$ and $\langle \mu^2 \rangle_0 / nm^2$, were computed for isotactic PPO chains using the RIS model with geometrical parameters listed in Table 4.1. The statistical weight matrices used in this calculation were from Eq (4.1). The results are summarized in Table 4.2.

Table 4.2 $\langle r^2 \rangle_0 / nl^2$, $\langle S^2 \rangle_0 / nl^2$ and $\langle \mu^2 \rangle_0 / nm^2$ for iso-PPO as estimated from the RIS model.

Properties	iso-PPO
$\langle r^2 \rangle_0 / nl^2$	8.20
$\langle S^2 \rangle_0 / nl^2$	12.30
$\langle \mu^2 \rangle_0 / nm^2$	0.36

Conformational dependent properties calculated from the RIS model give the values that are close to the experimental results. The characteristic ratio of 6.0 (i-C_8H_{18}) is observed at 50 $^\circ$C (Allen et al., 1967) and the dipole moment ratio of 0.47 (C_6H_{12}) is observed at 25 $^\circ$C (Hirano et al., 1979). These findings suggest that our simple RIS model derived from forcefield-based MM technique seems to be reasonable. Conformational dependent properties and the effect of stereochemical structure of syn-PPO are listed in Table 4.3.

Table 4.3 $\langle r^2 \rangle_0 / nl^2$, $\langle s^2 \rangle_0 / nl^2$ and $\langle \mu^2 \rangle_0 / nm^2$ for syn-PPO as estimated from the RIS model.

Properties	syn-PPO
$\langle r^2 \rangle_0 / nl^2$	6.04
$\langle s^2 \rangle_0 / nl^2$	9.06
$\langle \mu^2 \rangle_0 / nm^2$	0.46

The conformational dependent properties of syndiotactic PPO chains were calculated at 323 K. For comparison, experimental values from Allen *et al*. (1967) indicated that a decrease in isotacticity lead to a reduction in C_n from ~6.0 (isotactic) to ~4.5 (syndiotactic). Our result is about the same trend in that C_n value also decreases from ~8.20 (isotactic) to ~6.04 (syndiotactic). Unfortunately, there is no available experimental data for $\langle s^2 \rangle_0 / nl^2$ and $\langle \mu^2 \rangle_0 / nm^2$ reported so far, and that a comparison can not be made at the present.

Bond Conformation

In order to investigate the bond conformer, we calculated the proportions of *t*, *g^+* and *g^-* states about each of three types of skeletal bond. Experimentally, the bond conformer can be obtained from NMR vicinal coupling constant for a representative of short segment of polymer chain. In our work, we are interested in finding these quantities from *a priori* probabilities, p_t, p_{g^+} and p_{g^-}, using the statistical weight matrices U_{C-C}, U_{C-O} and U_{O-C}, for the *i*-th bond in PPO chain. The probability, for state η at bond *i*, denoted as $p_{\eta:i}$, is

$$p_{\eta:i} = Z^{-1}U_1 U_2 ....U_{i-1} U'_{\eta:i} U_{i+1} ....U_n \qquad \_\_\_\_ \ (4.3)$$

where Z is the conformational partition function, and $U'_{\eta:i}$ is obtained from U_i, by replacing all elements except those in column η by zeros. Thus, the priori probability $p_{\eta:i}$ is evaluated over all conformations with an η (*t*, g^+ *or* g^-) rotation about the *i*-th bond, and those values are the characteristics of that bond only. The bond conformations were computed for isotactic PPO chains by using RIS model, with geometrical parameters listed in Table 4.1, and with the set of statistical weight matrices from Eq. (4.1). The results are summarized in Table 4.4.

It should be noted that many researchers previously observed the gauche-oxygen effect in some polymers containing oxygen atoms in their backbone. This effect arises from the gauche conformation of fragment 2 (C-C and C-O) which shows lower energy than the corresponding trans conformation. So we expect to see this effect might presence in the case of PPO. Anyway, we found from our MM calculation that the trans conformation is more preferably than the

gauche conformation. The reason should be due to the difference between the force fields used in this work and those from earlier works. Even so, however, the bond conformation of bond 1 and bond 3 gives the same magnitude as NMR and theoretical works (Abe, 1979; Oguni, N., et al., 1973; Sasanuma, 1995; Stepto and Taylor, 1996)

Table 4.4 Bond conformations of isotactic PPO.

Source	Method	(O-C and C-C)			(C-C and C-O)			(C-O and O-C)		
		t	g^+	g^-	t	g^+	g^-	t	g^+	g^-
This study	RIS scheme	0.70	0.00	0.30	0.46	0.40	0.14	1.00	0.00	0.00
(Abe et al.,1979)	RIS scheme	0.57	0.00	0.43	0.35	0.45	0.20	0.93	0.04	0.03
(Oguni et al., 1973)	^{1}H-NMR (C_6H_6)		N/A		0.40	0.44	0.16		N/A	

Temperature Coefficients

As it is now well known, the temperature coefficient of a statistical property such as the unperturbed random-coil dimension $\langle r^2 \rangle_0$ assumes particular importance in the study of chain molecule. The coefficient was computed from the values of $d \ln \langle r^2 \rangle / dT$ and the result are used to interpret chain conformational energy. The data of the temperature-coefficient for PPO are shown in Table 4.5. Our finding seems to be reasonable as it is close to the reference value.

Table 4.5 Temperature coefficients $d \ln \langle r^2 \rangle / dT$, calculated for isotactic PPO.

Source	$d \ln \langle r^2 \rangle / dT$ (x 10^3, k^{-1})
This study	-1.49
(Abe *et al*. 1979)	-1.59

4.1.4 Intrinsic Viscosity Measurement

Using Huggins and Kraemer equations, the intrinsic viscosity of PPO MW molecular weight 4000 g/mole was measured at 20, 25, 30, 40, and 50°C in benzene. The intrinsic viscosities obtained by extrapolating the reduced viscosity to infinitely dilute concentration are shown in Table 4.6.

Table 4.6 Intrinsic viscosities for PPO MW 4000.

Temperature (°C)	$[\eta]\,(g/dl)$
20	0.0779
25	0.0447
30	0.0338
40	0.0083
50	0.0015

Then, molecular weights can be calculated by

$$[\eta] = KM^a \qquad \underline{\qquad} \ (4.4)$$

where K and a are known constants. For PPO solution in benzene at 20 °C, K and a are 11.1 x 10^3 ml/g and 0.79, respectively. M is a viscosity average molecular weight. We found that $[\eta]$ = 0.0779 g/dl and then M is equal to 4058 g/mole which is close to the actual value (ca. 4000 g/mole). From these results, we are confident on using these data to further calculate the size of PPO molecule.

From a well-known the intrinsic viscosity under the theta (θ) condition, ($[\eta]_\theta$) is related to $\langle r^2 \rangle_0$ that can be calculated from Eq (3.24).

From this relation, we can estimate $\langle r^2 \rangle_0$ and $\langle r^2 \rangle_0 / nl^2$ from the viscosity experiment equal to 3380 Å^2 and 7.94, respectively.

4.1.5 Nuclear Magnetic Resonance (NMR) Experiment

A. One-Dimensional NMR Spectroscopy (1D-NMR)

PPO (MW 4000) was first studied using 1D-NMR technique. The ^{1}H-NMR experiment is performed to give all protons signal. The ^{1}H-NMR spectrum of PPO, as shown in Figure 4.5, represents the peak position and integration numbers of CH_2, CH and CH_3 groups of PPO unit. However, ^{1}H-NMR technique has not been completely successful in establishing the microstructure presented in PPO. ^{13}C-NMR generally offers the potential for greater spectroscopic resolution than ^{1}H-NMR and is expected to be better suit for the analysis for PPO microstructure.
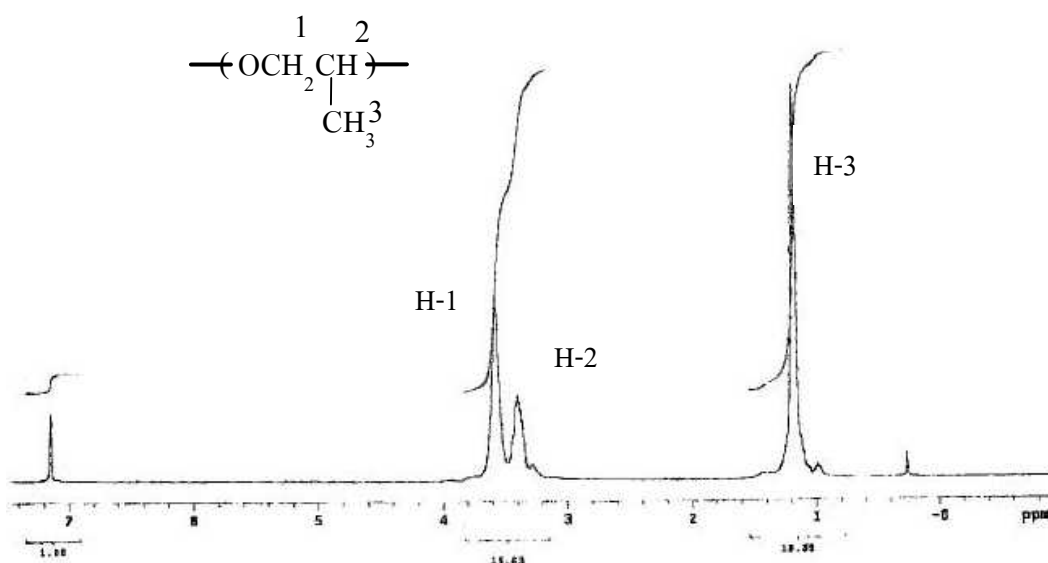
Figure 4.5 ^{1}H-NMR spectrum of PPO measured from 300 MHz of Unity Inova NMR spectrometer. ^{1}H-NMR ($C_6 D_6$) δ (ppm): 1.2 (s, 2H), 3.4 (s, 1H), 3.6(s, 3H), 7.05 (s, OH-terminal).

The ^{13}C-NMR spectrum, in Figure 4.6, gives all carbon signals in chemical structures (the ^{13}C-NMR spectrum in the region 80-20 ppm for the lower and in the region 76.0-73.1 and 18.0-17.0 ppm for the upper). The positions of chemical shift and carbon types of PPO are characterized in Table 4.7. Different carbon characteristics were distinguished by DEPT experiment. DEPT is performed to characterize carbon signals in the polymer structure. The DEPT-45 spectrum, shown in Figure 4.7, is conducted to provide information for methine carbon, CH, which represents for carbon peak at ~75 ppm, methylene carbon, CH_2, which represents for carbon peak at ~73 ppm and methyl carbon, CH_3, which represents for carbon peak at ~17 ppm.

Figure 4.6 ^{13}C-NMR spectrum of PPO measured from 300 MHz of Unity Inova NMR spectrometer. The chemical shift and carbon types of PPO are characterized in Table 4.7.

Figure 4.7 DEPT-45 spectrum of PPO measured from 300 MHz Unity Inova NMR spectrometer.

B. Two-Dimensional NMR Spectroscopy (2D-NMR)

To assign all carbon peaks in PPO, 2D-NMR technique, namely Heteronuclear Chemical Shift Correlation (HETCOR) was used. The HETCOR experiment provides a relationship between ^{1}H-NMR and ^{13}C-NMR spectra by elucidating the specific protons attached to each carbon atoms. ^{1}H-^{1}H COSY (COrrelated SpectroscopY) technique also leads to greater separation of the overlapping proton resonances. However, even the application of this spectroscopic technique, it has not been completely successful in establishing the microstructures presented in PPO. Therefore, COSY technique was not used in this research. Only the result for HETCOR experiment is presented here.

HETCOR Experiment

Figure 4.8 shows the HETCOR spectra of PPO. The ^{13}C-NMR spectrum is presented on the vertical axis and the ^{1}H-NMR spectrum is presented on the horizontal axis. The [1]H-^{13}C correlation is shown by a cross peak contour at the intersection of a horizontal line drawn from a ^{13}C peak and a vertical line drawn from a proton peak. The signals of carbons numbered 1 appearing at ~75 ppm is matched to proton signals #1 and #2 (methylene groups). The methin carbons at ~77 ppm, representing carbons #2 is paired with proton #2. At ~17 ppm carbons #3 is related to protons #3 (CH_3 groups)
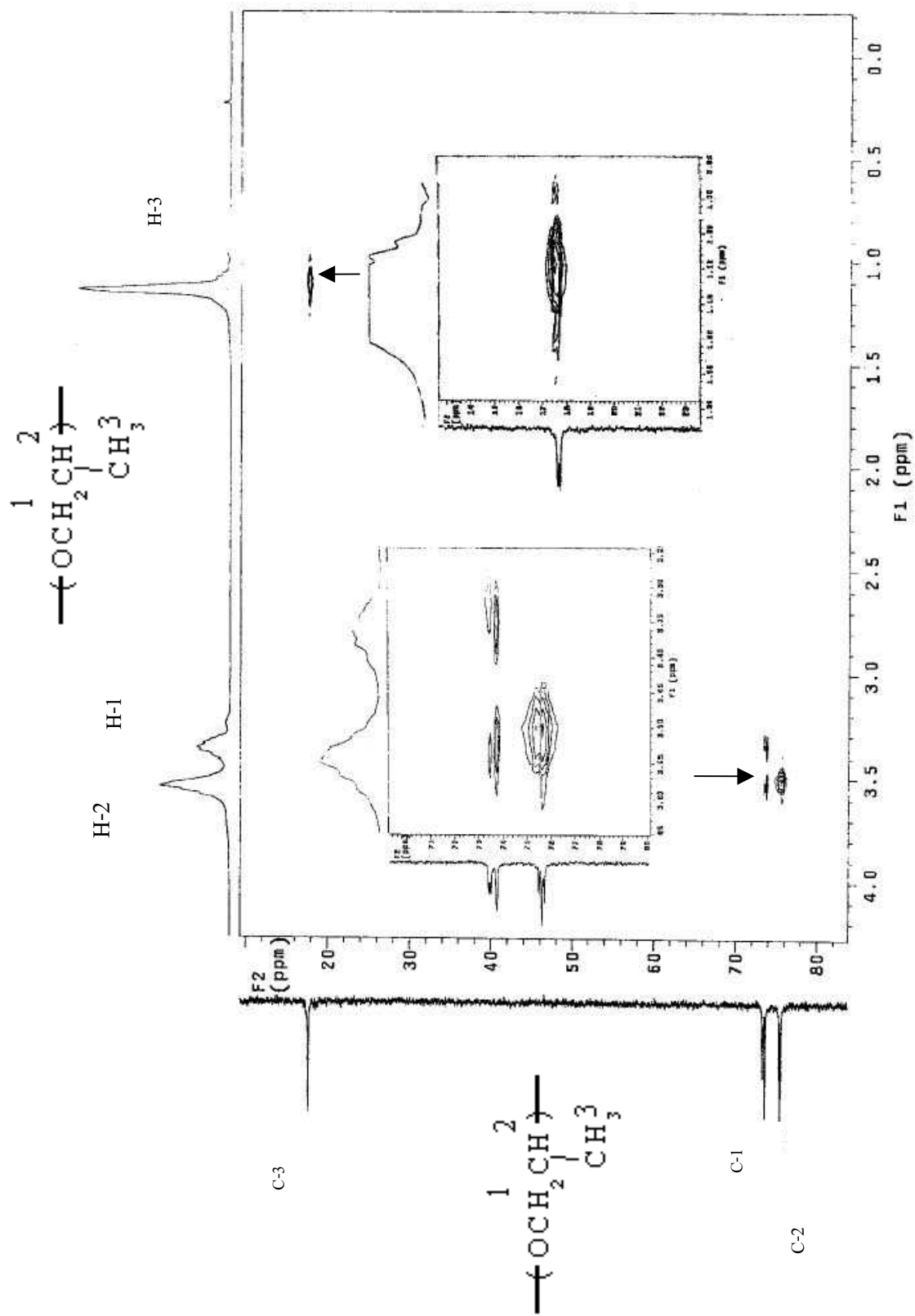
Figure 4.8 HETCOR relationship of PPO measured from 300 MHz Unity Inova NMR spectometer.

Our approach in analyzing the ^{13}C-NMR spectra of PPO was to define the type of carbon represented by each resonance, i.e. methine, methylene, or methyl as presented in Figure 4.9. Schilling *et al*. (1986) studied on the stereochemical arrangement for two types of PPO. They were atactic PPO (MW=4000) and isotactic PPO (MW=14500). Their ^{13}C-NMR spectra are shown in Figure 4.9.
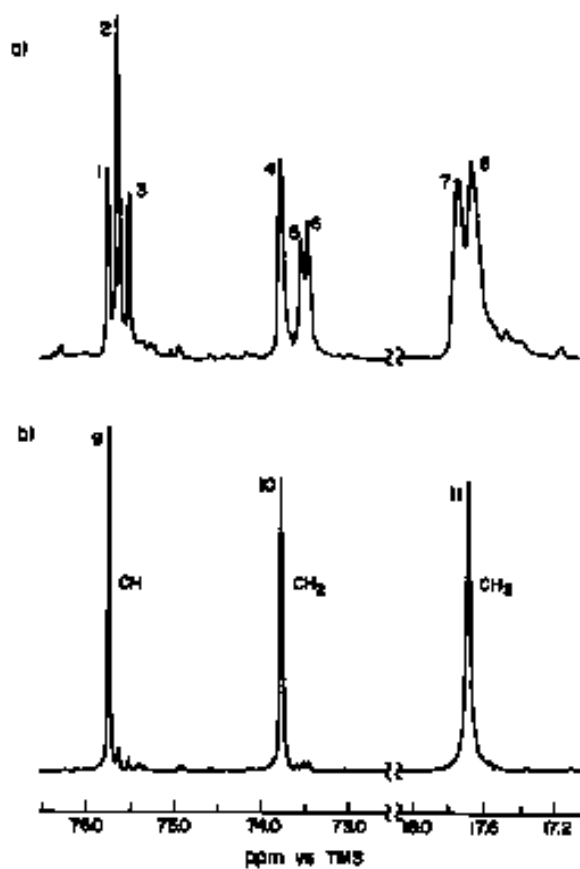
Figure 4.9 50.31 MHz ^{13}C-NMR spectra of (a) atactic PPO 4000, and (b) isotactic PPO, observed at 23 °C in C_6D_6 studied by Schilling *et al*. (1986).

Comparison of chemical shift to the stereochemistry and relaxation data of PPO between Schilling, *et al*. and this work for all three-carbon types are shown in Table 4.7. The ^{13}C-NMR spectrum from this work is similar to that of atactic PPO. In addition, the positions of the chemical shift of PPO are identical. However T_1 between this work and atactic PPO are different. This may be the temperature used in the work of Schilling, *et al*. which is less than our work. All above results of PPO derived from this study are very different from isotactic PPO spectra (as (b) in Figure 4.9). Therefore, we can conclude that the stereochemistry of PPO in this study is atactic arrangement.

Table 4.7 ^{13}C-NMR Chemical shifts and Relaxation data of PPO.

Resonance	Chem shift[a], ppm		T_1 , s		Peak	Carbon	Stereosequence
	This study[a]	Ref.[b]	This study[a]	Ref.[b]	height	type	
1	75.75	75.75	1.46	0.78	6.4	CH	mm
2	75.64	75.64	1.32	0.80	10.2	CH	mr + rm
3	75.50	75.50	1.54	0.81	5.3	CH	rr
4	73.77	73.78	0.85	0.51	7.8	CH_2	m
5	73.51	73.54	0.88	0.50	5.2	CH_2	r
6	73.44	73.47	0.95	0.50	5.2	CH_2	r
7	17.75	17.79	1.14	1.03	6.8	CH_3	rm, mr, rr
8	17.68	17.71	1.35	1.03	6.8	CH_3	mm, rm, mr, rr

[a] PPO (MW 4000) spectra were observed at 25 °C in C_6D_6.

[b] from Schilling *et al*. (1986) atactic PPO (MW 4000) were observed at 23 °C in C_6D_6.

4.2 Solid Polymer Electrolytes Films Characterization

    4.2.1 Effects of Salt Concentration

       The effects of salt concentration on structure and ionic conductivity of $(PEO)_n LiCF_3SO_3$ and $(PEO)_nKSCN$ systems were studied by using various analytical techniques such as XRD, DSC, FTIR and high resistance meter.

       4.2.1.1 Infrared Spectroscopy (IR)

       Ionic association and cation-polymer interaction are the main factors that play an important role in an ionic conduction. The factors are mutually dependent and it is essential to understand their significance in the polymer salt systems. Ionic association reflects the cation-anion interactions that vary from system to system. It is expected that ionic association is mediated through cation-polymer interactions. The different ionic species may range from "free" anion through ion pairs to ion aggregates or clusters. All these species have different mobilities, thereby significantly affecting the ionic conductivity. The addition of salt to polymers leads to a reduction in the segmental motion of the polymer owing to an increase in the cation-ether oxygen interactions. Therefore, changes in the conformation of polymer backbone are likely to occur [5]. Thus, it is also necessary to study the changes in polymer conformation in these complexes. In this part, the spectroscopic results of ionic association in $LiCF_3SO_3$ and KSCN complexes of PEO and the conformational changes in PEO complexes of $LiCF_3SO_3$ and KSCN as a function of salt concentration are presented.

       The frequencies and assignments of pure PEO and polymer-salt complexes $((PEO)_9LiCF_3SO_3$ and $(PEO)_nKSCN)$ are summarized in Table 4.8 (Dissanayake and Frech, 1995; Sekhon et al., 1995).

Table 4.8 Selected frequencies (wavenumber, cm^{-1}) and assignments of infrared active bands of PEO in the amorphous phase (A), the crystalline phase (X) and the polymer-salt complex ((PEO)$_9$ LiCF$_3$SO$_3$ and (PEO)$_n$KSCN).

PEO (A)	PEO (X)	(PEO)$_9$ LiCF$_3$SO$_3$	(PEO)KSCN	Peak assignment
			2090-2020	-SCN asym. stretching
		1367 (C)		
	1361	1361 (P)		$w_s(CH_2) + v(CC)$
1350				
		1353 (C)		
	1343	1343 (P)		$w_{as}(CH_2)$
		1340 (C)		
1325				
		1309 (C)		
		1298 (C)		$v_{as}(SO_3)$
1294				
		1288 (C)		$v_{as}(SO_3)$
	1280	1280 (P)		$t_{as}(CH_2) + t_s(CH_2)$
		1263 (C)		$v_{as}(SO_3)$
1250				
	1244	1244 (P)		$t_{as}(CH_2)$
	1236			$t_{as}(CH_2) - t_s(CH_2)$
		1233 (C)		$v_s(CF_3)$
		1179 (C)		
		1160 (C)		$v_{as}(CF_3)$
	1150	1150 (P)		$v(CC) - v_{as}(COC)$
	1144	1144 (C, P)		$v(CC) - v_{as}(COC)$
1142				

Table 4.8 *(continued).*

PEO (A)	PEO (X)	$(PEO)_9$ $LiCF_3SO_3$	(PEO)KSCN	Peak assignment
		1138 (C)		
	1113			v_s(COC) or v_{as}(COC)
1110	1111	1111		v_s(COC) or v_{as}(COC)
		1092 (C)		
		1082 (C)		
	1061	1061 (P)		v_{as}(COC) + r_s (CH$_2$)
		1045 (C)		v_s(SO$_3$)
1040				
993				
		969 (C)		
	963	964 (P)		r_{as} (CH$_2$)
		952 (C)		
948	949			r_s (CH$_2$) − v_{as}(COC)
		940 (C)		
	934			
		927 (C)		
		860 (C)		
856	857			
	844	844 (P)		r_{as} (CH$_2$)
		833 (C)		
	828	828 (P)		
		760 (C)		δ_s(CF$_3$)
			746	-SCN sym. stretching
			470	SCN bending

A. (PEO)$_n$LiCF$_3$SO$_3$ System

Ionic association as a function of salt concentration

Ionic association in (PEO)$_n$LiCF$_3$SO$_3$ system was studied as a function of ether oxygen to lithium ion molar ratio (O:Li) using infrared spectroscopy. The symmetric stretching (v_s(SO$_3$)) mode is sensitive to change in the ionic environment of the triflate anion and the solvent-cation interaction. The symmetric vibrations (δ_s(CF$_3$)) mode gives a better description of the ionic association as the band due to different triflate species are well-separated (Chintapalli, 1996). Figure 4.10 shows the spectra for the (PEO)$_n$LiCF$_3$SO$_3$ complexes as a function of O:Li ratio in the symmetric vibrations of δ_s(CF$_3$) spectra region. At dilute concentration (40:1 ratio), the peak appears at 757 cm^{-1}. There is a broad peak and it shifts to 760 cm^{-1} with increasing salt concentration. There is a sharp peak growing in the 5:1 and 3:1 complexes. The peaks at 757 and 760 cm^{-1} are attributed to ion-pair and (PEO)$_n$LiCF$_3$SO$_3$ compound, respectively. This is in consistent with an *ab initio* calculations and normal coordinate analysis (Huang et al., 1994). It can be seen that an increase in the salt concentration leads to ionic association.
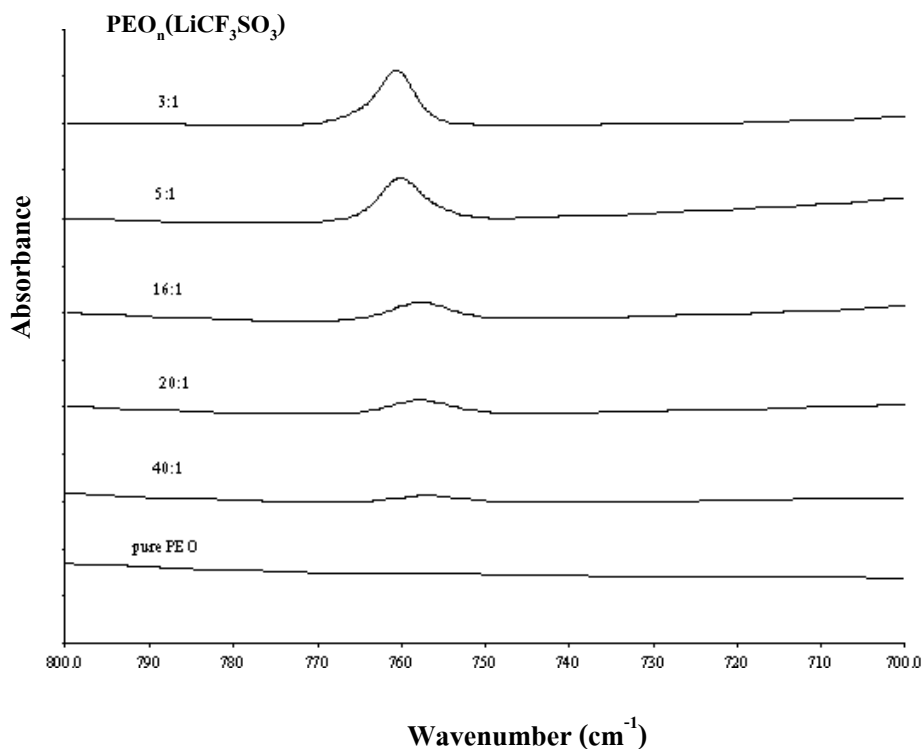
Figure 4.10 IR spectra of (PEO)$_n$LiCF$_3$SO$_3$ complexes in the 800-700 cm^{-1} spectra region.

PEO Conformation as a function of salt concentration

Figure 4.11 shows IR spectra for these complexes in the 1400-1300 cm^{-1} spectra region. The peaks at 1361 cm^{-1} and 1342 cm^{-1} are the CH$_2$ wagging modes characteristic of crystalline PEO. With an increase in salt concentration, a peak starts to appear at 1353 cm^{-1} in the 5:1 and 3:1 complexes. This peak is the characteristic of amorphous PEO. At 5:1 and 3:1 ratio, the intensity of peaks at 1361 cm^{-1} and 1342 cm^{-1} are decreased drastically. The peak due to the compound appears at 1367 cm^{-1} (Chintapalli, 1996). The compound peak increases in intensity in the 5:1 and 3:1 complexes.
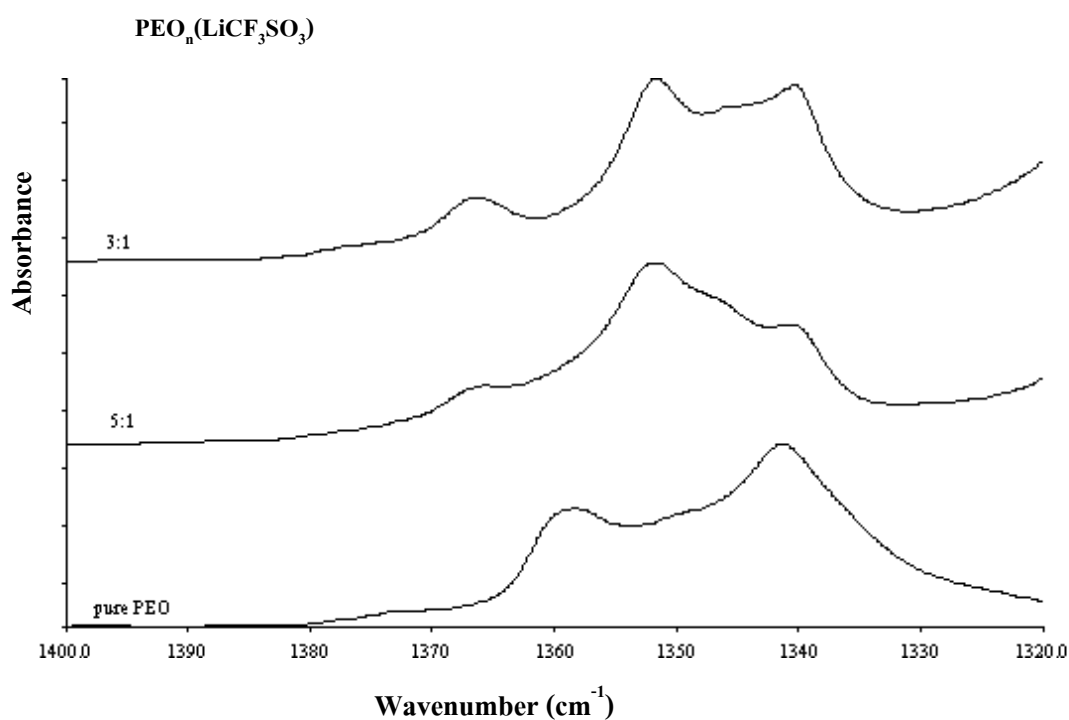
Figure 4.11 IR spectra of (PEO)$_n$ LiCF$_3$SO$_3$ complexes in the 1400-1320 cm^{-1} spectra region.

The spectra region of between 900-800 cm^{-1} (Figure 4.12) is the characteristics of C-O stretching and CH$_2$ rocking modes (Yoshihara et al., 1964). Pure PEO is also presented for comparison. The peak at 844 cm^{-1} is from CH$_2$ rocking mode coupled with a little C-O stretching modes. With an increase in salt concentration, new peaks at 860 and 834 cm^{-1} become visible at the salt concentration of 5:1ratio. These bands are ascribed to the complex. The peak at 860 cm^{-1} is the CH$_2$ rocking motion, which appears at the higher frequency due to the wrapping of the lithium ion by ether oxygens of PEO backbone. This assignment has been established based on *ab initio* calculations (Huang et al., 1994), again consistent with the crystal structure of (PEO)$_3$ LiCF$_3$SO$_3$ which belongs to the monoclinic space group P2$_1$/a(C$_{2h}^5$) and has a center of symmetry. A similar observation by Chintapalli for (PEO)$_n$ LiCF$_3$SO$_3$ system is that an increase in the salt concentration leads to the formation of (PEO)$_3$LiCF$_3$SO$_3$ at the expense of "free" ions and ion pairs.
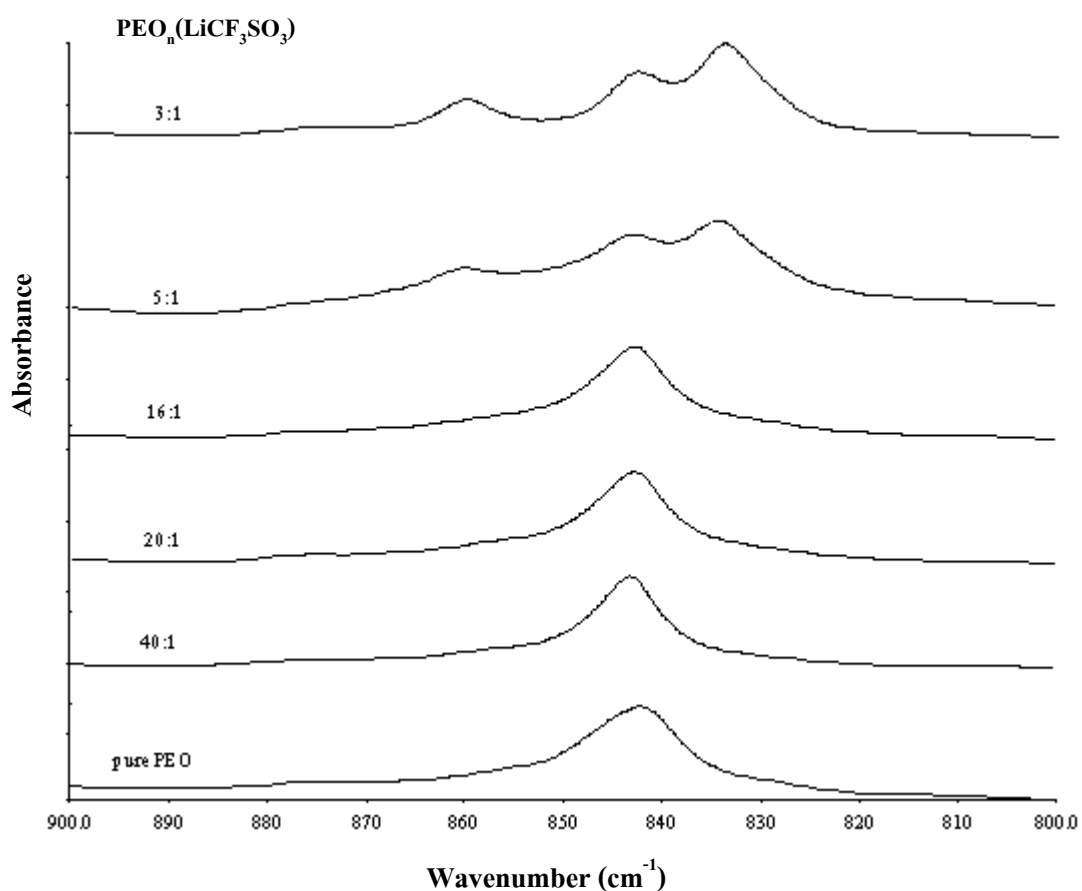
Figure 4.12 IR spectra of (PEO)$_n$ LiCF$_3$SO$_3$ complexes in the 900-800 cm^{-1} spectra region.

B. (PEO)$_n$KSCN System

Ionic association as a function of salt concentration

Ionic association in the (PEO)$_n$KSCN system was studied as a function of ether oxygen to potassium ion molar ratio (O:K$^+$) using FTIR spectroscopy. The frequencies and assignments of (PEO)$_n$KSCN system are summarized in Table 4.9. Figure 4.13 shows the spectra for the pure PEO and the (PEO)$_n$KSCN system as a function of O:K$^+$ ratio in the –SCN asymmetric stretching region (2600-1800 cm^{-1}). The peak at 2090-2020 cm^{-1} is due to –SCN asymmetric stretching. From Figure 4.13, the intensity of –SCN stretching peaks increases when salt concentration increases. This finding is similar to the characteristics of PEO$_n$(LiCF$_3$SO$_3$) system.
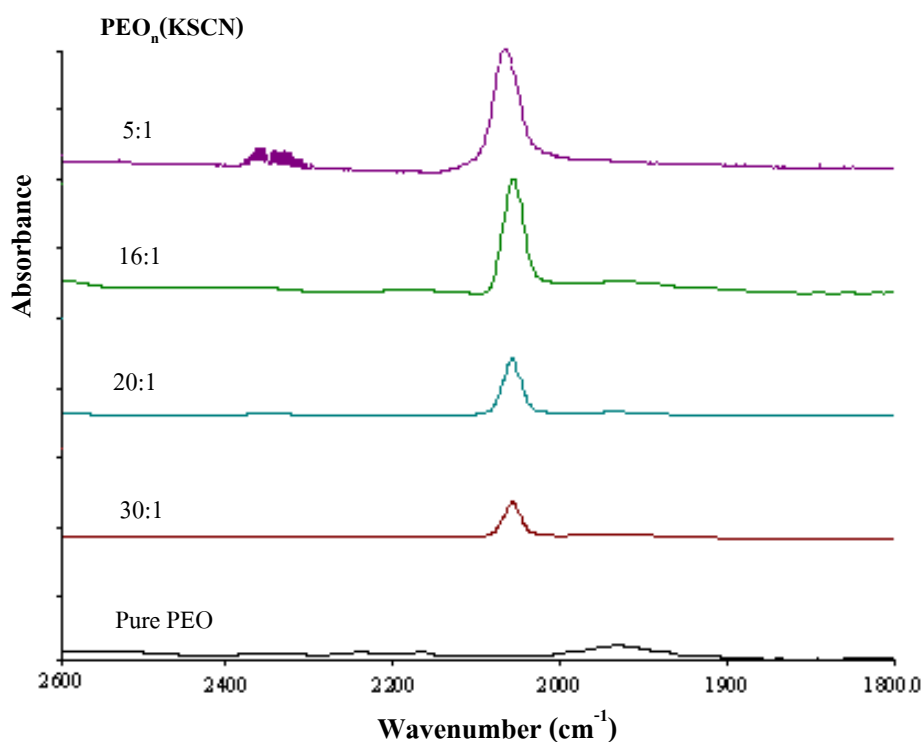
Figure 4.13 IR spectra of (PEO)$_n$KSCN complexes in the 2600-1800 cm^{-1} spectra region.

PEO conformation as a function of salt concentration

Figure 4.14 shows IR spectra of $(PEO)_nKSCN$ as a function of salt concentration in the region 1400-1260 cm^{-1}. The doublet peaks at 1343 and 1360 cm^{-1} are due to the CH_2 wagging of crystalline PEO. With increasing salt concentration, the peak at 1360 cm^{-1} in 16:1 and 5:1 complexes is replaced by a broad band at 1352 cm^{-1}. This peak is arisen from an amorphous PEO. Next, the intensity of the peak at 1278 cm^{-1} (CH_2 twisting of crystalline PEO) decreases with an increasing salt concentration. From these results, it suggests that the crystalline content of PEO complex decreases when the salt concentration increases.
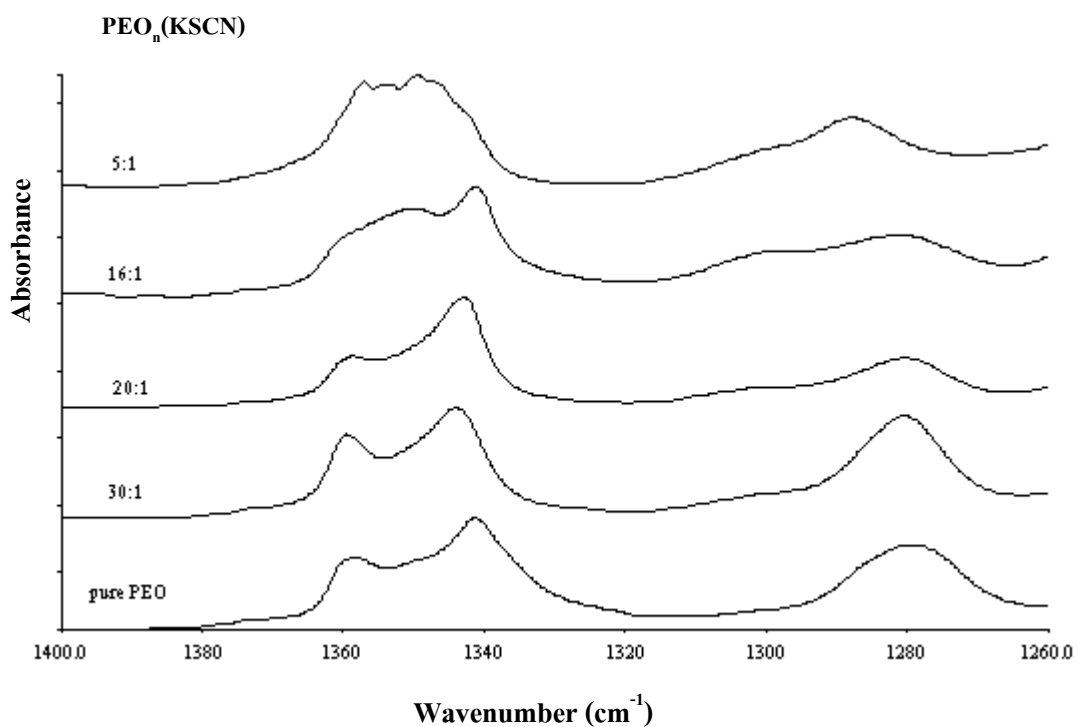
Figure 4.14 IR spectra of $(PEO)_nKSCN$ complexes in the 1400-1260 cm^{-1} spectra region.

Figure 4.15 shows IR spectra of (PEO)$_n$KSCN complexes in the region 900-800 cm^{-1}. This region is the characteristics of C-O stretching and CH$_2$ rocking modes. The peak at 844 cm^{-1} is CH$_2$ rocking coupled with C-O stretching vibrations of PEO molecules. This band is sensitive to the interaction of the cation with polymer backbone and hence is ideal for monitoring the changes in the conformation of PEO with the salt concentration. The band at 844 cm^{-1} begins to decrease in its intensity with increasing salt concentration and the peak at 834 cm^{-1} becomes visible at 16:1. This peak suggests a formation of the compound between polymer and salt.
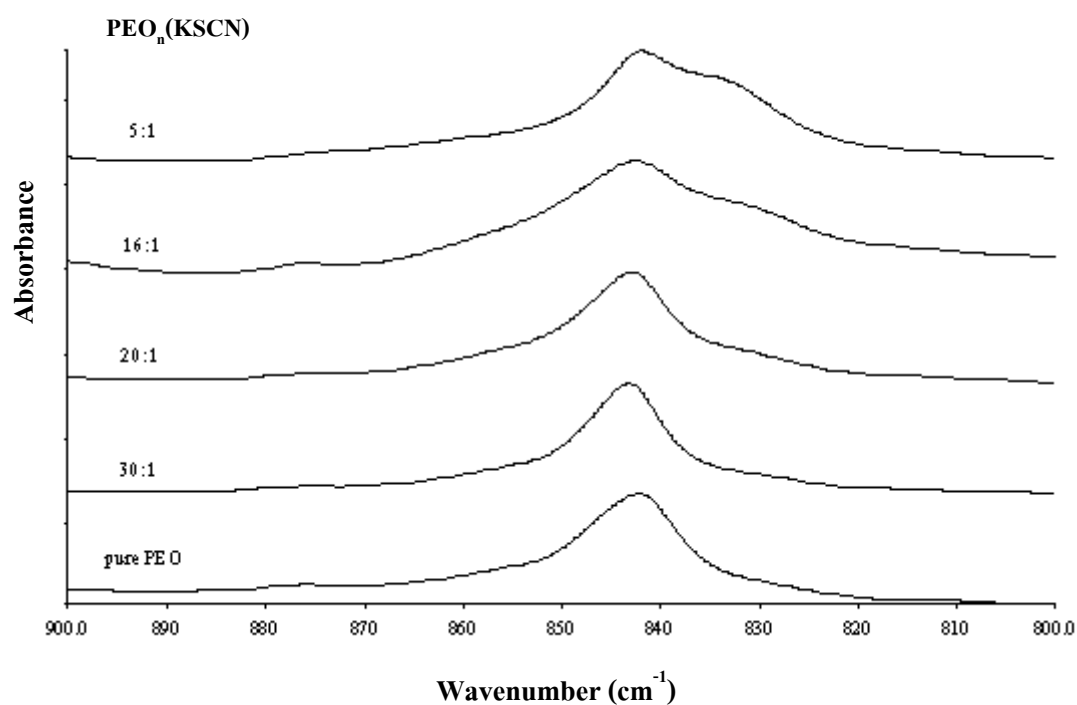
Figure 4.15 IR spectra of (PEO)$_n$KSCN complexes in the 900-800 cm^{-1} spectra region.

4.2.1.2 X-ray Diffraction (XRD)

For the purpose of an investigation on the changes in crystalline PEO matrices due to the incorporation of $LiCF_3SO_3$ or KSCN into the PEO, the XRD was performed to study on the crystalline PEO and its complex films. The results are described as followings.

The XRD patterns of pure PEO, pure $LiCF_3SO_3$ and pure KSCN for 2θ values between 5-40° are shown in Figure 4.16. The crystalline PEO reflection peaks at 15.3°, 19.3° and 23.3° are assigned to (110), (120) and (023) planes, respectively, as described by Bortel *et al.* (1979), Kitao *et al.* (1972) and Tandel *et al.* (1994). The XRD pattern in the $LiCF_3SO_3$ salt reflects many peaks, and it suggests that many crystalline phases exist. No peak in XRD pattern of pure KSCN is observed, suggesting that there is no crystalline salt phase. Figure 4.17 presents the XRD patterns of $(PEO)_n LiCF_3SO_3$ system as a function of salt concentration for 2θ values between 5-40°. The 40:1 and 16:1 complexes also give diffraction peaks at the same positions as PEO but the peak at 19.3° is narrower and more intense with an increase in salt concentration. Therefore, it suggests that the complexation occurs in the crystalline phase. The peak at 23.3° exhibits lower intensity at high salt concentration. It can be concluded that the crystalline phase in the film has the same structure as PEO, but at a lower percentage of the crystalline phase. The 3:1 complex shows absolutely different pattern from that of pure PEO. The peaks at 15.3°, 19.3° and 23.3° disappear, suggesting that there is no free crystalline PEO phase. Many new sharp peaks exist implying that (1) a new crystalline complex with well defined structure is presented (Preechatiwong et al., 1996; Rhodes et al., 2001; Zahurak et al., 1988) (2) the $LiCF_3SO_3$ salt does not totally dissociate in the polymer electrolytes, then some peaks of $LiCF_3SO_3$ salt can be observed in the pattern of polymer electrolytes. Combining our XRD and FTIR results, it can be said that PEO has limit solubility for $LiCF_3SO_3$ and salt will associate at high concentration.
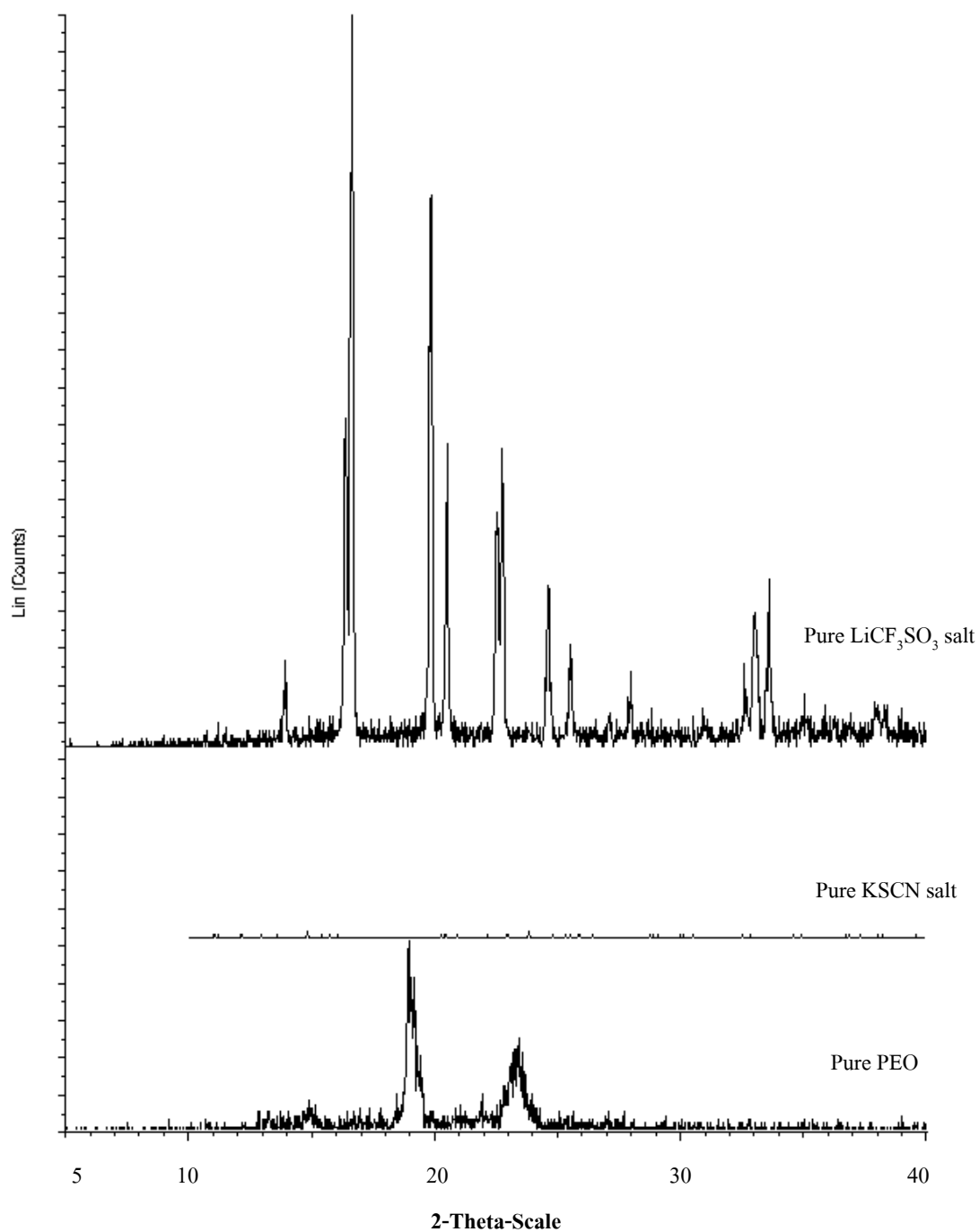
Figure 4.16 XRD pattern of pure LiCF₃SO₃ salt, pure KSCN salt and pure PEO.

(PEO)$_n$LiCF$_3$SO$_3$ System
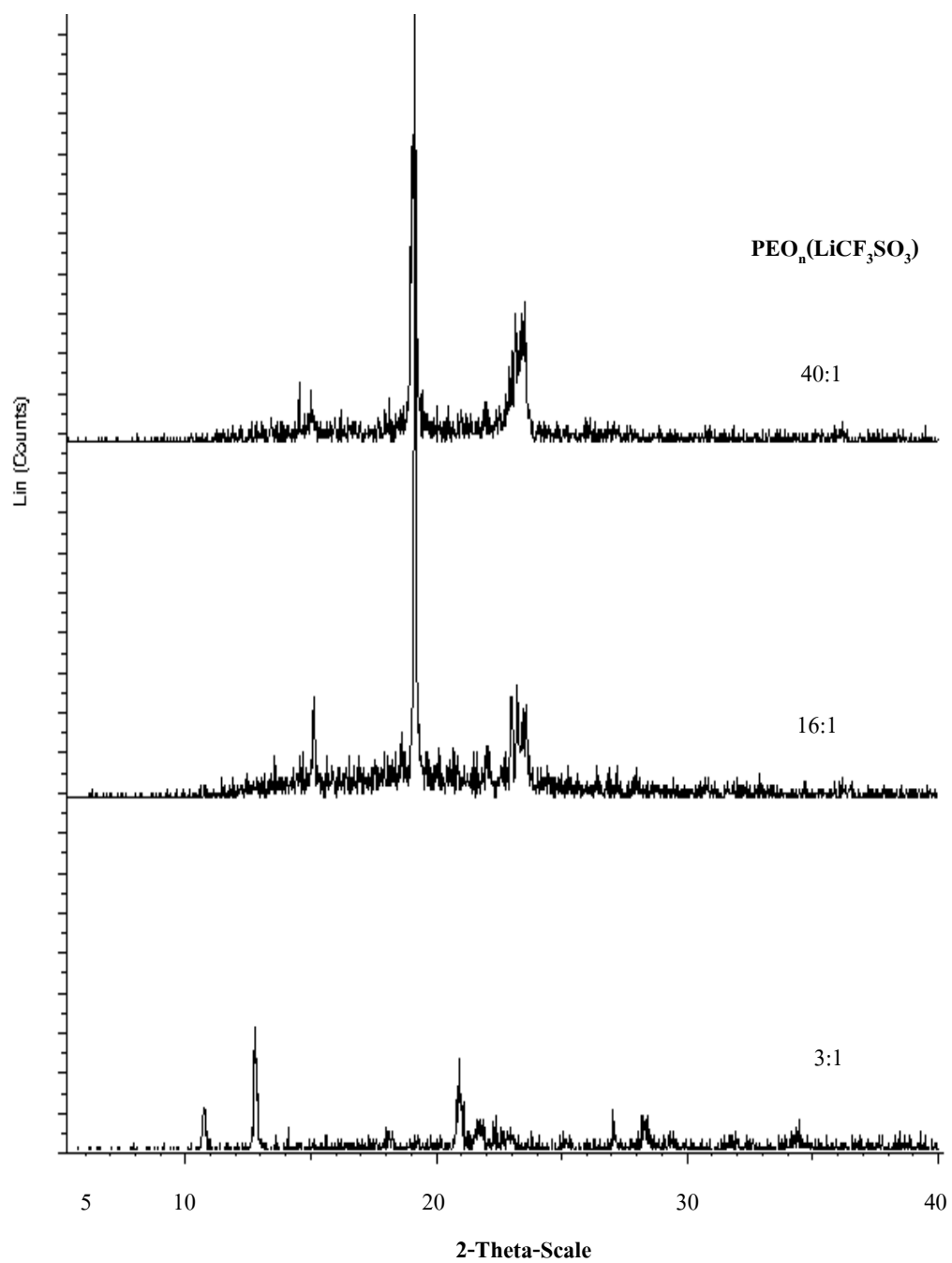
Figure 4.17 XRD pattern of (PEO)$_n$LiCF$_3$SO$_3$ electrolytes as a function of salt concentration.

Zahurak *et al*. (1988) studied XRD of the series of polymer salt concentration for PEO/LiBF$_4$ and PEO/LiCF$_3$SO$_3$, they found that both systems reflected a progressive change in the diffraction pattern with crystalline PEO peak losing intensity as more salt is added to the pure polymer. For both complexes, all traces of free crystalline PEO disappear at stoichiometry (PEO)$_{3.5}$ salt, indicating full complexation of the crystalline PEO.

Figure 4.18 shows the XRD patterns of (PEO)$_n$KSCN system as a function of salt concentration for 2θ values between 5-40°. The 40:1, 20:1 and 16:1 complexes also give peaks at the same positions (15.3°, 19.3° and 23.3°) as PEO but the peak at 19.3° is narrower and its intensity is higher for the 40:1 and 20:1 complex. However, the intensity of 19.3° peak for the 16:1 a complex is lower. It indicates that the content of crystalline PEO phase becomes smaller at this stoichiometry (Preechatiwong et al., 1996). The intensity of the peak at 23.3° is lower at high salt concentration. It can be suggested that the crystalline phase in the film has the same structure as PEO, but at a lower percentage. No peak occurs in the 5:1 complex, implying that the higher salt concentration at 5:1 has some undissolved KSCN (beyond solubility limit) which is also evidenced by an XRD pattern of pure KSCN. Again, with increasing the salt concentration, the percentage of the crystalline phase decreases. This trend is similar to that in the (PEO)$_n$LiCF$_3$SO$_3$ system.

(PEO)$_n$KSCN System
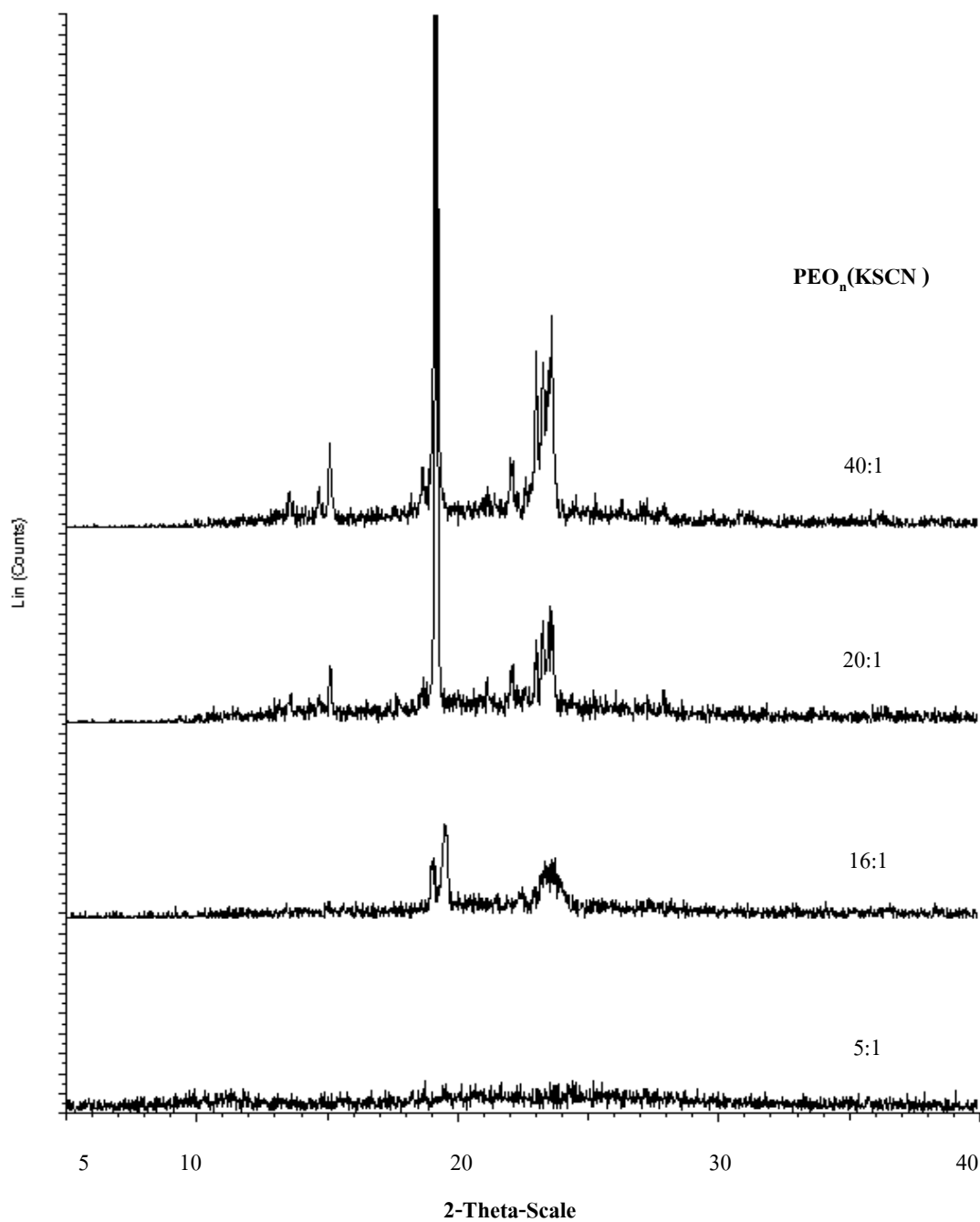
Figure 4.18 XRD pattern of (PEO)KSCN electrolytes as a function of salt concentration.

4.2.1.3 Differential Scanning Calorimeter (DSC)

Thermal characterization of the complexes is carried out by using differential scanning calorimeter (PYRIS Diamond DSC). The DSC experiment was performed to study the melting temperature (T_m), heat of fusion (ΔH) of PEO and its salt complex. It was expected that the changes in T_m and ΔH were from an incorporation of $LiCF_3SO_3$ and KSCN into the PEO, which gave rise to important changes in the PEO matrix. The DSC thermograms were recorded and the percentages of crystallinity (%X) were evaluated from Eq. (3.27).

The DSC thermograms of pure PEO and $(PEO)_nLiCF_3SO_3$ specimens at ratios of 3:1 and 16:1 complexes are presented in Figure 4.19. Both pure PEO and $(PEO)_{16}LiCF_3SO_3$ complex films clearly show the presence of an endotherm peak at 69 °C which is the melting temperature of a pure polymer phase. In addition, $(PEO)_{16}LiCF_3SO_3$ complex has a weak endotherm peak at 148 °C similar to the result observed by Rhodes *et al.* (2001). According to the phase diagram, it is the presences of very small amounts of the crystalline complex. For $(PEO)_3LiCF_3SO_3$ complex, the endotherm associated with pure PEO disappears, leaving a single melting endotherm of fully complex polymer/salt phase. This ratio exhibits a high melting point (Chintapalli, 1996; Rhodes et al., 2001; Zahuraket al., 1988) at 189.5 °C suggesting that salt does not only dissolves in PEO but also forms a new crystalline complex. For pure $LiCF_3SO_3$ salt, there is only a single melting temperature at 226.1 °C (Kim et al., 1998).

T_m and the percentage crystallinity of PEO-salt specimen are summarized in Table 4.9. ΔH and percentage crystallinity of $(PEO)_nLiCF_3SO_3$ are lower than that of pure PEO (see Figure 4.19 and Table 4.9). It is seen that percentage crystallinity decreases when the salt concentration increases. A similar dependence of percentage crystallinity on salt concentration is also observed from XRD results at high salt contents.

Table 4.9 Melting temperatures and percentage crystallinity of $(PEO)_nLiCF_3SO_3$ and PEO_nKSCN electrolytes.

Composition	Thermal behavior					
	T_{m1}	ΔH_1	(X_1)	T_{m2}	ΔH_2	(X_2)
	(°C)	(J g^{-1})	%	(°C)	(J g^{-1})	%
PEO	69.0	140.36	74.58			
PEO-LiCF$_3$SO$_3$ 16:1	69.0	73.14	38.88			
PEO-LiCF$_3$SO$_3$ 3:1				189.5	62.74	
^{c}LiCF$_3$SO$_3$	226.1					
PEO-KSCN 16:1	60.2	40.04	21.28			
PEO-KSCN 5:1			-*			
KSCN	179.7					

^{c} from Kim et al., 1998

* no peak

Next, DSC thermograms of the $(PEO)_nKSCN$ 16:1 and 5:1 samples were compared to thermogram of pure PEO as displayed in Figure 4.20. The ratio of 16:1 clearly exhibits the presence of an endotherm peak at 60.2 °C corresponding to the melting of crystalline PEO. The melting endotherm at lower temperature of $(PEO)_nKSCN$ film can possibly be explained by small crystalline sizes at this ratio (Robitaille et al., 1987). The trend for heat of fusion and percentage crystallinity is similar to that of LiCF$_3$SO$_3$ salt, in which the crystalline content decreases as the salt concentration increases (Preechatiwong, 1996; Robitaille, 1987). The percentage crystallinity of $(PEO)_nKSCN$ system is much lower than that of $(PEO)_nLiCF_3SO_3$ system. The endotherm of ratio 5:1 complex associated with pure PEO disappears and no peak is observed at this ratio. Therefore, it suggests that there is no free crystalline PEO to form complexes with KSCN (beyond the solubility limit). This result is also evidenced by XRD pattern shown earlier in Figure 4.18.
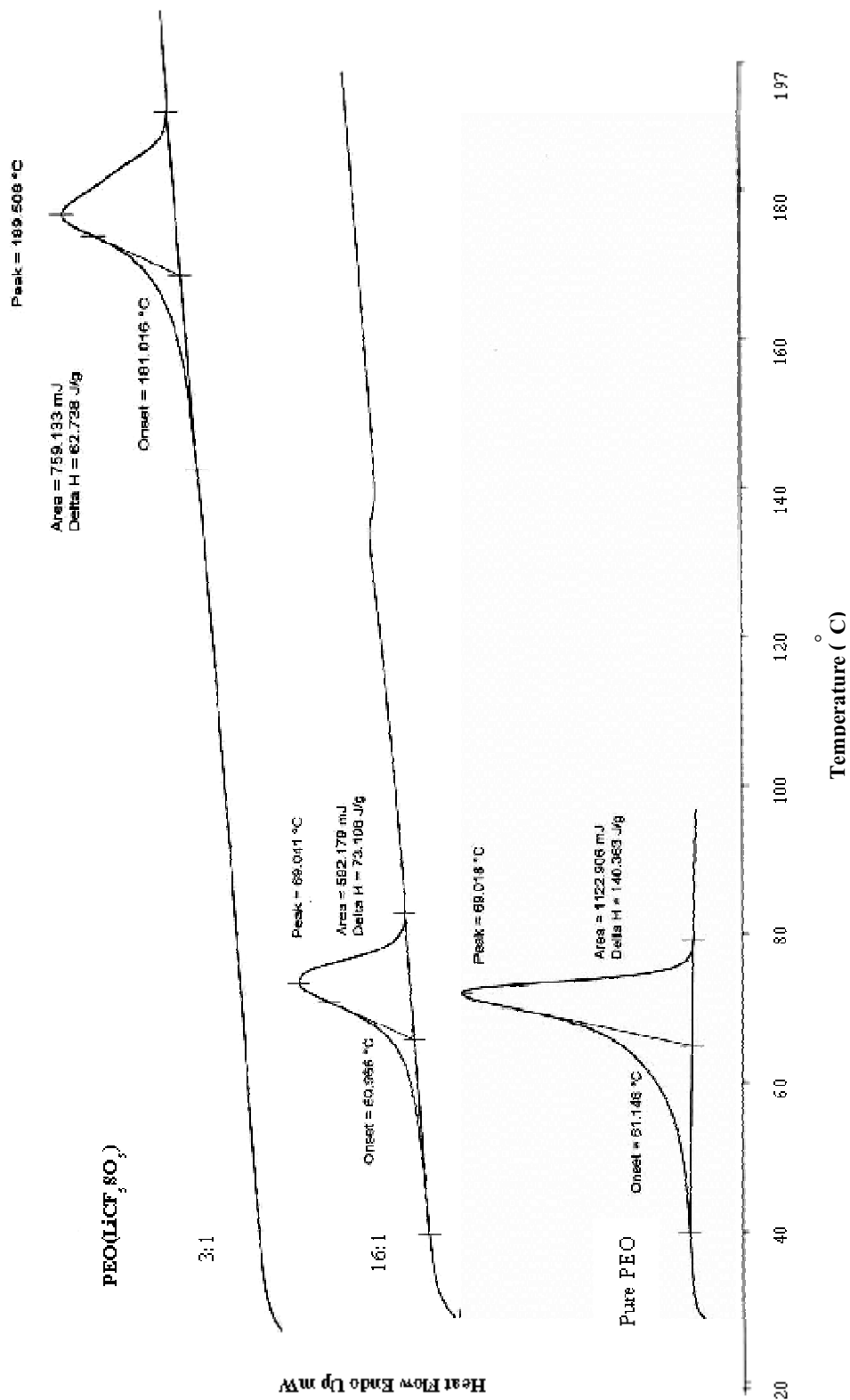
Figure 4.19 DSC thermograms of the crystalline of pure PEO and (PEO)LiCF$_3$SO$_3$ 16:1 and 3:1.
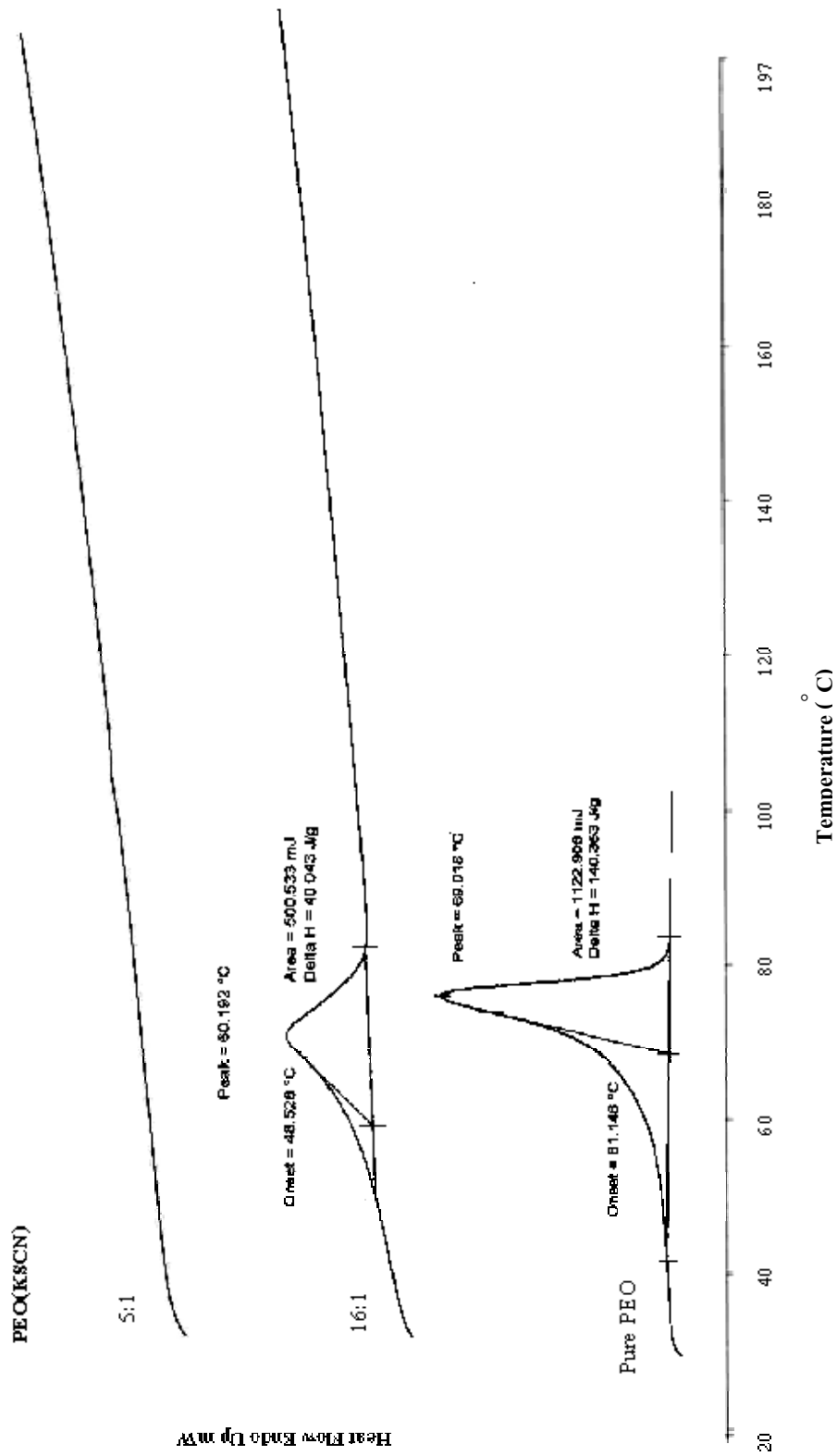
Figure 4.20 DSC thermograms of the crystalline of pure PEO and (PEO)KSCN 16:1 and 5:1.

4.2.1.4 Conductivity Measurement

In this part, the ionic conductivities of $(PEO)_n LiCF_3SO_3$ and $(PEO)_n KSCN$ electrolytes as a function of salt concentration are presented.

A. $(PEO)_n LiCF_3SO_3$ System

The results of volume conductivity measurements by using high resistance meter carried out at the room temperature on samples of various $LiCF_3SO_3$ salt content are presented in Table 4.10 and Figure 4.21. The conductivity value for $(PEO)_n LiCF_3SO_3$ ($\sim 10^{-9}$ S/cm) is about 10 times higher than that are observed for PEO ($\sim 10^{-10}$ S/cm). This value is acceptable since the room temperature conductivity of pure PEO reported by Sekhon *et al.* (1995) is $\sim 10^{-9}$ S/cm. It should also be noted that our measurement was derived from the method to determine the volume resistivity which was different from other works. The ionic conductivity increases when the salt concentration increases until the ratio O:Li$^+$ equal to 16:1 (similarly observed by Zahurak *et al.* (1988) who found that the highest conductivity for PEO/$LiCF_3SO_3$ was at O:Li$^+$ = 16:1). After this point, the conductivity decreases at higher salt concentrations (12:1 > 5:1 > 3:1). This variation is similar to the one observed for other polymer electrolytes. An initial rise of the ionic conductivity is due to the availability of conducting ions supplied by the polymer + salt complex (Robitaille et al., 1987; Sekhon *et al.*, 1995; Zahurak *et al*., 1988). In the region of high salt concentration, the ionic conductivity decreases because of an ion-association or segregation from the uncomplexed salt. Spectroscopic data, XRD patterns and DSC thermograms are also supported this conclusion. Infrared spectroscopic studies of $(PEO)_n LiCF_3SO_3$ complexes in the $\delta_s(CF_3)$ region show that at very high salt concentrations the peak at 760 cm^{-1} due to ion-pair becomes sharper and more intense. In addition, XRD and DSC results also show that a new crystalline complex with well-defined structure is presented at very high salt concentrations.

Table 4.10 Ionic conductivity of pure PEO and $(PEO)_nLiCF_3SO_3$ electrolytes at room temperature.

Composition (O:Li$^+$ ratio)	Mole Fraction salt	Weight Fraction salt	Conductivity (S/cm)
3:1	0.248	0.542	0.39×10^{-9}
5:1	0.167	0.415	0.77×10^{-9}
12.1	0.076	0.228	1.89×10^{-9}
16:1	0.059	0.181	2.27×10^{-9}
20:1	0.048	0.151	0.83×10^{-9}
30:1	0.033	0.105	0.71×10^{-9}
40:1	0.025	0.081	0.33×10^{-9}
60:1	0.016	0.056	0.31×10^{-9}
Pure PEO	0.000	0.000	0.13×10^{-9}
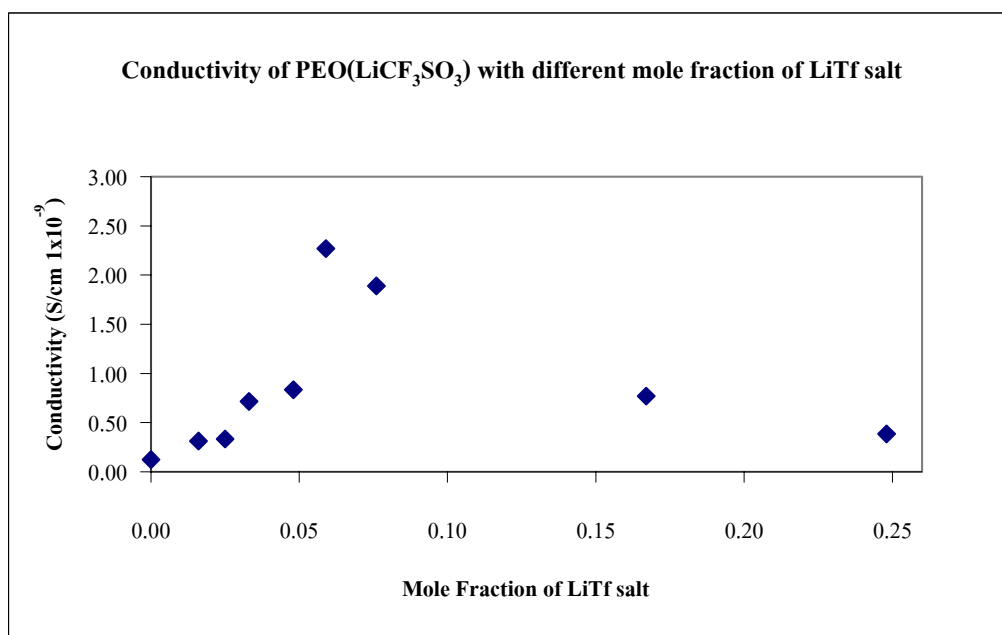
Figure 4.21 Ionic conductivity of pure PEO and $(PEO)_nLiCF_3SO_3$ electrolytes.

B. (PEO)$_n$KSCN System

Table 4.11 and Figure 4.22 show the results of conductivity measurements carried out at room temperature for samples varying KSCN salt content. A similar trend to the system of LiCF$_3$SO$_3$ salt is observed as the conductivity increases with increasing salt concentration. The maximum conductivity lies at the point between the ratio 16:1 and 5:1. Prechatiwong *et al*. (1996) found that the 8:1 ratio exhibited the highest conductivity and these complexes were almost completely amorphous. Unfortunately, the sample at this ratio could noy be prepared in this work. After 16:1 point, the conductivity decreases at very high salt concentration. Therefore, the ionic conductivity obtained in PEO complexes is depend on the amount of salt (or charge carriers) allowed in the host polymer (Dias et al., 2000).

Table 4.11 Ionic conductivity of pure PEO and (PEO)$_n$KSCN electrolytes.

Composition (O:K$^+$ ratio)	Mole Fraction salt	Weight Fractionsalt	Conductivity (S/cm)
5.1	0.166	0.306	1.15×10^{-9}
16:1	0.059	0.121	1.43×10^{-9}
20:1	0.047	0.099	0.71×10^{-9}
30:1	0.033	0.068	0.40×10^{-9}
40:1	0.024	0.052	0.39×10^{-9}
60:1	0.017	0.035	0.30×10^{-9}
Pure PEO	0.000	0.000	0.13×10^{-9}
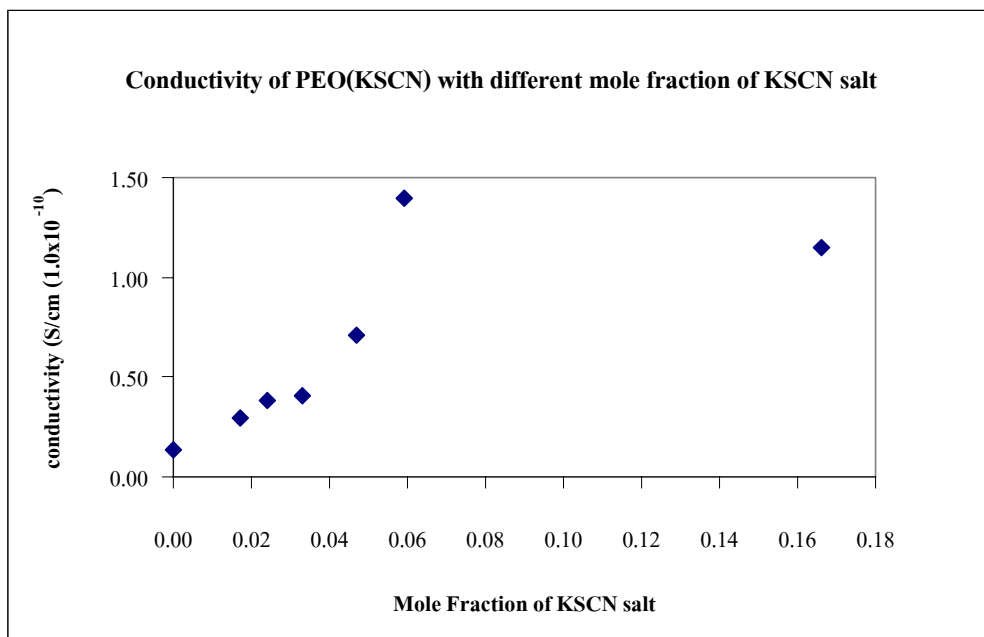
Figure 4.22 Ionic conductivity of pure PEO and $(PEO)_n KSCN$ electrolytes.

A maximum in the ionic conductivity as a function of salt concentration has long been observed in many solid polymer electrolytes systems. In this research, the ionic conductivity of $(PEO)_n LiCF_3 SO_3$ and $(PEO)_n KSCN$ electrolytes were studied. The $(PEO)_n LiCF_3 SO_3$ electrolyte gives higher ionic conductivity than the $(PEO)_n KSCN$ system. This can be understood from the following discussion. Kovac *et al*. (1998) quoted that the ionic transport in the SPEs was strongly related to the cation-ether oxygen coordination bonds (bond with a very strong interactions reduces cation mobility). In addition, there was an explanation of the coordination complex formation studied by Bruce (1995) to support the above reason. It was indicated in Ref. [6] that $PEO_3(LiCF_3SO_3)$, Li^+ was five coordinate composed of the three etheroxygens from PEO and one oxygen from each of two trifate groups. In the case of $PEO_4(MSCN)$ where $M = K^+$, NH_4^+ or Rb the cation were seven coordinate (five ether oxygens and two nitrogens from the thiocyanate anions). As a function of salt concentration, the conductivity increases and reaches a maximum value at a certain point because of the availability of conducting ions supplied by the polymer/salt complex. After this maximum point, the conductivity decreases with salt addition. This is due to hindrance to the motion of polymer chains accompanying ion mobility in crystalline PEO and

formation of ion pairs which lower the amount of the free ions available for conduction. These results were confirmed by FTIR, XRD and DSC techniques explained earlier.

4.2.2 Effect of Adding Poly(propylene oxide)

Although PEO is a good solvent for alkali metal salts owing to its excellent solvating properties, its crystallinity is a drawback for electrochemical applications because ion-conduction appears to occur in the amorphous domains. Chintapalli (1996) studied on the structure and phase diagram of $(PEO)_n LiCF_3SO_3$ system found that at least three phases exist in this system: (a) crystalline PEO below the melting point at 60 °C, (b) the crystalline compound $(PEO)_3 LiCF_3SO_3$ and (c) amorphous PEO with dissolved salt. The latter, an amorphous phase is believed to be responsible for the ionic conduction. Decreasing the crystalline domains and increasing main-chain segmental motions of SPEs can enhance the ionic conductivity of SPEs. Electrolytes with higher ionic conductivities can be made by introduction of plasticizer. Plasticizing additives decrease the content of the PEO crystalline phase in polymer electrolytes at room temperature. Low molecular weight polyethers and polar organic solvents are two commonly used plasticizers (Dias et al., 2000; Quartarone et al., 1998; Song et al., 1999). Kovac *et al.* (1998) studied on the effect of plasticizer for a $(PEO)_n LiAl(SO_3Cl)_4$ (using a mixture of propylene carbonate (PC) and dimethylether (DME) as a plasticizer) and found that this combination reduced the crystallinity of PEO by more than 50%. The reduction of crystallinity was proportional to the increasing of Li-salt concentration.

In this work, an attempt to improve the conductivity of PEO based electrolytes has come up with plasticization of polymer electrolytes with low molecular weight PPO molecule. The effect of adding PPO on the structure and ionic conductivity of PEO/salt systems were investigated using various of techniques, such as XRD, DSC, FTIR, and high resistance meter. In particular, PEO, PPO and salt ($LiCF_3SO_3$ and KSCN) were used as a polymer host, a plasticizer and ionic charge for this SPE system, respectively.

4.2.2.1 Infrared Spectroscopy (IR)

An addition of plasticizer to polymers-salt electrolytes leads to a change in the conformation of polymer backbone, cation-polymer interactions and ionic association. Thus, it is also necessary to study the changes in polymer conformation and ionic association in these complexes. In this part, vibrational spectroscopic studied for the role of plasticizer in the PEO-$LiCF_3SO_3$ system and PEO-KSCN system are reported.

A. $(PEO)_n LiCF_3SO_3$ + % wt PPO System

Effect of PPO on ionic association

As mensioned before, it is seen that more associated ionic species are formed with increasing $LiCF_3SO_3$ concentration. The bands at 753, 757 and 760 cm^{-1} correspond to the symmetric deformation of CF_3 [denoted as $\delta_s(CF_3)$] of the "free" triflate ion, ion pair, and the compound, $(PEO)_3 LiCF_3SO_3$, respectively. These assignments are consistent with an *ab initio* calculation and a normal coordination analysis (Huang et al., 1994). For the 16:1 sample, the infrared spectra of $(PEO)_{16} LiCF_3SO_3$ + PPO with different %wt PPO in the region 790-730 cm^{-1} are shown in Figure 4.23. The band of 758 cm^{-1} due to the ion pair is presented even after the addition of PPO. There is a very slightly change in the intensity of this band. With increasing plasticizer content, the intensity of the ion pair band at 758 cm^{-1} is as same as the $(PEO)_{16} LiCF_3SO_3$ complex. The absence of any change upon adding PPO content suggests that the Li^+ ions preferentially interact with PEO as a polymer host more than PPO as a plasticizer. The IR results of $PPO/LiCF_3SO_3$ (see Appendix B (Figure B1)) and $PEO/LiCF_3SO_3$ (Figure 4.10) also support this suggestion. It is found that peaks at 757 cm^{-1} due to ion pair of $PPO/LiCF_3SO_3$ becomes visible at 16:1, while this peak becomes visible at 40:1 for $PEO/LiCF_3SO_3$ system. Chintapalli studied the effect of adding plasticizer on ionic association and conductivity in $PEO/LiCF_3SO_3$ system. In their works, propylene carbonate (PC), ethylene carbonate (EC), tetraethylene glycol (TEG) and tetraethylene glycol dimethylether (TEGDME) were chosen as plasticizer. They found that PC, EC and TEG tend to increase the concentration of the less

associated species while TEGME tend to increase the concentration of more associated species relative with plasticizer.
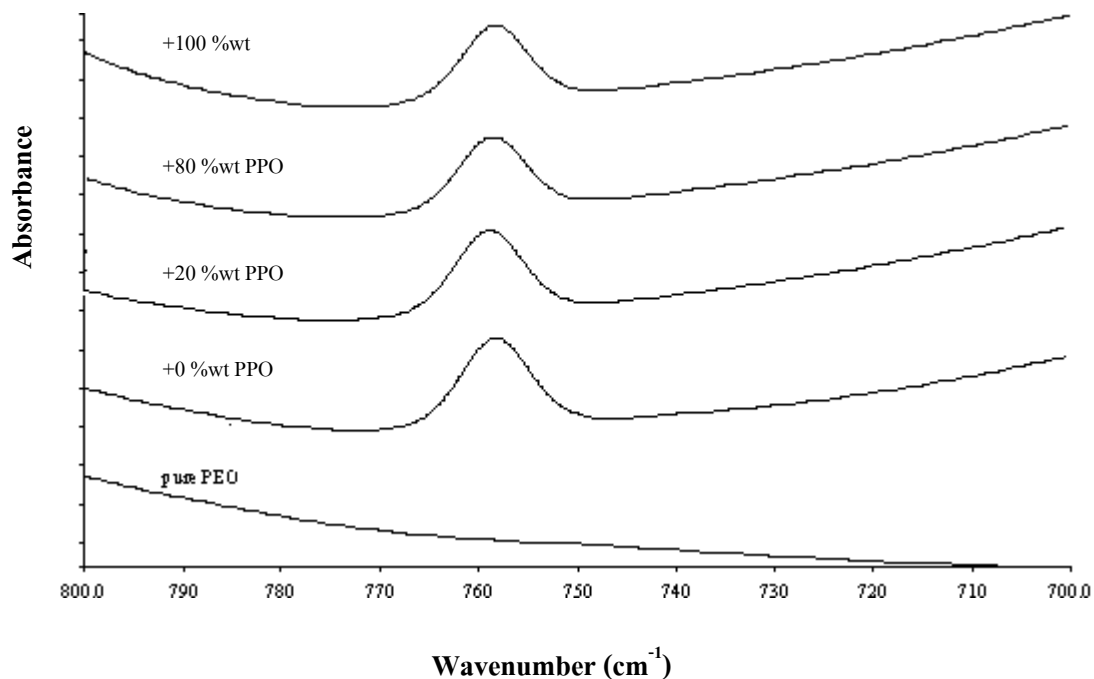
Figure 4.23 IR spectra of $(PEO)_{16}LiCF_3SO_3$ + %wt PPO in the 800-700 cm^{-1} spectra region.

Effect of adding PPO on local PEO conformation

Vibrational bands in the region 1000-800 cm^{-1} (Figure 4.24) are associated with vibrational modes of CH_2 rocking coupled with C-O stretching vibrations of the PEO molecule. As mentioned before, the band at 844 cm^{-1} is ascribed primarily to the rocking motion of CH_2 units [symbolized as $r_a(CH_2)$]. From Figure 4.24, it can be seen that the intensity of the crystalline PEO band at 844 cm^{-1} decreases when PPO is added. IR result of PEO+PPO blend (see Appendix (Figure B3)) also confirms this conclusion.

PEO(LiCF$_3$SO$_3$) 16:1

Absorbance

+100 %wt

+80 %wt PPO

+20 %wt PPO

+0 %wt PPO

pure PEO

900.0   890   880   870   860   850   840   830   820   810   800.0

Wavenumber (cm^{-1})
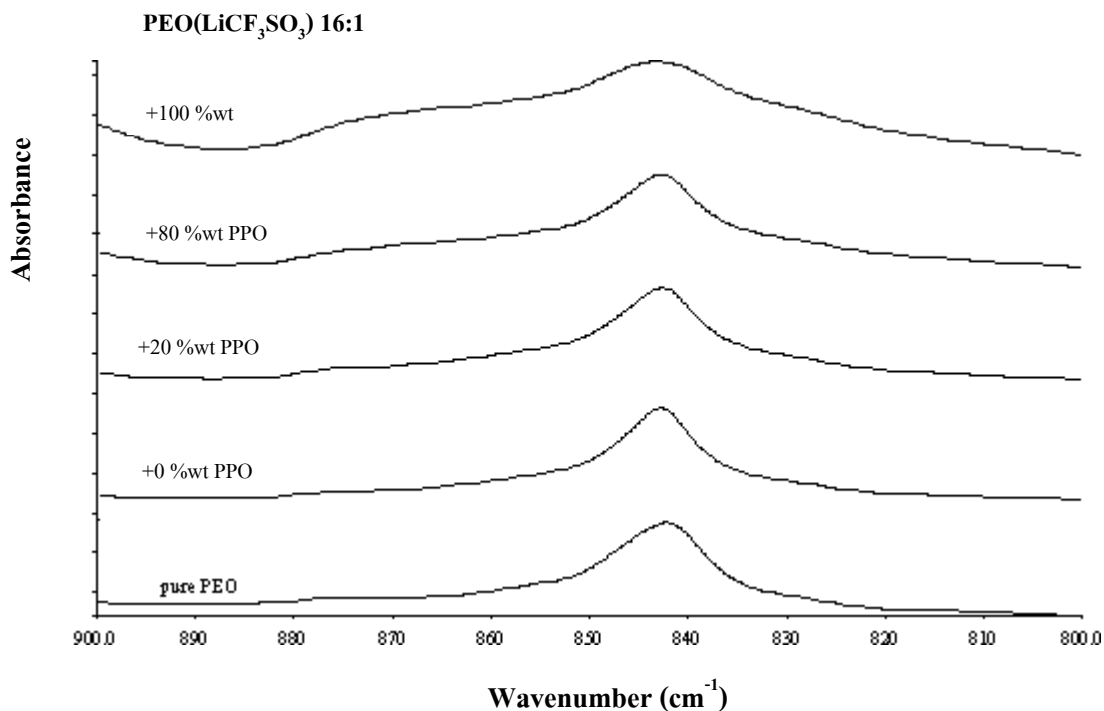
Figure 4.24 IR spectra of (PEO)$_{16}$LiCF$_3$SO$_3$ + %wt PPO in the 880-800 cm^{-1} spectra region.

B. (PEO)$_n$KSCN + %wt PPO System

Figure 4.25 demonstates the IR spectra of (PEO)$_n$KSCN + %wt PPO system as a function of different %wt PPO in the −SCN asymmetric stretching. The frequency and intensity of the IR spectra slightly change with an addition of PPO content. In the same way, the IR spectra in the region 900-800 cm^{-1} for (PEO)$_{20}$KSCN complex in Figure 4.26 is the characteristics of C-O stretching and CH$_2$ rocking modes. The peak at 844 cm^{-1} is due to CH$_2$ rocking coupled with C-O stretching vibrations of the PEO molecules. This band slightly decreases with increasing PPO content. However, it can be seen that the intensity of crystalline PEO decreases when PPO is added. A similar trend is observed in (PEO)$_{16}$LiCF$_3$SO$_3$ system.
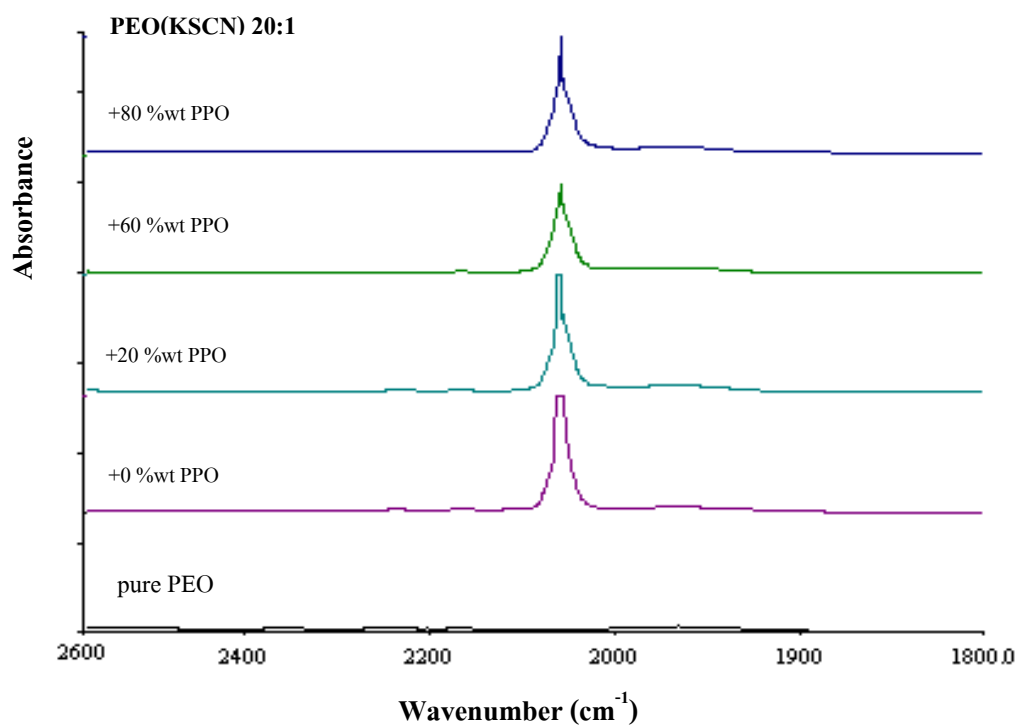
Figure 4.25 IR spectra of $(PEO)_{20}KSCN$ + %wt PPO in the 2600-1800 cm^{-1} spectra region.
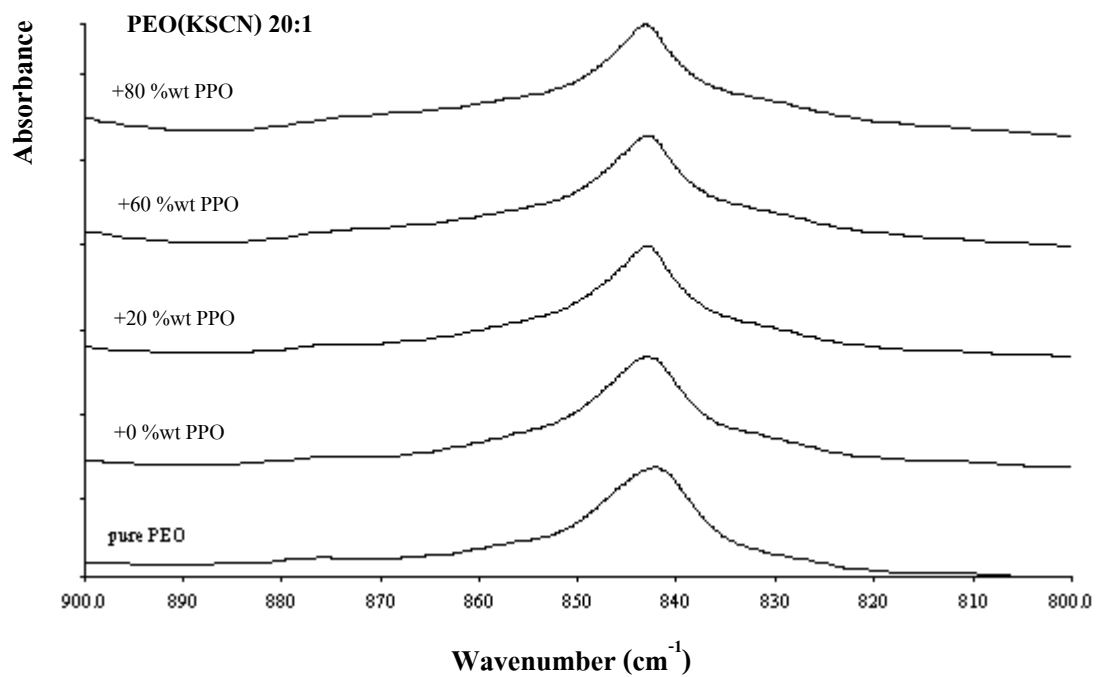
Figure 4.26 IR spectra of $(PEO)_{20}KSCN$ + %wt PPO in the 900-800 cm^{-1} spectra region.

4.2.2.2 X-ray Diffraction (XRD)

The incorporation of PPO into polymeric PEO phase was studied. Figure 4.27 shows the XRD patterns of pure PEO and PEO + %wt PPO for 2θ values between 5- 40°. The results are presented in the crystalline PEO reflection peak at 15.3°, 19.3° and 23.3°. For the PEO + 33 %wt PPO and PEO + 100 %wt PPO, the intensity of crystalline PEO peaks decreases with adding PPO content. The magnitude of crystalline peaks for PEO+PPO mixture is higher for 33 %wt PPO than 100 %wt PPO.

The XRD patterns of $(PEO)_{16} LiCF_3SO_3$ + %wt PPO system with different %wt PPO content for 2θ values between 5-40° are shown in Figure 4.28. With increasing plasticizer content, the intensity of crystalline peaks are about the same as the $(PEO)_{16}LiCF_3SO_3$ complexes. However, there is more the amorphous halo at baseline with increasing plasticizer content which implies that the crystalline PEO regions become amorphous.

Next, the XRD patterns of $(PEO)_{20}KSCN$ + %wt PPO system with different %wt PPO content for 2θ values between 5-40° are shown in Figure 4.29. The intensity of crystalline peaks decrease with increasing plasticizer content (50 and 100 %wt PPO). It is clearly seen that diffraction peaks of crystalline PEO decrease with addition 100 %wt PPO than 50 %wt PPO. It points out that PPO is incorporated into PEO and the crystalline PEO regions become more amorphous.

PEO + %wt PPO
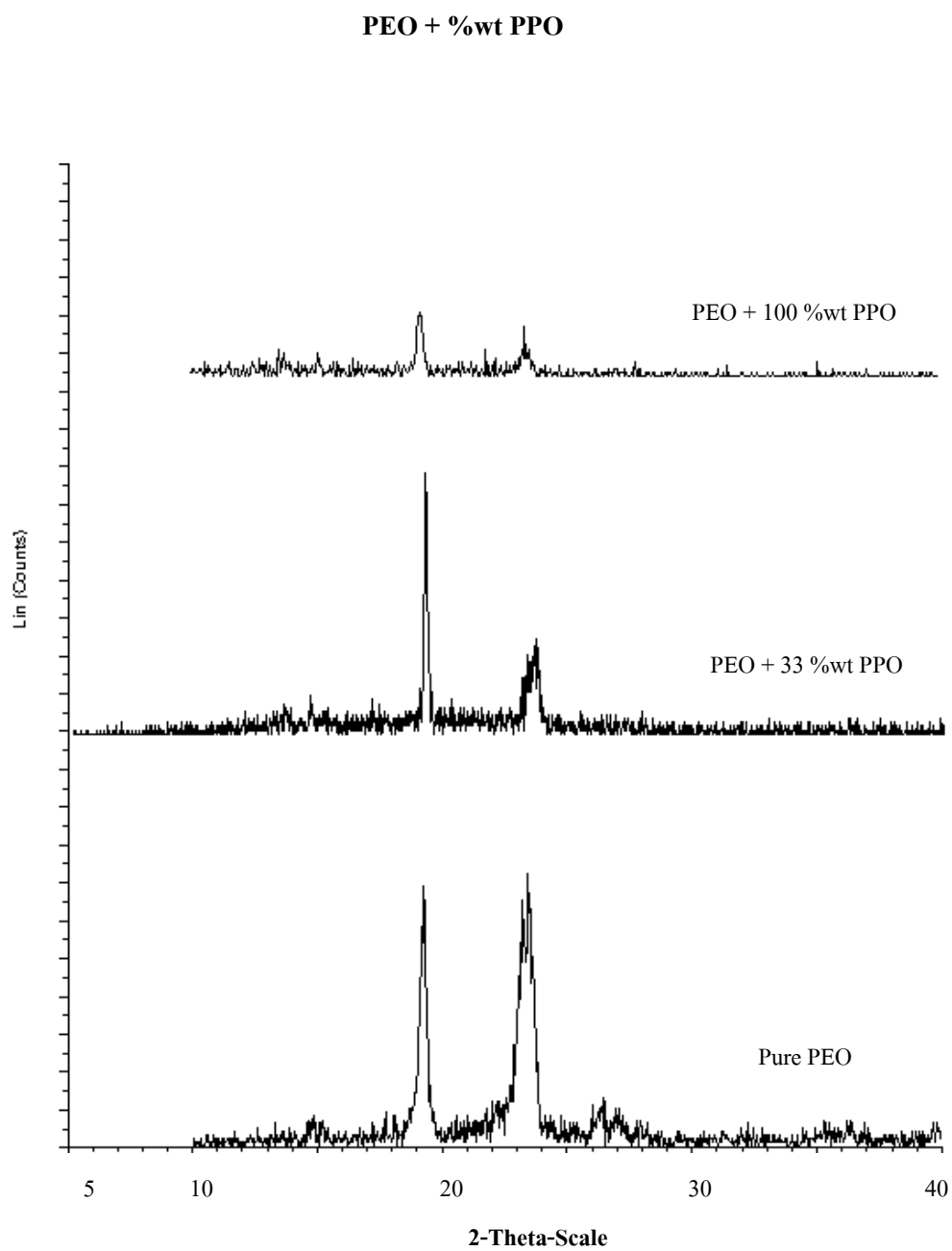
Figure 4.27 XRD patterns of PEO + PPO as a function of different %wt PPO content.

(PEO)$_n$LiCF$_3$SO$_3$ + %wt PPO System
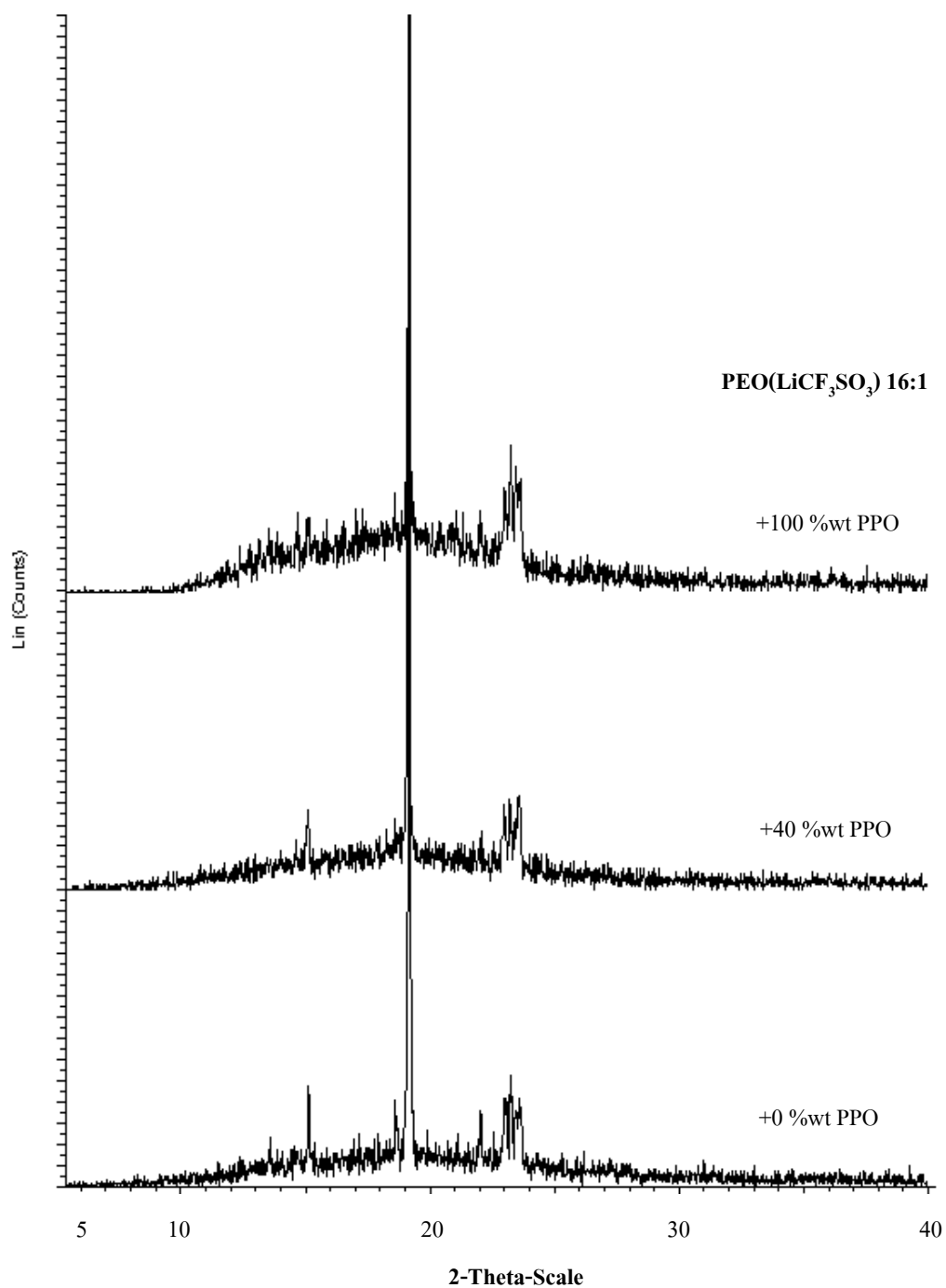
Figure 4.28 XRD patterns of PEO$_{16}$(LiCF$_3$SO$_3$) + %wt PPO as a function of adding %wt PPO content.

(PEO)ₙKSCN + %wt PPO System
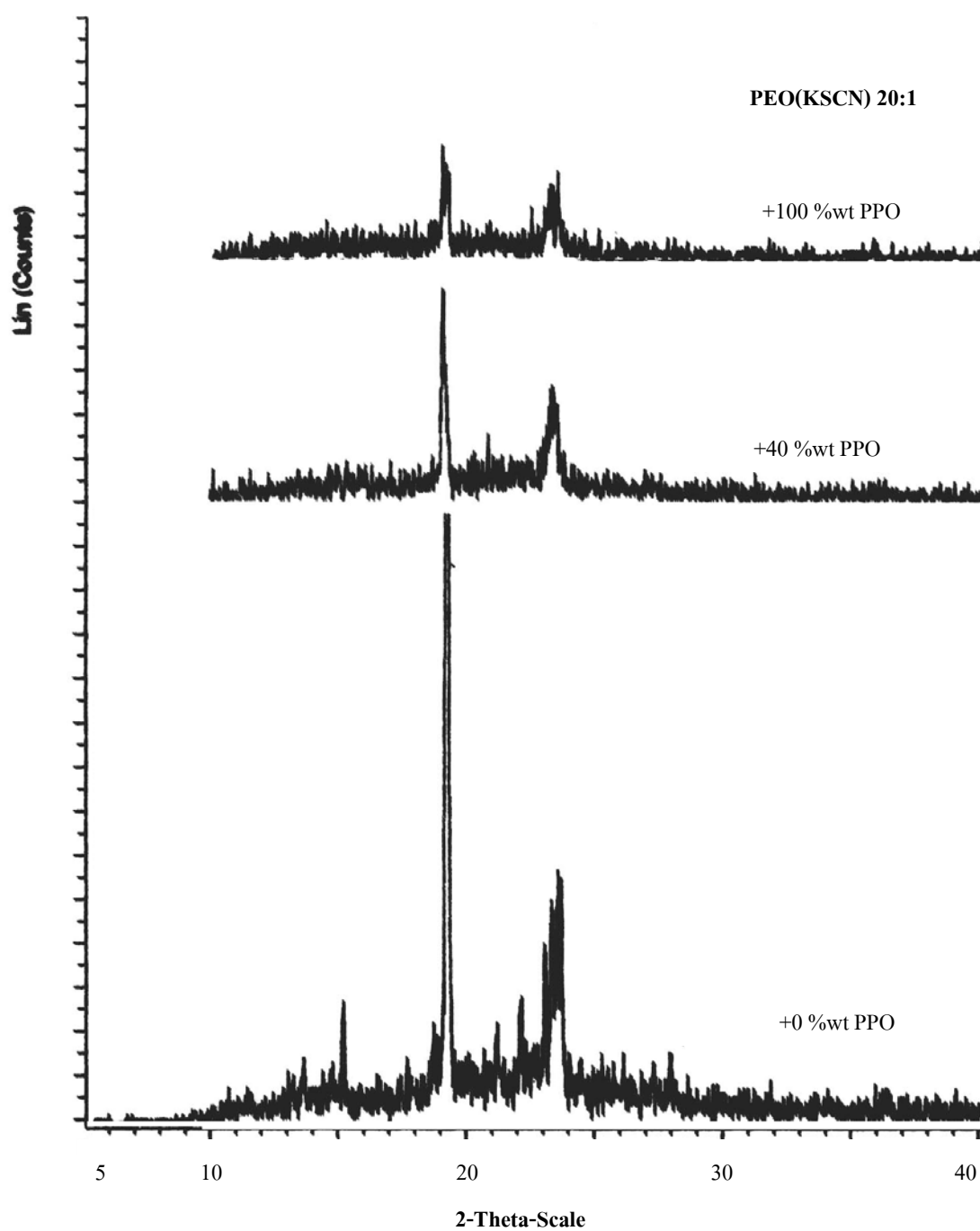
Figure 4.29 XRD patterns of $PEO_{16}(KSCN)$ + %wt PPO as a function of adding %wt PPO content.

4.2.2.3 Differential Scanning Calorimeter (DSC)

The effect of adding PPO on the changes of T_m and ΔH of PEO and PEO-salt were investigated using DSC technique. T_m, ΔH and the percentages crystallinity for each specimen are shown in Table 4.12.

Table 4.12 Melting temperatures and percentage crystallinity of polymer electrolytes as a function of adding PPO.

Composition		Thermal behavior						
PEO/PPO	**O/M$^+$**	T_g	T_{m1}	ΔH_1	(X_1)	T_{m2}	ΔH_2	(X_2)
		(°C)	(°C)	(J g^{-1})	%	(°C)	(J g^{-1})	%
100/0	0 (Li$^+$)	-58.1	69.0	140.36	74.58			
[a]0/100	0 (Li$^+$)				-[b]			
100/80	0 (Li$^+$)		63.8	58.98	31.34			
100/0	16 (Li$^+$)		69.0	73.14	38.88			
100/80	16 (Li$^+$)		64.91	52.69	28.00	164.4	5.87	
100/0	16 (K$^+$)		60.2	40.04	21.28			
100/80	16 (K$^+$)		56.5	30.85	16.39			

[a] from Song *et al*.

[b] Amorphous polymer 100 %.

The DSC thermograms of PEO + PPO and PEO-LiCF$_3$SO$_3$ 16:1 + 80 %wt PPO specimens are shown in Figure 4.30. The plasticizing effect of PPO is clearly seen as a shift in the melting temperature of PEO from 69.0 °C to 63.8 °C. It suggests that there is more amorphous domain in the complex due to the miscibility of PPO with PEO. ΔH and the percentages crystallinity of PEO + 80 %wt PPO are lower than that of PEO. It reveals that PPO is compatible with PEO and PPO reduces the crystallinity of PEO. XRD results of PEO + PPO system also support this idea. The melting peak of PEO-LiCF$_3$SO$_3$ 16:1 is equal to that of pure PEO.

However, ΔH and the percentages crystallinity of PEO-LiCF$_3$SO$_3$ 16:1 are lower than those of pure PEO. A similar trend is observed in PEO-KSCN system which shows that crystallinity decreases as the salt concentration increases. For the PEO-LiCF$_3$SO$_3$ specimen at ratios of 16:1 with 80 %wt PPO, there are two melting peaks at 64.9 °C (T$_{m1}$), and 164.4 °C (T$_{m2}$). The first peak is due to salt associated with pure PEO and a new endotherm peak at high melting temperature (164.4 °C) suggests the presence of complex phase. Supportive evidence is obtained by XRD results for PEO-LiCF$_3$SO$_3$ + %wt PPO shown in Figure 4.28. It is found that only the amorphous halo at baseline increases with increasing plasticizer content, while the intensity of crystalline PEO did not change. A reduction in T$_{m1}$ of PEO-LiCF$_3$SO$_3$ 16:1 from 69.0 °C to 64.9 °C as the addition amount of PPO suggests that PPO is compatible with PEO and there is more amorphous domain in the complex.

For comparison, the DSC thermogram of PEO-KSCN 16:1 + 80 %wt PPO is also shown in Figure 4.31. For the PEO-KSCN specimen at ratios of 16:1 with 80 %wt PPO, there is a shift in the T$_m$ of PEO (69.0 °C) and PEO-KSCN 16:1 (60.2 °C) to 56.5 °C. The melting temperature of PEO in PEO-KSCN 16:1 complex shifts from 69.0 °C to 60.2 °C. It suggests that cation is attracted to the oxygen atoms and formed the covalent bonds between carbon and oxygen atoms thereby weakening the polymer backbone (Kim et al., 1998). ΔH and the percentages crystallinity of both polymer-salt complexes decrease ordering as PEO-salt 16:1 + %wt PPO > PEO-salt > PEO. ΔH and the percentages crystallinity for PEO-KSCN are lower than that of PEO-LiCF$_3$SO$_3$ salt. From these results, it confirms the plasticizing effect of PPO for PEO-salt. A decrease in percentages crystallinity in PEO and PEO-salt, shown by IR spectra, DSC and XRD diffractograms upon adding PPO indicates that there is more amorphous phase in the complex.
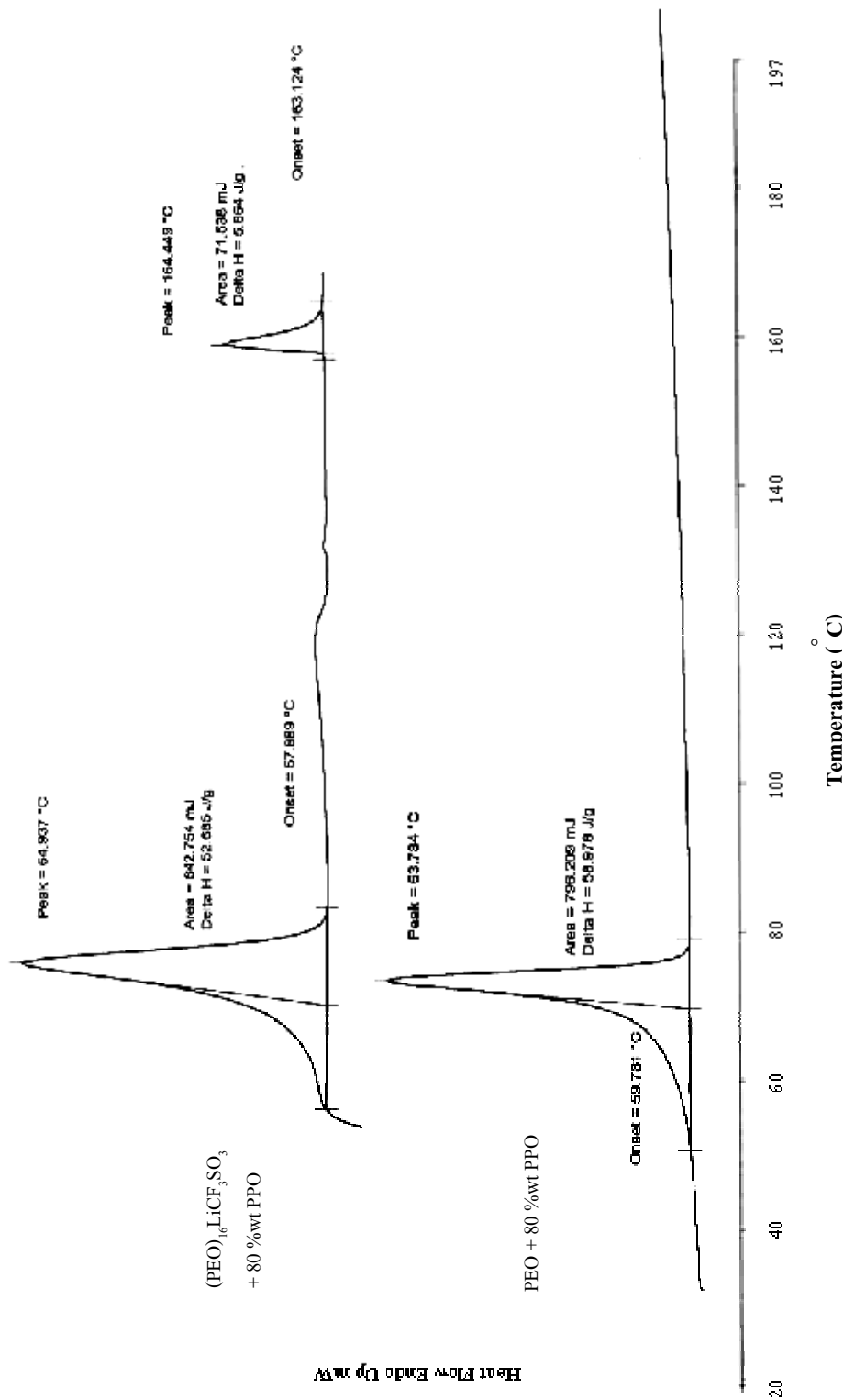
Figure 4.30 DSC thermograms of the crystalline of PEO + 80 %wt PPO and (PEO)$_{16}$LiCF$_3$SO$_3$ + 80 %wt PPO.
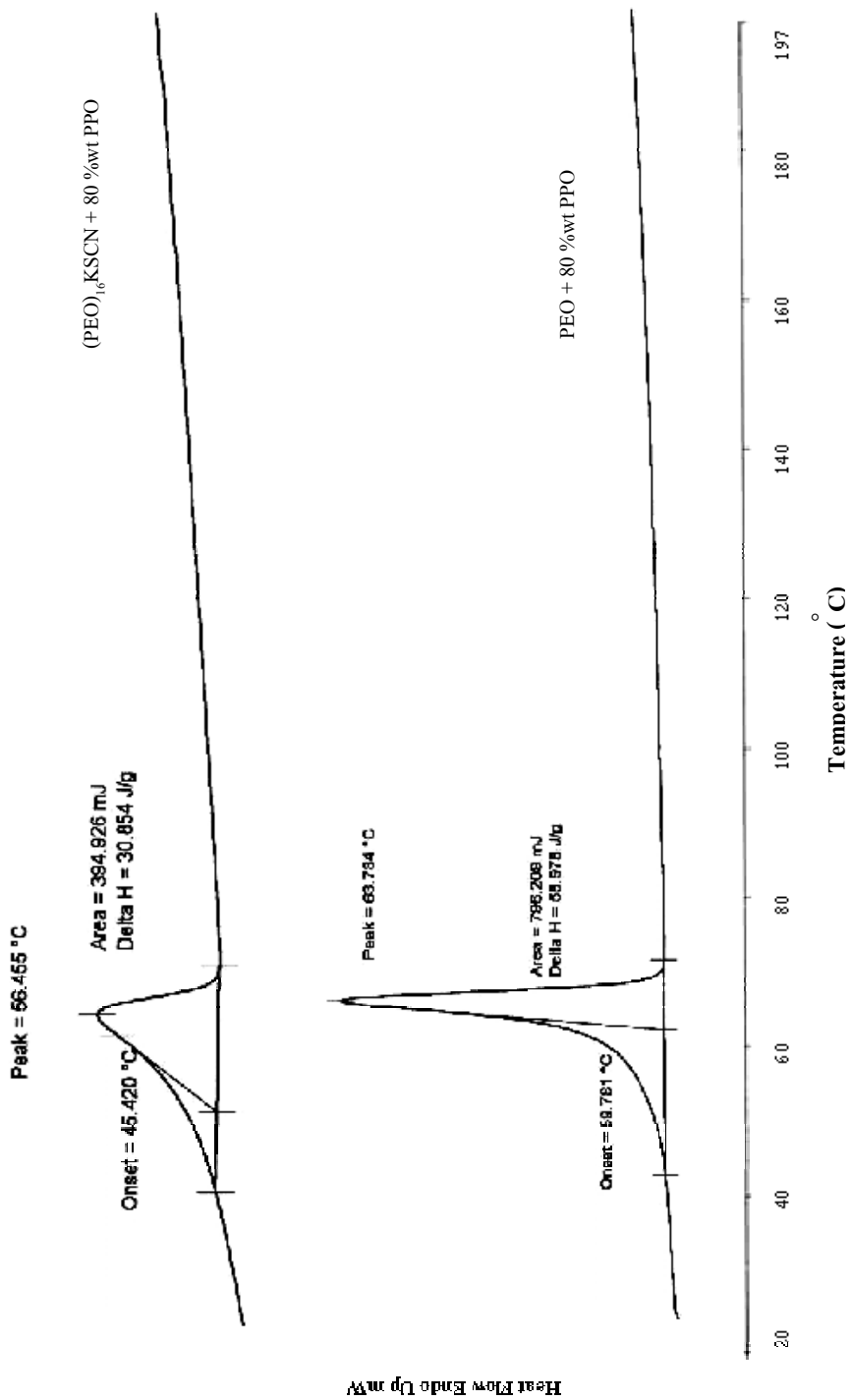
Figure 4.31 DSC thermograms of the crystalline of PEO + 80 %wt PPO and (PEO)$_{16}$KSCN + 80 %wt PPO.

4.2.2.4 Conductivity Measurement

The ionic conductivity in the SPEs is found to be accompanied by polymer chain mobilities. Conductivity and ion transport are restricted to the amorphous of polymer electrolytes. The phenomenon of plasticization has been found to improve the conductivity of PEO based electrolytes because it can disrupt PEO crytallinity so as to increase the fraction of the conductive amorphous phase. In this part, the ionic conductivity of $(PEO)_n LiCF_3SO_3$ and $(PEO)_n KSCN$ electrolytes as a function of salt concentration and $(PEO)_n LiCF_3SO_3$ + %wt PPO and $(PEO)_n KSCN$ + %wt PPO electrolytes as a function of addition %wt PPO content are presented.

A. $(PEO)_n LiCF_3SO_3$ +wt% PPO System

The conductivity measurements were carried out at the room temperature. The results of samples of varying $LiCF_3SO_3$ salt and %wt PPO content are presented in Table 4.13 and Figure 4.32. Figure 4.32a displays the ionic conductivity against mole fraction of $LiCF_3SO_3$ salt while Figure 4.32b shows the ionic conductivity against %wt PPO content. Ionic conductivities increase with the salt concentration upto the ratio $O:Li^+$ equal to 16:1 and then decrease at very high salt concentration. A decrease in ionic conductivity with increasing salt concentration at high content were suggested to higher percentage of associated ions, ion pairs or ions acting as a transient cross-linking agent (Prechatiwong et al., 1996; Sekhon et al., 1995). The FTIR, XRD, and DSC results shown earlier also confirm this discussion.

Polymer electrolytes with plasticizer show better ionic conductivity. The ionic conductivity of $PEO(LiCF_3SO_3)$ + %wt PPO ($\sim10^{-7}$ S/cm) is about 100 times higher than those for $PEO(LiCF_3SO_3)$ ($\sim10^{-9}$ S/cm). The conductivity is improved due to an increase in the amorphous phase, which enhance the ion mobility. The FTIR, XRD, and DSC results also support this conclusion as a substantial amount of PPO plasticizer is incorporated in SPEs films. PPO reduces the crystallinity of PEO and $PEO(LiCF_3SO_3)$ system by more than 50% and 20%, respectively. The ionic conductivity increases with increasing %wt PPO content to 60%, 80%, 100% and 120% for the ratio of 5:1, 12:1, 16:1 and 20:1, respectively, then it decreases at very high PPO content.

It should be noted that the increase in an ionic conductivity to a maximum point for each sample depended on the amount of salt and PPO. The maximum value of an ionic conductivity is seen when O:Li ratio is 16:1 while the rest are slightly significant. In addition, adding 80 %wt PPO in that system gives the highest conductivity. This emphasizes that PEO/PPO/LiCF$_3$SO$_3$ electrolyte has the best ionic conductivity when ratio of O:Li is 16:1 with 80 %wt PPO.

Table 4.13 Ionic conductivity of $(PEO)_n LiCF_3SO_3$ electrolytes and $(PEO)_n LiCF_3SO_3$ + %wt PPO electrolytes.

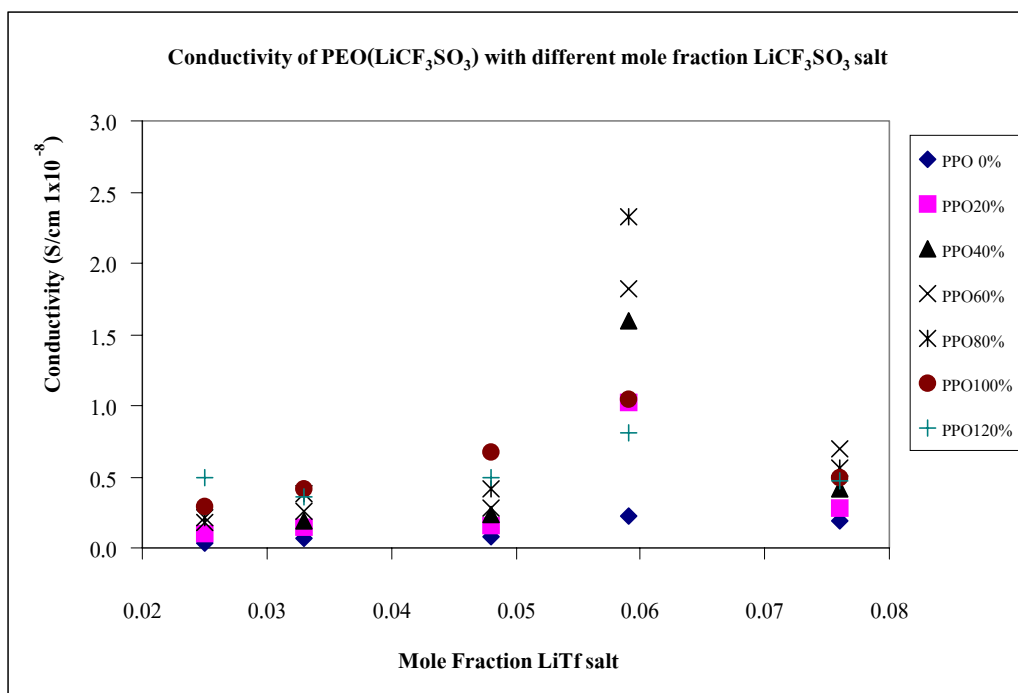| Composition		conductivity	Composition		Conductivity
O:Li$^+$	%wt PPO	(S/cm)	O:Li$^+$	%wt PPO	(S/cm)
5:1	0	0.075×10^{-8}	20:1	0	0.083×10^{-8}
5:1	20%	0.286×10^{-8}	20:1	20%	0.156×10^{-8}
5:1	40%	0.526×10^{-8}	20:1	40%	0.233×10^{-8}
5:1	60%	0.333×10^{-8}	20:1	60%	0.286×10^{-8}
5:1	100%	0.400×10^{-8}	20:1	80%	0.417×10^{-8}
12:1	0	0.189×10^{-8}	20:1	100%	0.676×10^{-8}
12:1	20%	0.286×10^{-8}	20:1	120%	0.500×10^{-8}
12:1	40%	0.412×10^{-8}	30:1	0	0.071×10^{-8}
12:1	60%	0.699×10^{-8}	30:1	20%	0.143×10^{-8}
12:1	80%	0.565×10^{-8}	30:1	40%	0.196×10^{-8}
12:1	100%	0.500×10^{-8}	30:1	60%	0.256×10^{-8}
12:1	120%	0.476×10^{-8}	30:1	80%	0.379×10^{-8}
16:1	0	0.277×10^{-8}	30:1	100%	0.413×10^{-8}
16:1	20%	0.102×10^{-7}	30:1	120%	0.357×10^{-8}
16:1	40%	0.159×10^{-7}	40:1	0	0.033×10^{-8}
16:1	60%	0.182×10^{-7}	40:1	20%	0.100×10^{-8}
16:1	80%	0.233×10^{-7}	40:1	60%	0.175×10^{-8}
16:1	100%	0.105×10^{-7}	40:1	80%	0.217×10^{-8}
16:1	120%	0.806×10^{-8}	40:1	100%	0.294×10^{-8}
			40:1	120%	0.500×10^{-8}

Figure 4.32a Ionic conductivity against mole fraction of $LiCF_3SO_3$ salt of $(PEO)_n LiCF_3SO_3 +$ %wt PPO electrolytes.
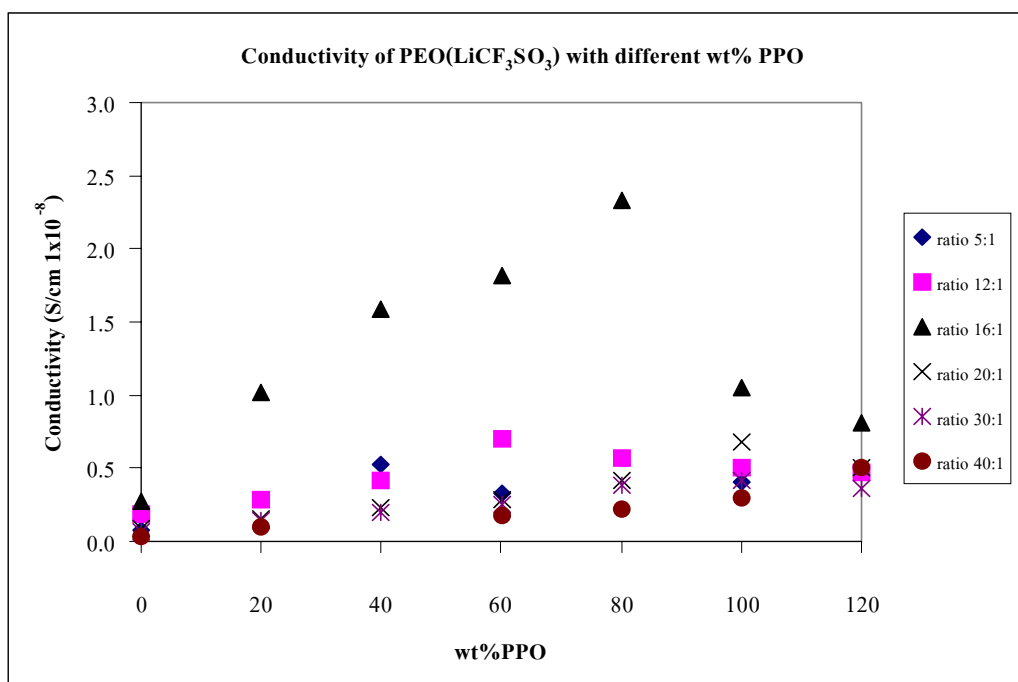
Figure 4.32b Ionic conductivity against %wt PPO of $(PEO)_n LiCF_3SO_3 +$ %wt PPO electrolytes.

B. (PEO)$_n$KSCN + %wt PPO System

The conductivity values at the room temperature of samples which KSCN salt was added at the ratio of 16:1 and 20:1 (with various %wt PPO content) are presented in Table 4.14. The ionic conductivities against %wt PPO of (PEO)$_n$KSCN electrolytes are shown in Figure 4.33. The ionic conductivities increases rapidly with increasing of PPO up to 20 %wt. After this point, the conductivity values slightly increases. The best composition that gives the highest ionic conductivity of PEO/PPO/KSCN electrolyte is PEO:salt of 16:1 with 100 %wt PPO. Although this composition gives the highest ionic conductivity, it may be not useful since its conductivity is rarely different from the samples in which 20 %wt PPO is added. It should be noted that the ionic conductivity of (PEO)$_n$KSCN + %wt PPO is lower than that of (PEO)$_n$ LiCF$_3$SO$_3$+ %wt PPO system. This trend is similar to the (PEO)$_n$KSCN system (without plasticizer) explained earlier.

Table 4.14 Ionic conductivity of (PEO)$_n$KSCN electrolytes and (PEO)$_n$KSCN + %wt PPO electrolytes.

Composition		conductivity	Composition		Conductivity
O:K$^+$	%wt PPO	(S/cm)	O:K$^+$	%wt PPO	(S/cm)
16:1	0	0.143×10^{-8}	20:1	0	0.071×10^{-8}
16:1	20%	0.250×10^{-8}	20:1	20%	0.233×10^{-8}
16:1	60%	0.278×10^{-8}	20:1	60%	0.303×10^{-8}
16:1	80%	0.333×10^{-8}	20:1	80%	0.286×10^{-8}
16:1	100%	0.345×10^{-8}	20:1	100%	0.303×10^{-8}
16:1	120%	0.333×10^{-8}	20:1	120%	0.313×10^{-8}

Figure 4.33 Ionic conductivity against %wt PPO of $(PEO)_nKSCN$ + %wt PPO electrolytes.

The observed results from this work indicate that the composition between polymer host, salt and plasticizer is important for an improvement of an ionic conductivity. More ionic transportation on main-chain segmental motions in system of SPEs can enhance the ionic conductivity. The IR and XRD results show that the crytallinity of PEO decreases with the adding of PPO content. A trend is observed in which the conductivity increases with increasing %wt PPO content to a maximum point, then decreases at very high %wt PPO content. The $PEO/PPO/LiCF_3SO_3$ electrolyte gives higher ionic conductivity than the PEO/PPO/KSCN electrolyte. The best composition that gives the highest ionic conductivity of their two polymer electrolytes are (1) PEO:salt 16:1 with 80 %wt PPO for $PEO/PPO/LiCF_3SO_3$ electrolyte and (2) PEO:salt 16:1 with 100 %wt PPO for PEO/PPO/KSCN electrolyte.

CHAPTER V

CONCLUSION

1. The RIS model provided conformational dependent properties in good agreement with the experimental observations, including the characteristic ratio, the dipole moment ratio and bond conformation. Our findings suggested that the simple RIS model derived from forcefield-based MM technique seemed to be reasonable.

2. A trend was observed in which the conductivity increased with increasing salt concentration to a maximum ratio O:M 16:1, then decreased at very high salt concentration. The PEO/LiCF$_3$SO$_3$ electrolyte gave higher ionic conductivity than the PEO/KSCN electrolyte.

3. The FTIR, XRD and DSC results showed that the PPO was able to decrease the crytallinity of PEO and improve the ionic conductivity of PEO-salts (LiCF$_3$SO$_3$ or KSCN) systems. The PEO/PPO/LiCF$_3$SO$_3$ electrolyte displayed higher ionic conductivity than the PEO/PPO/KSCN electrolyte. The best composition that gave the highest ionic conductivity for two electrolytes were (1) PEO:salt 16:1 with 80 %wt PPO for PEO/PPO/LiCF$_3$SO$_3$ electrolyte and (2) PEO:salt 16:1 with 100 %wt PPO for PEO/PPO/KSCN electrolyte.

References

References

Abe, A. (1979). Conformational energies and the random-coil configuration of poly (propylene oxide). **Macromolecules** 6: 1092 - 1100.

Acosta, J. L. and Morales, E. (1996). Structural, morphological characterization of polymer electrolytes based on PEO/PPO blends. **Solid State Ionic** 85: 85 - 90.

Ahlstrom, P., Borodin, O., WahnstrÖm, G., Wensink, E. J. W., Carlsson, P. and Smith, G. D. (2000). Molecular- dynamics simulation of structural and conformational properties of poly (propylene oxide). **J. Chem. Phys.** 112: 10669 - 10679.

Allen, G., Booth, C. and Price, C., (1967). **Polymer** 6:459. Quoted in Stepto, R. F. T., and Taylor, D. J. R. (1996). The conformational properties of polyoxypropylene chains -A critical correlation of theory and experiment. **Computational and Theoretical Polymer Science** 6: 49-60.

Armand, M. B. (1979). **Fast Ion Transport in Solids**. Elsevier North-Halland. Quoted in Puatrakul, T. (2000). **Studies of Ionic Conductivity of Uniaxially Stretched Polymer Electrolytes Films.** Ph.D. Thesis, University of Akron, USA.

Armand, M. B. (1987). **Polymer Electrolyte Review-1**. Elsevier Applied Science. Quoted in Puatrakul, T. (2000). **Studies of Ionic Conductivity of Uniaxially Stretched Polymer Electrolytes Films.** Ph.D. Thesis, University of Akron, USA.

Billmeyer, F. W. JR. (1984). **Textbook of polymer science.** (3rd ed.). New York: John Wiley & Sons.

Blythe, A. R. (1979). **Electrical Properties of polymers**. United Kingdom: Cambridge University Press.

Botel, E. Hodorowicz, S., and Lamot, R. (1979). **Makromol. Chem** 180: 2491. Quoted in Puatrakul, T. (2000). **Studies of Ionic Conductivity of Uniaxially Stretched Polymer Electrolytes Films.** Ph.D. Thesis, University of Akron, USA.

Bruce, P. G. (1995). **Solid state electrochemistry.** United Kingdom: Cambridge University Press.

CambridgeSoft Corporation. (1986-2000). CS Chem3D Molecular Modeling and analysis User'Guide [computer softwere]. USA: Cambridge Scientific Computing.

Chen, T. (1991). **Conformational–Configurational characteristics of water–soluble acylamide polymers.** Ph. D. Dissertation, Massachusetts Institute of Technology, USA.

Chintapalli, S. (1996). **Structural characterization of polymer – salt complexes and the role of plasticizers in ionic transport.** Ph. D. Dissertation, University of Oklahoma Graduate College, USA.

Dias, B. F., Plomp, L. and Veldhuis, J. B. J. (2000). Trends in polymer electrolytes for secondary lithium batteries**. J. Power sources** 88: 169 – 191.

Dissanayake, M. A. K. L. and Frech, R. (1995). Infrared Spectroscopic Study of the Phases and Phase Transitions in Poly(ethylene oxide) and Poly(ethylene oxide)-Lithium Trifluoromethanesulfonate Complexes. **Macromolecule** 28: 5312-5319.

Duke, C. B. and Gibson, H. W. (1978). **Encyclopedia of Chemical Technology** (Vol. 18). 3rd ed. New York: John Wiley & Sons.

Gauthier, M., Armand, M. and Muller, A. (1988). **Electroresponsive Molecular an Polymeric Systems** (Vol. 1). New York: Marcel Dekker. Quoted in Puatrakul, T. (2000). **Studies of Ionic Conductivity of Uniaxially Stretched Polymer Electrolytes Films.** Ph.D. Thesis, University of Akron, USA.

Gray, F. M. (1991). **Solid Polymer Electrolytes: Fundamental and Technological Applications.** New York: VCH. Quoted in Puatrakul, T. (2000). **Studies of Ionic Conductivity of Uniaxially Stretched Polymer Electrolytes Films.** Ph.D. Thesis, University of Akron, USA.

Gutmann, F. and Lyons, L. E. (1976). **Organic Semiconductors**. (n.p.) John Wiley & Sons.

Hirano, T., Khanh, P. H., Tsuji, K., Sato, A., Tsuruta, T., Abe, A., Shimozawa, T., Kotera, A., Yamaguchi, N. and Kitahara, S. (1979). **Polym. J**. 11:905. Quoted in Sasanuma, Y. (1995). Conformational analysis of poly(propylene oxide) and its model compound 1,2-Dimethyloxypropane. **J. Am. Chem. Soc.** 28: 8629 - 8638.

Huang, W., Frech, R. and Wheeler, R. A. (1994). Molecular structure and normal vibration of $CF_3SO_3^-$ and itd lithium ion pairs and aggregates. **J. Phys. Chem** 98: 100-110.

Kim, J. Y., Noh, S. T. and Bae, Y. C. (1998). Phase behaviours of solid polymer electrolytes: applicability of the melting point depression. **Polymer** 39: 3473-3477.

Kitao, T., Yamada, K., Yamazaki, T. and Oya, S. (1972). **Sen'I Gakkaishi** 28: 2, 61. Quoted in Puatrakul, T. (2000). **Studies of Ionic Conductivity of Uniaxially Stretched Polymer Electrolytes Films.** Ph.D. Thesis, University of Akron, USA.

Kovac, M., Gaberscek, M. and Grdadolnik, J. (1998). The effect of plasticizer on microstructural and electrochemical properties of a $(PEO)_n$ $LiAl(SO_3Cl)_4$. **Electrochim. Acta.** 44: 863 – 870.

Law, R. V. and Sasanuma, Y. (1998). Conformational characteristics of poly (tetramethylene oxide). **Macromolecules** 31: 2335 - 2342.

Lightfoot, P., Metha, M. A. and Bruce, P. G. (1993). **Science** 262:883. Quoted in Puatrakul, T. (2000). **Studies of Ionic Conductivity of Uniaxially Stretched Polymer Electrolytes Films.** Ph.D. Thesis, University of Akron, USA.

MacCallum, J. R. and Vincent, C. A. (1987). **Polymer Electrolyte Review I. Elsevier Applied Science.** New York. (n.p.). Quoted in Puatrakul, T. (2000). **Studies of Ionic Conductivity of Uniaxially Stretched Polymer Electrolytes Films.** Ph.D. Thesis, University of Akron, USA.

Nishimoto, A., Agehara, K., Furuya, N., Watanabe, T. and Watanabe, M. (1999). High ionic conductivity of polyether-based network polymer electrolytes with hyperbranched side chains. **Macromolecules** 32: 1541 - 1548.

Oapke, B. L., Ratner, M. A. and Shriver, D. F. (1982). **J.Electrochem.Soc**. 129:1694. Quoted in Puatrakul, T. (2000). **Studies of Ionic Conductivity of Uniaxially Stretched Polymer Electrolytes Films.** Ph.D. Thesis, University of Akron, USA.

Oguni, N., Maeda, S. and Tani, H. (1973). Structure Analysis of Poly(propylene-α-d oxide) by Proton Nuclear Magnetic Resonance Spectroscopy. **Macromolecules** 6: 459.

Oguni, N., Watanabe, S., Maki, M. and Tani, H. (1973). Structure analysis of poly(propylene oxide) by High-Resolution Nuclear Magnetic Resonance Spectroscopy. **Macromolecules** 6: 195-199.

Pearson, R. G. (1963). Hard and soft Acids and Bases. **J.Am.Chem.Soc**. 85:3533-3539.

Preechatiwong, W. and Schultz, J. M., (1996). Electrical conductivity of poly(ethylene oxide)-alkali metal salts systems and effects of mixed salts and mixed molecular weights. **Polymer** 37: 5109 – 5116.

Puatrakul, T. (2000). **Studies of Ionic Conductivity of Uniaxially Stretched Polymer Electrolytes Films.** Ph.D. Thesis, University of Akron, USA.

Quartarone, E., Mustarelli, P. and Magistris, A. (1998). PEO – based composite polymer electrolytes. **Solid State Ionics** 110: 1 – 14.

Ratner, M. A., MacCallum. J. R. and Vincent, C.A. (eds.). (1987). **Polymer Electrolyte Review I.** New York: Elsevier Applied Science. Quoted in Puatrakul, T. (2000). **Studies of Ionic Conductivity of Uniaxially Stretched Polymer Electrolytes Films.** Ph.D. Thesis, University of Akron, USA.

Rhodes, C. P. and Frech, R. (2001). Local structures in crystalline and amorphous phases of Diglyme-LiCF$_3$SO$_3$ and poly(ethylene oxide)- LiCF$_3$SO$_3$ systems: Implications for the mechanism of ionic transport. **Macromolecules** 34: 2660-2666.

Robitaille, C., Marques, S., Boils, D. and Prud'homme, J. (1987). Thermal properties of poly (ethylene oxide) complexed with NaSCN and KSCN. **Macromolecules** 20: 3023-3034.

Sasanuma, Y. (1995). Conformational analysis of poly(propylene oxide) and its model compound 1,2-Dimethyloxypropane. **J. Am. Chem. Soc.** 28: 8629 - 8638.

Sasanuma, Y., Iwata, T., Kato, Y., Kato, H., Yarita, T., Kinugasa, S. and Law, R. V. (2001). Carbon-13 NMR chemical shifts of dimeric model compounds of poly(propylene oxide): A proof of existence of the (C-H)…O attraction. **J. Phys. Chem. A** 105: 3277 - 3283.

Schilling, F. C. and Tonelli, A. E. (1986). Carbon-13 NMR determination of poly(propylene oxide) microstructure. **Macromolecules** 19: 1337-1343.

Sekhon, S. S., Singh, G., Agnihotry, S. A. and Chandra, S. (1995). Solid polymer electrolytes based on polyethylene oxide-silver thiocynate. **Solid State Ionics** 80: 37-44.

Shriver, D. F. and Farrington, G. C. (1985, May 20). **Chem.Eng.News** 63: 42. Quoted in Puatrakul, T. (2000). **Studies of Ionic Conductivity of Uniaxially Stretched Polymer Electrolytes Films.** Ph.D. Thesis, University of Akron, USA.

Smith, G. D., Borodin, O. and Bedrove, D. (1998). Quantum chemistry based force field for simulations of poly(propylene oxide) and it oligomers. **J. Phys. Chem. A** 102: 10318 - 10323.

Smith, G. D., Jaffe, R. L. and Yoon, D. Y. (1996). Conformational characteristics of 1,3-Dimethyloxypropane and poly(oxytrimethylene) based upon ab initio electronic structure calculations. **J. Phys. Chem.** 100: 13439 - 13446.

Smith, G. D., Jaffe, R. L. and Yoon, D. Y. (2000). **Conformations of 1,2-Dimethoxypropane and 5-methoxy-1,3-diaoxane: Are ab initio quantum chemistry predictions accurate?.** [On- line]. Available: http:// www.che.utah.edu/~gdsmith/publications/45/ conformations. PDF

Song, J. Y., Wang, Y. Y. and Wan, C. C. (1999). Review of gel – type polymer – electrolytes for lithium – ion batteries. **J. Power Sources** 77: 183 – 197.

Stepto, R. F. T. and Taylor, D. J. R. (1996). The conformational properties of polyoxypropylene chains — A critical correlation of theory and experiment. **Computational and Theoretical Polymer Science** 6: 49-60.

Stowe, M. K. (2001). **PEO-Based Polymer Electrolytes for Secondary Lithium Batteries.** Ph.D. Dissertation, Michigan State University, USA.

Takahashi, Y. and Tadokoro, H. (1973). **Macromolecules** 6: 672. Quoted in Puatrakul, T. (2000). **Studies of Ionic Conductivity of Uniaxially Stretched Polymer Electrolytes Films.** Ph.D. Thesis, University of Akron, USA.

Tandel, V. P. (1994). Master Thesis, University of Akron. Quoted in Puatrakul, T. (2000). **Studies of Ionic Conductivity of Uniaxially Stretched Polymer Electrolytes Films.** Ph.D. Thesis, University of Akron, USA.

Tonelli, A. E. (1976). Conformational characteristics of poly(vinylidene fluoride). **Macromolecules** 547 - 550.

Watanabe, M., Nagono, S., Sanui, K. and Ogata, N. (1986). **Polymer. J.** 18 (11): 809. Quoted in Puatrakul, T. (2000). **Studies of Ionic Conductivity of Uniaxially Stretched Polymer Electrolytes Films.** Ph.D. Thesis, University of Akron, USA.

Wright, P. V.,Br. (1975). **Polym. J**. 7:319. Quoted in Puatrakul, T. (2000). **Studies of Ionic Conductivity of Uniaxially Stretched Polymer Electrolytes Films.** Ph.D. Thesis, University of Akron, USA.

Yang, L. L., McGhie, A. R. and Farrington, G. J. (1986). **Electrochem. Soc.** 133: 1380. Quoted in Puatrakul, T. (2000). **Studies of Ionic Conductivity of Uniaxially Stretched Polymer Electrolytes Films.** Ph.D. Thesis, University of Akron, USA.

Yoshihara, T., Tadokoro, H. and Murahashi, S. (1964). **J. Chem. Phys.** 41: 2909. Quoted in Chintapalli, S. (1996). **Structural characterization of polymer – salt complexes and the role of plasticizers in ionic transport.** Ph. D. Dissertation, University of Oklahoma Graduate College, USA.

Zahurak, S. M., Kaplan, M. L., Rietman, E. A., Murphy, D. W. and Cava, R. J. (1988).Phase relationships and conductivity of the polymer electrolytes poly(ethylene oxide)/ Lithium Tetrafluoroborate and poly(ethylene oxide)/ Lithium Trifluoromethanesulfonate. **Macromolecules** 21: 654-660.

References

Appendix A

Statistical Weight Matrices of PPO for Each Bond at Various Temperature

Temperature 293 K

$$U_{OC-CC} = \begin{pmatrix} SW_{tt} & SW_{tg^+} & SW_{tg^-} \\ SW_{g^+t} & SW_{g^+g^+} & SW_{g^+g^-} \\ SW_{g^-t} & SW_{g^-g^+} & SW_{g^-g^-} \end{pmatrix} \qquad \begin{pmatrix} 0.78 & 0.73 & 0.67 \\ 0.02 & 0.13 & 0.00 \\ 0.00 & 0.00 & 0.00 \end{pmatrix}$$

$$U_{CC-CO} = \begin{pmatrix} SW_{tt} & SW_{tg^+} & SW_{tg^-} \\ SW_{g^+t} & SW_{g^+g^+} & SW_{g^+g^-} \\ SW_{g^-t} & SW_{g^-g^+} & SW_{g^-g^-} \end{pmatrix} \qquad \begin{pmatrix} 0.11 & 0.04 & 0.16 \\ 0.09 & 0.05 & 0.01 \\ 0.00 & 0.00 & 0.00 \end{pmatrix}$$

$$U_{CO-OC} = \begin{pmatrix} SW_{tt} & SW_{tg^+} & SW_{tg^-} \\ SW_{g^+t} & SW_{g^+g^+} & SW_{g^+g^-} \\ SW_{g^-t} & SW_{g^-g^+} & SW_{g^-g^-} \end{pmatrix} \qquad \begin{pmatrix} 0.58 & 0.00 & 0.01 \\ 0.34 & 0.00 & 0.01 \\ 0.59 & 0.00 & 0.20 \end{pmatrix}$$

Temperature 298 K

$$U_{OC-CC} = \begin{pmatrix} SW_{tt} & SW_{tg^+} & SW_{tg^-} \\ SW_{g^+t} & SW_{g^+g^+} & SW_{g^+g^-} \\ SW_{g^-t} & SW_{g^-g^+} & SW_{g^-g^-} \end{pmatrix} \qquad \begin{pmatrix} 0.79 & 0.73 & 0.68 \\ 0.02 & 0.13 & 0.00 \\ 0.00 & 0.00 & 0.00 \end{pmatrix}$$

$$U_{CC-CO} = \begin{pmatrix} SW_{tt} & SW_{tg^+} & SW_{tg^-} \\ SW_{g^+t} & SW_{g^+g^+} & SW_{g^+g^-} \\ SW_{g^-t} & SW_{g^-g^+} & SW_{g^-g^-} \end{pmatrix} \qquad \begin{pmatrix} 0.11 & 0.05 & 0.17 \\ 0.10 & 0.05 & 0.01 \\ 0.00 & 0.00 & 0.00 \end{pmatrix}$$

$$U_{CO-OC} = \begin{pmatrix} SW_{tt} & SW_{tg^+} & SW_{tg^-} \\ SW_{g^+t} & SW_{g^+g^+} & SW_{g^+g^-} \\ SW_{g^-t} & SW_{g^-g^+} & SW_{g^-g^-} \end{pmatrix} \qquad \begin{pmatrix} 0.58 & 0.00 & 0.01 \\ 0.35 & 0.00 & 0.01 \\ 0.60 & 0.00 & 0.21 \end{pmatrix}$$

Temperature 303 K

$$U_{OC-CC} = \begin{pmatrix} SW_{tt} & SW_{tg^+} & SW_{tg^-} \\ SW_{g^+t} & SW_{g^+g^+} & SW_{g^+g^-} \\ SW_{g^-t} & SW_{g^-g^+} & SW_{g^-g^-} \end{pmatrix} \qquad \begin{pmatrix} 0.79 & 0.74 & 0.68 \\ 0.02 & 0.14 & 0.01 \\ 0.00 & 0.00 & 0.00 \end{pmatrix}$$

$$U_{CC-CO} = \begin{pmatrix} SW_{tt} & SW_{tg^+} & SW_{tg^-} \\ SW_{g^+t} & SW_{g^+g^+} & SW_{g^+g^-} \\ SW_{g^-t} & SW_{g^-g^+} & SW_{g^-g^-} \end{pmatrix} \qquad \begin{pmatrix} 0.11 & 0.05 & 0.18 \\ 0.10 & 0.05 & 0.01 \\ 0.00 & 0.00 & 0.00 \end{pmatrix}$$

$$U_{CO-OC} = \begin{pmatrix} SW_{tt} & SW_{tg^+} & SW_{tg^-} \\ SW_{g^+t} & SW_{g^+g^+} & SW_{g^+g^-} \\ SW_{g^-t} & SW_{g^-g^+} & SW_{g^-g^-} \end{pmatrix} \qquad \begin{pmatrix} 0.59 & 0.00 & 0.01 \\ 0.36 & 0.00 & 0.00 \\ 0.60 & 0.00 & 0.21 \end{pmatrix}$$

Temperature 313 K

$$U_{OC-CC} = \begin{pmatrix} SW_{tt} & SW_{tg^+} & SW_{tg^-} \\ SW_{g^+t} & SW_{g^+g^+} & SW_{g^+g^-} \\ SW_{g^-t} & SW_{g^-g^+} & SW_{g^-g^-} \end{pmatrix} \qquad \begin{pmatrix} 0.80 & 0.74 & 0.69 \\ 0.03 & 0.15 & 0.01 \\ 0.00 & 0.00 & 0.00 \end{pmatrix}$$

$$U_{CC-CO} = \begin{pmatrix} SW_{tt} & SW_{tg^+} & SW_{tg^-} \\ SW_{g^+t} & SW_{g^+g^+} & SW_{g^+g^-} \\ SW_{g^-t} & SW_{g^-g^+} & SW_{g^-g^-} \end{pmatrix} \qquad \begin{pmatrix} 0.12 & 0.05 & 0.18 \\ 0.11 & 0.06 & 0.01 \\ 0.00 & 0.00 & 0.00 \end{pmatrix}$$

$$U_{CO-OC} = \begin{pmatrix} SW_{tt} & SW_{tg^+} & SW_{tg^-} \\ SW_{g^+t} & SW_{g^+g^+} & SW_{g^+g^-} \\ SW_{g^-t} & SW_{g^-g^+} & SW_{g^-g^-} \end{pmatrix} \qquad \begin{pmatrix} 0.60 & 0.00 & 0.02 \\ 0.37 & 0.00 & 0.01 \\ 0.63 & 0.00 & 0.22 \end{pmatrix}$$

Temperature 323 K

$$U_{OC-CC} = \begin{pmatrix} SW_{tt} & SW_{tg^+} & SW_{tg^-} \\ SW_{g^+t} & SW_{g^+g^+} & SW_{g^+g^-} \\ SW_{g^-t} & SW_{g^-g^+} & SW_{g^-g^-} \end{pmatrix} \qquad \begin{pmatrix} 0.80 & 0.75 & 0.70 \\ 0.03 & 0.16 & 0.01 \\ 0.00 & 0.00 & 0.00 \end{pmatrix}$$

$$U_{CC-CO} = \begin{pmatrix} SW_{tt} & SW_{tg^+} & SW_{tg^-} \\ SW_{g^+t} & SW_{g^+g^+} & SW_{g^+g^-} \\ SW_{g^-t} & SW_{g^-g^+} & SW_{g^-g^-} \end{pmatrix} \qquad \begin{pmatrix} 0.13 & 0.06 & 0.19 \\ 0.11 & 0.06 & 0.01 \\ 0.00 & 0.00 & 0.00 \end{pmatrix}$$

$$U_{CO-OC} = \begin{pmatrix} SW_{tt} & SW_{tg^+} & SW_{tg^-} \\ SW_{g^+t} & SW_{g^+g^+} & SW_{g^+g^-} \\ SW_{g^-t} & SW_{g^-g^+} & SW_{g^-g^-} \end{pmatrix} \qquad \begin{pmatrix} 0.61 & 0.00 & 0.02 \\ 0.38 & 0.00 & 0.01 \\ 0.63 & 0.00 & 0.23 \end{pmatrix}$$

Appendix B

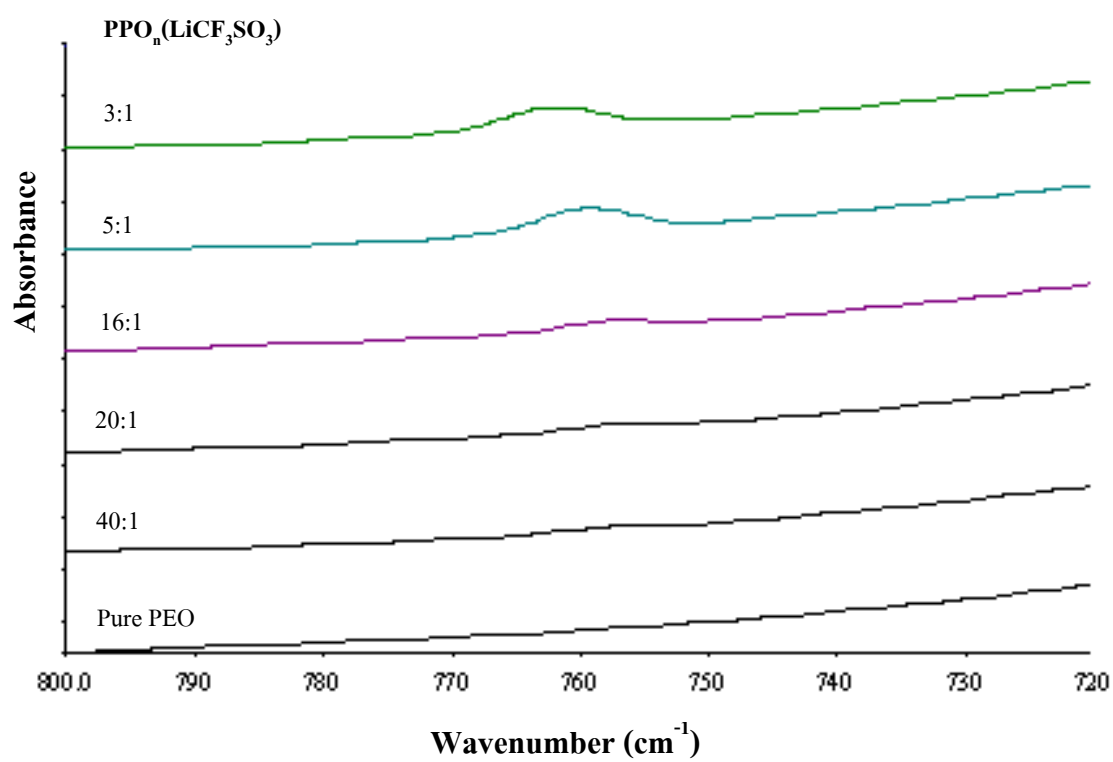## Infrared Spectra of PPO/salt and PEO + PPO

Figure B1 IR spectra of $(PEO)_n LiCF_3 SO_3$ complexes in the 800-720 cm^{-1} spectra region.

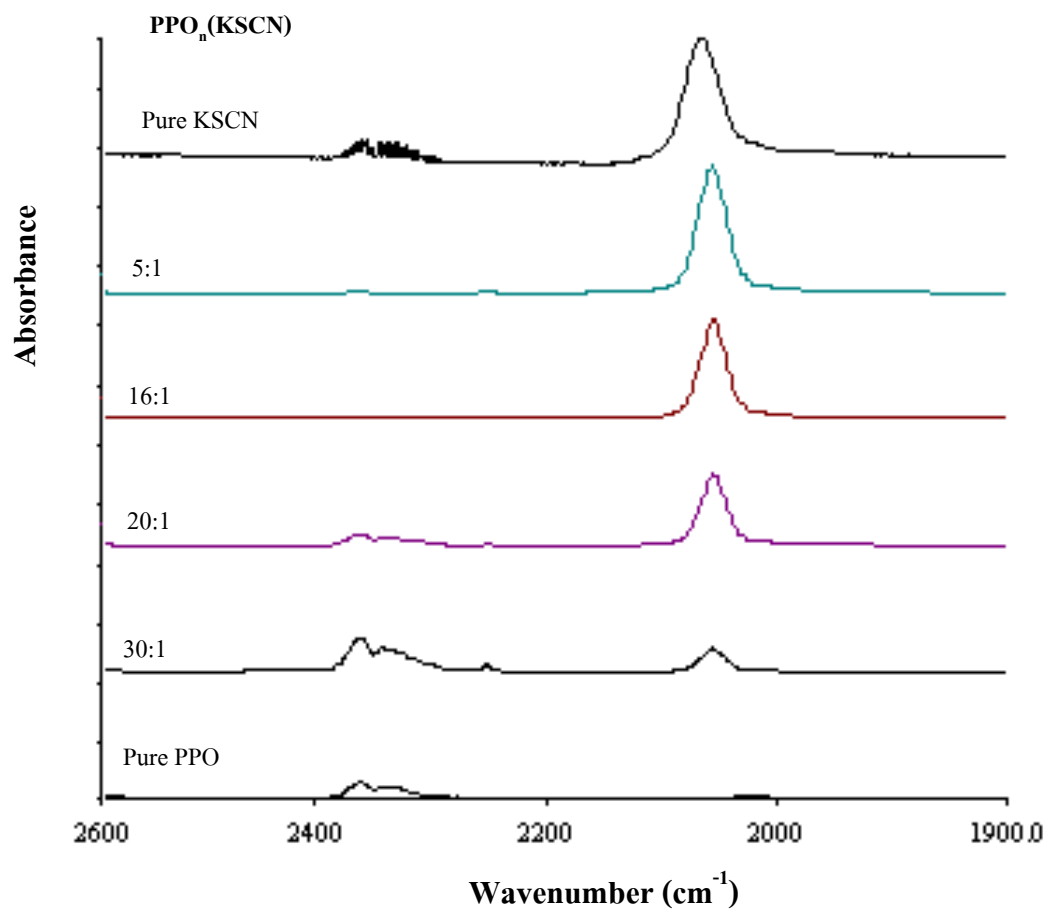**Figure B2** IR spectra of $(PEO)_nKSCN$ complexes in the 2600-1900 cm^{-1} spectra region.
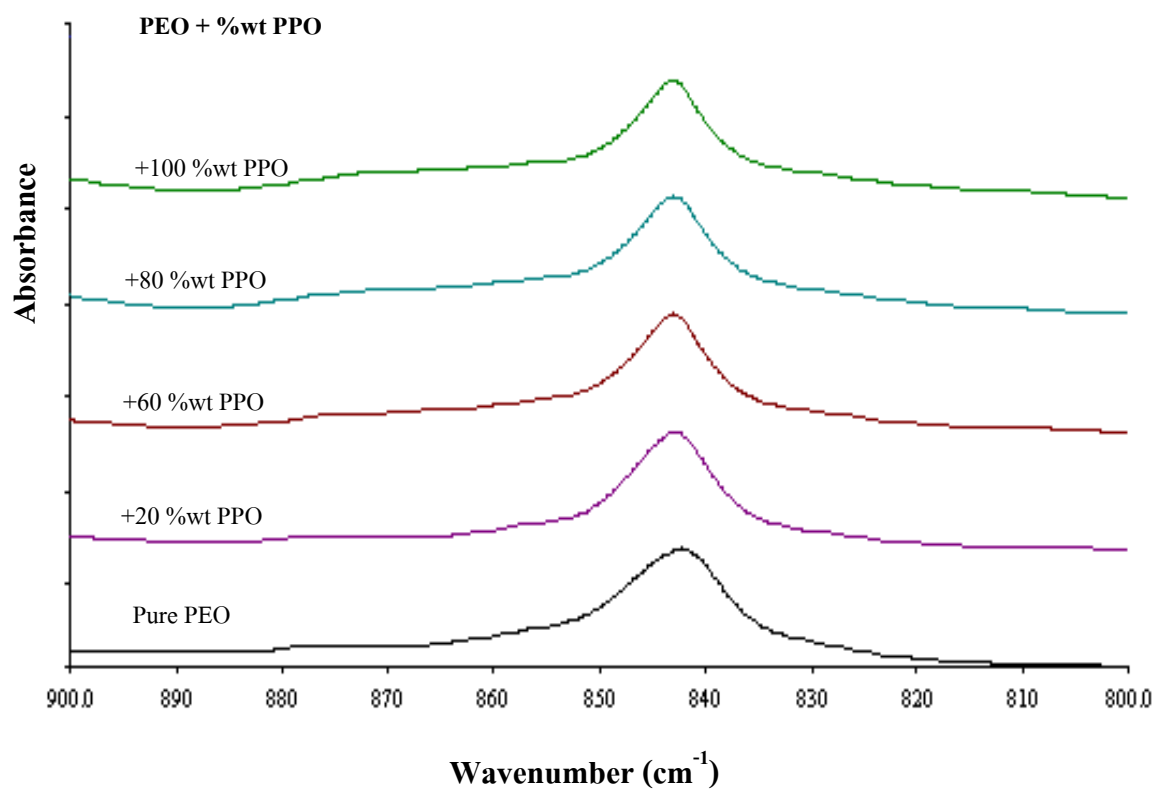
Figure B3 IR spectra of PEO+ %wt PPO complexes in the 900-8800 cm^{-1} spectra region.

Appendix C

Abstract of Presentation at the 3rd National Symposium on Graduated Research, Suranaree University of Technology, Thailand, 18-19 July 2002.

ชื่อบทความ : ภาษาไทย	สมบัติเชิงโครงรูปของพอลิโพรพิลีนออกไซด์
: ภาษาอังกฤษ	Conformational Properties of Poly(propylene oxide)
ผู้แต่ง :	Panita Decha[1] and Dr.Visit Vao-soongnern[2]
ผู้นำเสนอบทความ :	Panita Decha
สังกัด :	School of Chemistry, Institute of Science, Suranaree University of Technology, Nakhorn Ratchasima
อีเมล์ :	[1]p_decha@yahoo.com **Tel: (044) 223153**
กลุ่มวิชา :	Science and Technology

The conformational properties of poly(propylene oxide), [-CH$_2$CH(CH$_3$)O-]$_x$ or (PPO) has been investigated by both theoretical and experimental approach. PPO has two stereochemical arrangements ((R)- and (S)-optical form) due to methyl group in the repeating unit. The conformational energies and geometries of small segments of PPO were determined by the force-field based Molecular Mechanics (MM) technique. Various conformational dependent properties of PPO were then investigated by the Rotational Isomeric State (RIS) Theory. This theory made possible the fast and accurate calculations by generating properties of a single chain that representation of chain conformational statistics for molecule. Rotational isomers, local minima produced by internal rotation about main-chain bond, are considered as discrete state. The relative energies of those states were used to determine the probability as given conformation . Under an additional assumption of fixed bond lengths and bond angles, a set of rotational states along the bonds of a chain completely determines the chain geometry.

In this work, the conformational energies derived from MM technique were used to estimate the elements of statistical weight matrices required for the parameterization of RIS models. The RIS approximation for chain molecules are based on the first- and second-order interactions for three rotational isomeric states *i.e.* trans (t), gauche$^+$ (g$^+$), and gauche$^-$ (g$^-$). The RIS model with statistical weight matrices can be used to predict some conformational dependent properties including the mean square end-to-end distance $\langle r^2 \rangle_0$, the characteristic ratio C_n , the mean-square radius of gyration $\langle s^2 \rangle$, and fraction of bond conformer. These predictions were then be compared with the results obtained from the intrinsic viscosity measurement and NMR experiment.

Extended Abstract of Presentation at the 28th Congress on Science and Technology of Thailand, King Mongkut's Institute of Technology North Bangkok, 24-26 October 2002.

ผลของการเติมพอลิโพรพิลีนออกไซด์ต่อโครงสร้างและสมบัติของพอลิเมอร์อิเล็กโทรไลต์ของแข็ง:ระบบพอลิเอทธิลีนออกไซด์/เกลือ

EFFECT OF ADDING POLY(PROPYLENE OXIDE) ON STRUCTURES AND PROPERTIES OF SOLID POLYMER ELECTROLYTES: POLY(ETHYLENE OXIDE)/SALT SYSTEM

<u>พนิตา เดชา</u>* และ วิสิษฐ์ แววสูงเนิน

<u>Panita Decha</u>* and Visit Vao-soongnern
School of Chemistry, Institute of Science, Suranaree University of Technology, Nakhon Ratchasima 30000, Thailand;
e-mail address: p_decha@yahoo.com

บทคัดย่อ: พอลิเมอร์อิเล็กโทรไลต์ของแข็งเป็นพอลิเมอร์ที่มีสภาพนำไฟฟ้าเชิงไอออนิกซึ่งเตรียมได้จากการใช้เกลืออัลคาไลละลายในพอลิเมอร์ตัวกลางที่เหมาะสม ปัจจุบันมีการพัฒนาพอลิเมอร์อิเล็กโทรไลต์ของแข็งเพื่อนำมาประยุกต์ใช้เป็นอุปกรณ์ที่เกี่ยวข้องกับไฟฟ้าเคมีอย่างกว้างขวางโดยเฉพาะอย่างยิ่งการสร้างเป็นแบตเตอรี่แห้งที่สามารถอัดประจุใหม่ได้สำหรับเครื่องอิเล็กโทรนิกส์ขนาดเล็ก พอลิเอทธิลีนออกไซด์ (PEO) มักถูกใช้เป็นพอลิเมอร์ตัวกลางสำหรับการศึกษาพอลิเมอร์อิเล็กโทรไลต์ของแข็ง เนื่องจากพอลิเอทธิลีนออกไซด์มีสมบัติเป็นตัวทำละลายที่ดีสำหรับตัวนำประจุ อย่างไรก็ตามระบบพอลิเมอร์อิเล็กโทรไลต์ของพอลิเอทธิลีนออกไซด์/เกลือนั้น ให้สภาพนำไฟฟ้าเชิงไอออนิกต่ำที่อุณหภูมิห้อง เพื่อปรับปรุงสภาพนำไฟฟ้าเชิงไอออนิกระบบนี้ ผู้วิจัยใช้การเติมสารเจือพวกพลาสติไซเซอร์ลงไปเพื่อเพิ่มส่วนที่เป็นอสัณฐานของพอลิเอทธิลีนออกไซด์ ซึ่งทำให้สภาพนำไฟฟ้าเชิงไอออนิกเพิ่มมากขึ้น ในงานวิจัยนี้สนใจศึกษาพอลิเมอร์อิเล็กโทรไลต์ของแข็งของระบบพอลิเอทธิลีนออกไซด์/พอลิ- โพรพิลีนออกไซด์ / เกลือ โดยที่พอลิเอทธิลีนออกไซด์เป็นพอลิเมอร์ตัวกลาง พอลิโพรพิลีนออกไซด์ (PPO) เป็นพลาสติไซเซอร์ และใช้เกลือสองชนิดคือ $LiCF_3SO_3$ และ KSCN เป็นไอออน และศึกษาผลของการเติมพอลิโพรพิลีนออกไซด์ ซึ่งเป็นพลาสติไซเซอร์ต่อโครงสร้างและสมบัติของพอลิเมอร์อิเล็กโทรไลต์ของแข็ง:ระบบพอลิเอทธิลีนออกไซด์/เกลือด้วยเทคนิคต่างๆดังนี้ X-ray diffraction, Differential Scanning Calorimeter, Infrared Spectroscopy , และ High resistance meter ผลการทดลองพบว่า พอลิโพรพิลีนออกไซด์สามารถปรับปรุงสภาพนำไฟฟ้าเชิงไอออนของระบบพอลิเอทธิลีนออกไซด์/เกลือได้ และระบบ $PEO/PPO/LiCF_3SO_3$ แสดงสภาพนำไฟฟ้าเชิงไอออนที่สูงกว่าระบบ PEO/PPO/KSCN ส่วนประกอบที่ให้สภาพนำไฟฟ้าเชิงไอออนที่สูงที่สุดคือ PEO:salt ในอัตราส่วน 16:1 กับ PPO 80% สำหรับระบบ $PEO/PPO/LiCF_3SO_3$ และ PEO:salt ในอัตราส่วน 16:1 กับ PPO 100% สำหรับระบบ PEO/PPO/KSCN

Abstract: Solid polymer electrolytes (SPEs) have an ionic conductivity when modified by dissolving of alkali salts in suitable polymer matrix. They have a wide range of electrochemical applications especially the rechargeable batteries for some small electronic

devices. Poly(ethylene oxide), PEO, has been used as matrix polymers for studies of SPEs due to PEO contains ether coordination sites, which in assist the dissociation of salts incorporated in the polymer. However, PEO-salts polymer electrolytes showed low ionic conductivity at room temperature. Attempt to improve the conductivity of PEO based electrolytes researcher has come up with plasticization of polymer electrolytes to disrupt PEO crytallinity and increase the fraction of the conductive amorphous phase. In this research work, we are interested in polymer electrolytes based on PEO/PPO/salt and analyze the effect of adding PPO on the structure and ionic conductivity of these systems. In particular the system in which PEO, PPO and salt have been used as a polymer host, a plasticizer and ionic charge, respectively. Structure and properties of these systems are characterized by variety of techniques, such as x-ray diffraction, differential scanning calorimeter, infrared spectroscopy, and resistance meter. The results of this research work showed that PPO can improve the ionic conductivity of PEO-salts system and PEO/PPO/$LiCF_3SO_3$ electrolyte show higher ionic conductivity than PEO/PPO/KSCN electrolyte. The best composition that gives the highest ionic conductivity are PEO: salt 16:1 with PPO 80% for PEO/PPO/$LiCF_3SO_3$ electrolyte and PEO: salt 16:1 with PPO 100% for PEO/PPO/KSCN electrolyte.

Methodology: PEO (MW $4x10^6$), PPO (4000) are used as received while salt is dried at 100 °C in the oven for 24 h. A solution of the desired volume of PEO, PPO and salt dissolved in a sufficient amount of methanol is stirred overnight at room temperature. The concentration of salt in polymer-salt complexes is expressed in term of molar ratios of the ether oxygen in the polymer to metal cation of salt (O:M). After continuous stirring, the solution is allowed to stand at room temperature for 24 h to facilitate degasing. These solutions are cast on the glass plate. Solvent is removed slowly in vacuum oven at 50 °C for 24 h. The final films are stored in a dessicator before testing. Two main sets of solid polymer electrolytes are made. They are: 1) constant O:M ratio of PEO-salt with the different weight percent of PPO 2)constant weight percent of PPO with the different O:M ratio of PEO-salt. Structure and properties of these systems are characterized by variety of techniques, such as X-ray diffraction, Differential Scanning Calorimeter (DSC), Fourier Transform Infrared Spectroscopy (FTIR), and High resistance meter.

Results, Discussion and Conclusion: The results of this research work from IR and x-ray diffraction studies showed that the PPO can decrease crytallinity of PEO and improve the ionic conductivity of PEO-salts ($LiCF_3SO_3$ or KSCN) system. The PEO/PPO/$LiCF_3SO_3$ electrolyte shows higher ionic conductivity than the PEO/PPO/KSCN electrolyte. A trend was observed in which conductivity increased with increasing salt concentration to a maximum, then decreased at very high salt concentration. The best composition that gives the highest ionic conductivity of two above electrolytes are PEO:salt 16:1 with PPO 80% for PEO/PPO/$LiCF_3SO_3$ electrolyte and PEO:salt 16:1 with PPO 100% PEO/PPO/KSCN electrolyte.

References:
(1) Chintapalli, S. (1996). *Ph. D. Dissertation, University of Oklahoma Graduate College*, USA.
(2) Dias, B. F., Plomp, L., Veldhuis, J. B. J. (2000). *J. Power sources.* **88**, 169 – 191.
(3) Quartarone, E., Mustarelli, P., Magistris, A. (1998). *Solid State Ionics.* **110**, 1 – 14.
(4) Song, J. Y., Wang, Y. Y., Wan, C. C. (1999). *J. Power Sources.* **77**, 183 – 197.

Keywords: solid polymer electrolytes, poly(ethylene oxide), poly(propylene oxide)

Curriculum Vitae

PANITA DECHA

Born: April 27, 1976, Nakhon Si Thammarat

Citizenship: Thailand

Education

1995-1998   B.Sc. Chemistry

Ramkhamhaeng University, Bangkok, Thailand

Experience

1998-1999   Quality Control, Huhtamaki (Thailand) Ltd.

Samut sakhon, Thailand

2000-2002   Teacher Asistance, School of Chemistry, Institute of Science,

Suranaree University of Technology, Nakhon Ratchasima.

Presentation

1.   "Conformational Properties of Poly(propylene oxide)", (with Visit Vao-soongnern), The 3rd National Symposium on Graduated Research, 18-19 July 2002, Suranaree University of Technology, Thailand.

2.   "Effect of Adding Poly(propylene oxide) on Structures and Properties of Solid Polymer Electrolytes: Poly(ethylene oxide)/Salt System)", (with Visit Vao-soongnern), The 28th Congress on Science and Technology of Thailand, 24-26 October 2002, King Mongkut's Institute of Technology North Bangkok.